Evolution of Tectonic and Stratigraphic Geometries in the Southern Outeniqua Basin



Travis Smithard

Supervisor: Dr. Beth Kahle

Dr. Alastair Sloan

Department of Geological Sciences

University of Cape Town

This dissertation is submitted for the degree of

Master of Science

February 2019

University of Cape Town

The copyright of this thesis vests in the author. No quotation from it or information derived from it is to be published without full acknowledgement of the source. The thesis is to be used for private study or non-commercial research purposes only.

Published by the University of Cape Town (UCT) in terms of the non-exclusive license granted to UCT by the author.

University of Cape Town

Declaration

I hereby declare that except where specific reference is made to the work of others, the contents of this dissertation are original and have not been submitted in whole or in part for consideration for any other degree or qualification in this, or any other university. This dissertation is my own work and contains nothing which is the outcome of work done in collaboration with others, except as specified in the text and Acknowledgements.

Travis Smithard

February 2019

Acknowledgements

I would like to thank Total Exploration and Production for the opportunity to study the Southern Outeniqua Basin utilising their dataset. The support that I have received from the team has been unrivalled and I am incredibly grateful for the exposure that I have gained into the oil industry as a result of my working with them. I would also like to thank my supervisors Beth and Alastair who have both supported me in the duration of my masters not just through technically rigorous discussion but also outside of the office, I will forever be grateful for your direction and advice. Last, but certainly not least, I would like to thank my family and friends who have steadfastly believed in me and encouraged me throughout my thesis.

Abstract

The evolution of the Southern Outeniqua Basin has been analysed within a tectono-stratigraphic framework by the interpretation of 3,700km of 2D seismic data constrained by five exploration wells, drilled on the adjacent shelf. The mapping of different fault families into distinct structural orientations, NE-SW, NNE-SSW and NW-SE, was done and the basin sub-divided into four sectors (far-west, west, central and east) based on the geographical position of these faults. Sequence stratigraphic analysis of the basin lead to the identification of seven second-order unconformities which have been further defined into five main seismo-stratigraphic units. The variation in major structural orientations suggest the evolution of the basin developed during three phases of extension, which have been related to the broader plate tectonic context during the Mesozoic break-up of Gondwana. Early Jurassic (170-150Ma) rifting between West and East Gondwana is proposed to have created weaknesses in the crust along the Southern African margin in a NNE-SSW orientation leading to the development of small rift basins and the deposition of syn-rift sediments. A series of intra-continental strike slip faults, including the proto-Agulhas Falklands Fracture Zone, are proposed to have developed along the southern margin during the incipient formation of the Weddell Sea (147Ma) between Antarctica and West Gondwana. Later mid-Jurassic (150-130Ma) extension along the North-Falkland rift zone lead to the oblique extension along the southern margin and the development of normal faults orientated NE-SW. Continued rifting (134Ma) in the proto-South Atlantic lead to translation along the southern African margin and the coalescence of the individual segments of the intra-continental strike slip faults and ultimately

the formation of the Agulhas Falklands Fracture Zone. This phase of wrench faulting (134-130Ma) is characterised by the strike-slip deformation of syn-tectonic sediments defined by second-order unconformities BR and B - late Valanginian - Hauterivian (134-130Ma). The Diaz Marginal Ridge (DMR), which bounds the Southern Outeniqua Basin and AFFZ to the south and north respectively, shows a marked variation is seismic character along strike. In the eastern and western sectors of the basin the DMR is made of syn-rift sediments. The discontinuous and non-parallel seismic character of the DMR in the central sector of the basin is interpreted to be continental basement. Significant bevelling of the top of the DMR in this sector, along with on-lapping reflector geometries of horizon B, Hauterivian (130Ma), is proposed to signify that the continental block existed prior to the formation of the Southern Outeniqua Basin and remained a basement promontory until the development of horizon G - Tertiary (66Ma). The Southern Outeniqua Basin is therefore proposed to have formed through four periods of tectonism: 1) early Jurassic (170-150Ma) orthogonal rifting of West from East Gondwana; 2) late Jurassic to early Cretaceous (150-130Ma) oblique extension and translation along intra-continental strike-slip faults; 3) early-late Cretaceous deformation associated with transverse motion along the AFFZ and development of an active transform margin; 4) mid-late Cretaceous thermal uplift of the Southern Outeniqua Basin associated with migration of the Natal Valley spreading centre along the AFFZ. Thermal subsidence and true passive transform margin conditions developed in the Southern Outeniqua Basin from early Tertiary to present day.

Table of contents

List of figures **xiii**

List of tables **xxix**

1 Introduction **1**

1.1 Introduction 1

2 Geological background **5**

2.1 Plate Tectonic Setting 5

2.2 Sedimentation phases - Outeniqua Basin 7

2.2.1 Rift Phase 7

2.2.2 Transition Phase 8

2.2.3 Drift Phase 8

3 Methodology **13**

3.1 Datasets 13

3.1.1 Seismic Data 13

3.1.2 Well data 15

3.1.3 Checkshot data 15

3.1.4 Potential Field Data 16

3.2 Data Analysis 16

3.2.1 Seismic-well tie 17
3.2.2 Sequence Stratigraphy 18
3.2.3 Fault interpretation and mapping 20
3.2.4 Velocity analysis and depth conversion 20
3.2.5 Seismic artefacts 21
3.2.6 Isochron maps 21

4 Sequence Stratigraphy **27**
4.1 Introduction 27
4.2 Mapped seismic horizons 28
4.2.1 Horizon BR - Valanginian [134Ma] 30
4.2.2 Horizon B - Hauterivian [130Ma] 34
4.2.3 Horizon C - Aptian (120Ma) 37
4.2.4 Horizon D - Cenomanian (93Ma) 40
4.2.5 Horizon E - Campanian (80Ma) 42
4.2.6 Horizon F - late Campanian (76Ma) 45
4.2.7 Horizon G - Maastrichtian (66Ma) 49
4.2.8 Seabed 52
4.3 Seismic packages 55
4.3.1 Pre-rift package 55
4.3.2 Syn-rift package 58
4.3.3 Reflector BR to B: Package 1 (P1) 61
4.3.4 Reflector B to C: Package 2 (P2) 64
4.3.5 Reflector C to D - Package 3 (P3) 68
4.3.6 Reflector D to E - Package 4 (P4) 72
4.3.7 Reflector E to Seabed - Package 5 (P5) 73
4.4 Isochron maps 74

4.5 Summary 76

5 Structural Interpretation 81

5.1 Introduction 81

5.2 Interpretation of seismic data 86

5.2.1 Structural Orientation 1: NE-SW (045-065) 87

5.2.2 Structural Orientation 2: NNE-SSW (020-040) 96

5.2.3 Structural Orientation 3: NW-SE (135-155) 97

5.3 Variation in basin morphology along strike 102

5.3.1 Far-West 106

5.3.2 West 106

5.3.3 Centre 108

5.3.4 East 109

5.4 Diaz Marginal Ridge 110

5.5 Growth faults 114

5.6 Summary 116

6 Discussion 117

6.1 Structural evolution of the Southern Outeniqua Basin 117

6.1.1 Continental rifting between West-East Gondwana (170 - 150Ma) . . 118

6.1.2 Continental rifting between South America and Africa (150 -134Ma) 126

6.1.3 Development of structures associated with transform motion (134 - 80Ma) 126

6.1.4 Development of a passive transform margin (80Ma - Present Day) . 128

6.2 Diaz Marginal Ridge 130

6.3 Stratigraphic evolution of the Southern Outeniqua Basin 135

7 Conclusion 141

References **145**

List of figures

1.1 Map showing the position of the 2001 seismic survey (blue lines) used in the study, within the context of the Southern Outeniqua Basin, shown off the southern margin of South Africa. The five exploration wells, FL-1, FP-1, FS-1, GB-M1 and GB-L1 are shown by their names to the north of the survey. 4

2.1 Map showing a plate reconstruction from Jungslager (1999) of Late Jurassic to Early Cretaceous rift basins before the break-up of West Gondwana. An alternative position for the Falklands Islands is proposed, making the Outeniqua Basin conjugate to the North Falklands Basin. This study has a preference for the former position which implies conjugate margins between the Falklands Plateau basin and the Outeniqua Basin. 10

2.2 Sequence stratigraphic charts for the Bredasdorp and Pletmos Basins. These two charts are shown in order to elucidate on the stratigraphy of the shelfal basins that bound the western and eastern portions of the Southern Outeniqua Basin (modified after Brown et al. (1995). 11

2.3 The inset map shows the location of the seismic line across the shallow water Pletmos sub-basin, the Southern Outeniqua Basin and Diaz Marginal Ridge, from north-west to south-east. The seismic image shows the general structure of the Southern Outeniqua Basin in this area with horizon interpretations (Parsiegla et al., 2009). 12

List of figures

3.1 The 2001 survey shown off the southern margin of South Africa with the bathymetry contoured using a 1000m interval. The survey is transposed upon a hybrid map of the southern African coastline and shows the 5 wells used in order to calibrate the seismic and create a time-depth relationship. 14

3.2 Well FS-1 location shown in Fig. 3.1. The seismic well-tie was generated using calibrated sonic and density logs of the supplied well data. Reflectors shown are those which were interpreted by the precursor to PASA with their relevant polarity interpretations shown. A good correlation was found between the synthetic seismogram and the seismic from which a time-depth relation was calculated and run through the survey area. 18

3.3 Seismic line 2001-33, location shown in Fig.3.1. The interpreted seismic section shows the key second order unconformity surfaces, BR-G,that were mapped across the basin. Fault planes and sense of slip are annotated to show the normal and reverse faulting. 23

3.4 The graph shows the polynomial functions of check-shot velocities for each of the 4 wells that were used (see Fig. 3.1. for location). A regression function is then generated showing a correlation coefficient of 98,9 percent, with the function being used as a means of depth converting specific reflection horizons. 24

3.5 A crossplot showing the datapoints of the interval velocities as derived from a stacking velocity cube using the Dix equation. 24

3.6 Seismic line 63. The quality of the seismic is generally good. Some lines however do still contain processing artefacts and not all diffraction hyperbole have been collapsed back to the point source. These artefacts however can be useful in terms of identifying faults that lie in a similar plane to that of the line, helping to illuminate faults which may otherwise go by unnoticed. 25

4.1 A time structure map of the oldest mapped unconformity surface, BR (refer to Section 3.2.2), used to illustrate the sub-division of the basin into four regions based on morphological variation seen along strike. The regions are labelled Far-West, West, Central and East from the SW to NE along the strike of the basin 29

4.2 Seismic line L2001-9, located in the far-western sector, location shown in Fig. 4.1. The BR reflector truncates the deformed syn-rift sediment that form part of the Diaz Marginal Ridge in the far-western sector. Horizon B is only present in the northern part of the far-western sector where it onlaps onto the BR horizon towards the south. 32

4.3 Seismic line 2001-33, in the western sector, location shown in Fig. 4.1. The interpreted seismic section shows the key second order unconformity surfaces. Horizon BR truncates the syn-rift strata within the rotated fault blocks in the centre of the basin as well as the top of the DMR. Later faulting over the DMR displaces the BR reflector that forms the top of the structure; horizon E onlaps the surface, which is tilted to the north 33

4.4 Seismic line 2001-63, in the central sector, location shown in Fig. 4.1. The interpreted seismic section shows the unconformity surface B on-lapping the basin-bounding faults in this central sector of the basin. 35

4.5 Seismic line 2001-75, in the eastern sector, location shown in Fig. 4.1. The interpreted seismic section shows the unconformity surface C on-lapping the basin-bounding faults of the basement highs to the south of the basin. . . . 36

4.6 Seismic line 2001-19, in the western sector, location shown in Fig. 4.1. The interpreted seismic section shows the unconformity surface C mapped across the basin, with overlying sediments displaying down-lapping reflector geometries onto the surface. These down-lapping geometries are characteristic of basin-floor fan deposits onto underlying sequence boundaries (Vail et al., 1977) 38

4.7 a) Time structure maps within the context of the four sectors of the basin. A) Horizon BR - Valanginian (134Ma). The white ellipses on the structure map show three main depocentre geometries (NNE-SSW, NE-SW and NW-SE) at the beginning of transform motion along the AFFZ. B) Horizon B - Hauterivian (130Ma). The white ellipses show the change in depocentres relative to horizon BR; the horizon B surface is limited in areal extent when compared to the BR surface. C) Horizon C - Aptian (120Ma). The time structure map demonstrates a NE-SW trending depocentre in the western and central sectors and the development of an embayment in the far-western sector. The southern part of the far-western sector is elevated in the time structure map indicating a basinal high during the development of the unconformity. . . . 39

4.8 Seismic line 2001-61, in the central sector, location shown in Fig.4.1. The seismic section shows polygonal faulting, due to the de-watering of shale sediments, between reflectors D-G within the middle of the basin. 41

4.9 Seismic line 2001-13, in the far-western sector, location shown in Fig. 4.1. The seismic section shows unconformity horizon E gaining elevation from north to south as the reflector passes over the Diaz Marginal Ridge and is eventually truncated by the seafloor. 43

4.10 Seismic line 2001-63, in the central sector, location shown in Fig. 4.1. The interpreted seismic section shows the unconformity surface B on-lapping the basin-bounding faults in this central sector of the basin. 44

4.11 Seismic line 2001-75, in the eastern sector, location shown in Fig. 4.1. The interpreted seismic section shows the key first order unconformity surfaces, BR truncating the syn-rift strata within the rotated fault blocks in the centre of the basin. The BR surface in this part of the basin is also observed to be a part of and folded along the shoulder of the Diaz Marginal Ridge. 46

4.12 A) Seismic line 2001-33, in the western sector, location shown in Fig. 4.1. Interpreted sections shows Horizon F on-lapping older reflectors over the northern shoulder of the Diaz Marginal Ridge. 47

4.13 Time structure maps within the context of the four sectors of the basin. a) Horizon D - Cenomanian (93Ma). The white ellipse on the structure map shows the main depocentre straddling the central and western sectors of the basin. The wide contour space between contours suggests that the northern and south-western parts of the basin were characterised by a slope environment during the Cenomanian. b) Horizon E - Campanian (80Ma). The white ellipses shows a south-westward change the position of the depocentre relative to horizon D. The time structure map demonstrates a more defined embayment developing in the south-western part of the far-western sector. c) Horizon F - late Campanian (76Ma) showing the progradation of the shelf. . 48

4.14 Seismic line 2001-63, in the central sector, location shown in Fig. 4.1. Interpreted seismic section shows the tight concave geometry of reflector G as it approaches the DMR high. 50

4.15 Time structure map of horizon G over the study area of the Southern Outeniqua Basin. The reflector is eroded along the northern part of all sectors in the basin and shows a concave geometry in the eastern sector, becoming more concave in the central and far-western sectors where it seems to be defined by the Diaz Marginal Ridge. The surface in the western sector deepens to the south and is more planar in geometry where it overlies the marginal ridge structure. 51

4.16 Time structure map of the seabed in the study area of the Southern Outeniqua Basin. 53

4.17 Seismic line 2001-19, in the western sector, location shown in Fig. 4.1. Interpreted seismic section shows faults originating over the Diaz Marginal Ridge displacing the seabed. 54

4.18 A) Seismic line 2001-75, in the eastern sector, location shown in Fig. 4.1. Interpreted seismic section shows the clear syn-rift strata overlying the acoustically chaotic basement. 56

4.19 A) Seismic line 2001-63, in the eastern sector, location in Fig. 4.1. Interpreted seismic section shows syn-rift strata in the northern part of the basin but very little on the southern part of the basin. 57

4.20 A) Seismic line 2001-2, in the western sector, location in Fig. 4.1. Shows the variation in lithology that makes up the Diaz Marginal Ridge in the western sector of the basin. Syn-rift strata with divergent and parallel reflector geometries are identifiable and contrast with the acoustic chaotic basement that makes up portions of the ridge 59

4.21 Seismic line L2001-9, located in the far-western sector, location shown in Fig. 4.1. 60

4.22 A) Seismic line 2001-31, in the western sector, location shown in Fig. 4.1. Shows the thickening of the on-lapping reflectors of Package 1 towards the north. 62
4.23 A) Seismic line 2001-33, in the western sector, location shown in Fig. 4.1. Interpreted section shows deformation within the P1 (horizons BR - B) over the Diaz Marginal Ridge segment. 63
4.24 A) Seismic line 2001-75, in the eastern sector, location shown in Fig. 4.1. Interpreted seismic section shows the clear folding of the syn-rift strata overlying the acoustically chaotic basement. 65
4.25 A) Seismic line 2001-63, in the eastern sector, location shown in Fig. 4.1. Interpreted seismic section demonstrating the thin package of P2 over the northern part of the sector relative to the thicker package in the middle of the basin with reflections onlapping the DMR to the south 66
4.26 Interpreted line L2001-29, in the western sector, location shown in Fig. 4.1. In the north the sequence of P2 is very thin and indistinguishable from sediments onlapping onto unconformity BR, while the package thickens towards the DMR in the south. 67
4.27 A) Seismic line 2001-61, in the eastern sector, location shown in Fig. 4.1. Interpreted seismic section demonstrating the continuous, parallel, medium-high amplitude reflectors of P3 being truncated by wedge-shaped reflectors which appear to emanate from the northern shoulder of the DMR 70
4.28 A) Seismic line 2001-31, in the western sector, location shown in Fig. 4.1. Interpreted section shows deformation within the BR-B package over the Diaz Marginal Ridge segment. 71

4.29 Seismic line 2001-75, in the eastern sector, location shown in Fig. 4.1. Interpreted seismic section demonstrates the low-amplitude, low frequency, continuous reflection pattern of the lower part of P4, horizons D - E. The upper part of the package is markedly different with high-amplitude, high-frequency discontinuous reflectors onlapping the shoulder of the DMR. . . 73

4.30 Seismic line 2001-9, in the far-western sector, location shown in Fig. 4.1. Interpreted seismic section demonstrates the change from low-frequency, low-amplitude reflectors of P4 in the north to high-amplitude, high frequency internal reflector patterns in the south before the package pinches out against the DMR. 78

4.31 Seismic line 2001-10, crosses the far-western, western and central sectors of the basin, location shown in Fig. 4.1. Interpreted seismic section with megasequence boundaries delineated.The section shows deposition between reflectors E and F, thinning out towards the far-western and western sectors of the basin. Also shown is the change in reflector geometries between Package 5a and 5b, indicating a change in sedimentary provenance. 79

4.32 Isochron maps showing the variation in thickness between the seismic packages across the Southern Outeniqua Basin. P1 is the package defining sediments between BR and B. P2 is the package defining sediments between B and C. P3 is the package defining sediments between C and D. P4 is the package defining sediments between D and E. P5a is the package defining sediments between E and F. P5b is the package defining sediments between F and the seabed. 80

5.1 A) Reconstruction based on free-air satellite gravity data of western Gondwana around 160Ma; prior to any translation along the AFFZ. B) Dextral strike-slip movement along the AFFZ approximately 130Ma. C) Further translation along the fracture zone around 110Ma sees the Maurice Ewing Bank clearing the southern tip of the African plate. D) Gravity reconstruction around 90Ma with pronounced rotation of the African plate as the separation from the South American plates continues. E) Present day plate configuration with the AFFZ clearly visible as a distinct quasi-linear gravity low. SAM - South America, AFR - Africa, FI - Falklands Islands, FPB - Falklands Plateau Basin, MEB - Maurice Ewing Bank, SOB - Southern Outeniqua Basin. 84

5.2 A) Bouguer correction applied to gravity image highlights the trace of the AFFZ and the gravity signatures around the South African margin. The mass deficiency in the crust is highlighted as the bounds of the Southern Outeniqua Basin (SOB) with the faint trace of a fault bounding the northern part of the basin. A sinuous trace inboard of the coastal margin shows the trend of the Cape Fold Belt. B) An EMAG 2 image is annotated to show the different crustal provinces along the offshore South African margin. A change in the magnetic fabric is visible across the trace of the AFFZ outboard of the Southern Outeniqua basin, separating continental from oceanic lithosphere. COB- Continent-Ocean Boundary; LIP - Large Igneous Province; SOB - Southern Outeniqua Basin. 85

5.3 A) The mapped base unconformity (BR - refer to Chapter 4.1) surface is shown, overlain by the observed structural trends and basinal regions in plan view. The structural trends were mapped using the morphological variations in the horizon governed by the inferred existence of faults. B) The mapped faults of this study, in black, are digitised onto the BR surface as well as their corresponding orientations quantified using inset rose-diagram. Shelf area faults were digitised from literature and are shown in green (Broad et al., 2006; Brown et al., 1995; Roux, 1997). 89

5.4 Shows the: A) Mapped BR surface and faults in the Southern Outeniqua Basin. Faults which are in the S.O. 1 orientation are highlighted in red with corresponding seismic lines interpreted in Figs. 5.6-8. 90

5.5 Shows the: The mapped Graben geometries along the strike of the Southern Outeniqua basin. The general trend of the graben is in a NE-SW orientation with a complicating geometry in a NNE-SSW orientation caused by normal faults i that developed during the opening of the Weddell Sea at ca. 147Ma. 92

5.6 A) Seismic line 2001-63, in the central sector. B) Interpreted line with major stratigraphic horizons and faults annotated; shows the NE-SW trending DMR bounding faults as well as a strike slip fault zone and secondary intra-basinal strike slip fault. See Fig. 5.4 for location. 93

5.7 Seismic line 2001-77, in the eastern sector. The interpreted seismic line indicates the second-order stratigraphic unconformities as well as major faults. The large displacement syn-rift fault defines the overall geometry of the basin in this area with smaller, planar-normal faults creating the northern and southern graben seen in the BR reflector interpretation. 94

5.8 Seismic line 2001-71, in the eastern sector. Faults displaying normal and strike slips sense of displacement, with associated folding, found within the basement and syn-kinematic strata. Reactivation of faults to the Tertiary is seen above the shoulder of the Diaz Marginal Ridge segment to the south of the basin. 95

5.9 Faults that are mapped within structural orientation 2 are highlighted in red. Individual seismic lines which show the mapped faults are presented as Figs. 5.10-12. 97

5.10 Seismic line 2001-19, in the western sector. The interpreted section shows the block rotation and half-graben deepening to the south of the basin. . . . 99

5.11 Seismic line 2001-29, in the western sector. Showing block rotation and two half-grabens deepening towards the DMR to the south. A ca. 15km long S.O.1 strike slip fault can be seen propagating on the northern side of the basin where it deforms and interacts with the growth faults in this region. . 100

5.12 Seismic line 2001-33, in the western sector. Shows block rotation and a half-graben deepening towards the southern part of the basin. 101

5.13 Faults that are mapped within structural orientation 3 are highlighted in red. An individual seismic line, L2001-2, which shows the mapped fault is presented as Fig. 5.14. 102

5.14 Seismic line 2001-2 in the western sector. The single mapped fault trending in S.O.3 truncates the shoulder of the DMR in the NE of the section, with syn-rift strata being deposited in the subsequently generated accommodation space. Also visible is the deformed and inverted BR surface towards the SW of the section with multiple later generation faults cutting this unit. 103

5.15 A) The annotated BR-surface time structure map shows the location of figures, labelled Fig. 5.16a-c and Fig. 5.17, chosen in order to display the variation in basin morphology along strike. 104

5.16 This figure shows: Interpreted seismic sections along the basin strike, with locations for Figs. 5.16a-c. A noticeable increase in deformation complexity can be seen towards the western, central and eastern sectors of the basin. . . 105

5.17 A) Seismic Line 2001-79, in the eastern sector. The interpreted section with major structural and stratigraphic relationships highlighted, showing the folding and faulting of basement arches and the DMR across the basin profile. For reflector ages refer back to stratigraphy section. 107

5.18 Seismic line 2001-29, in the western sector. Interpreted seismic section shows the tight concave geometry of reflector G as it approaches the DMR high. 111

5.19 Seismic line 2001-63, in the central sector. Interpreted seismic section shows the major strike-slip zone that is present in the northern part of the central sector. 112

5.20 .Seismic line 2001-77, in the eastern sector. Interpreted seismic section shows normal slip along portions of the syn-rift faults and inversion on the upper segments. 113

5.21 Seismic line L2001-61, in the central sector. The interpreted section highlights the complex growth fault deformation seen along the shelf-side of the basin. 115

6.1 A time structure map of the Valanginian (134Ma) aged unconformity surface, BR, used to illustrate the three depression geometries observed within the basin. The basin has been defined into four sectors given the variation of morphology along strike and are labelled far-west, west, central and east from the SW to NE. 118

6.2 Conceptual cartoon of the first proposed model of the tectonics and structure of the southern margin of South Africa. The cartoon is drawn from regional gravity and magnetic data and the the position of the Maurice Ewing Bank (MEB) during the time of Weddell Sea Rifting. The model shows initial rifting in the Mid-Jurassic and formation of NNE-SSW trending faults. Further extension during the Late Jurassic is proposed to initiate transcurrent motion along intra-continental strike slip faults which then translate the fault blocks from the north-east towards the south-west. A later proposed re-organisation of strain lead to the formation of the incipient AFFZ. 121

6.3 Conceptual cartoon of the second proposed model of the tectonics and structure of the Southern margin of South Africa. The cartoon is drawn from seismic lines in the Central, Western and far-Western sectors of the basin. The lineations labelled F1 and F3 are strike-slip faults visible in seismic in the east and central sectors but lose their character in the western and far-western sectors of the basin (refer to Chapter 4.) 124

6.4 Conceptual cartoon of the third proposed model of the tectonics that created the NNE-SSW trending fault geometries in the far-western sector of the basin. The cartoon is drawn from regional gravity and magnetic data and shows the orientation and position of the extinct spreading ridge between the Maurice Ewing Bank (MEB) and the Falklands Islands (FI). 125

6.5 A proposed break up model of Gondwana during the evolution of the Southern Outeniqua Basin. The ages depicted for each phase of the break-up sequence were calibrated by the oceanic magnetic striping interpretation done by Jokat and Herter (2016); Jordan et al. (2017); König and Jokat (2006). 160Ma) Initial NW-SE extension between East and West Gondwana and the development incipient Weddell Sea produces rift shoulder faults that strike NE-SW. 147Ma) The initiation of intracontinental strike slip motion of the proto-Agulhas Falklands Fracture Zone along a new plane of weakness derived during orthogonal rifting of East and West Gondwana. 138Ma) Transform motion along the Agulhas Falklands Fracture Zone juxtaposes the Falkland Plateau Basin and Maurice Ewing Bank against the southern margin of the proto-Southern Outeniqua Basin producing transpression and uplift of a continental sliver, the Diaz Marginal Ridge. 120Ma) True passive margin conditions begin as free connection occurs between the South Atlantic and South Indian Oceans with later (80Ma) transient uplift occurring along the southern African margin with the passage of the Natal Valley Spreading centre. 129

6.6 Seismic line 2001-53. Interpretation shows the sediments on the southern (oceanward) side of the DMR are deformed between horizons Br-E, Valanginian - Cenomanian (134-93Ma). Deformation is is assumed to be associated with the transform motion along the AFFZ during this time. . . . 132

6.7 Seismic line 2001-61, in the central sector. Interpreted line with major horizons, faults and the DMR annotated. The sediments between horizon B and F, Hauterivian - Campanian (134-80Ma) on the northern shoulder of the DMR show inclined reflector geometries. This is interpreted to be the result of rotation of the fan sediments due to transpression along the AFFZ and the later transient thermal uplift associated with the migrating Natal Valley spreading centre. 133

6.8 A chronostratigraphic chart with regional, basin and feature specific annotations for the area under study. Relative timings of the various picked reflectors are given alongside the interpreted structural and stratigraphic mega-themes. 134

6.9 Seismic line 17, in the far-western sector. Interpreted line with major horizons and faults annotated. The south-eastern portion of the line shows a basement promontory that is dissected by faults that show sediments with divergent reflector geometries, typical of syn-rift deposits. Downlapping reflector geometries near the northern shoulder of the DMR, in the far-western sector, create a mounded feature which is typical of basin floor fan deposits. A number of truncational, onlapping and downlapping reflector geometries indicates the multiple phases of subsidence and uplift that have occurred along the trace of the DMR. 138

6.10 A) A cartoon drawn to reflect the proposed mass transport processes that governed the deposition of Packages 3 and 4, Aptian - Campanian (120-80Ma), along the strike of the basin. 139

6.11 A chronostratigraphic chart with regional, basin and feature specific annotations for the area under study. Relative timings of the various picked reflectors are given alongside the interpreted structural and stratigraphic mega-themes. 140

List of tables

3.1 Horizons mapped and informally named in this study have been correlated with Type-1, second-order unconformities as defined by Brown et al. (1995) and in use at the Petroleum Agency of South Africa. Horizons with their corresponding ages and seismic response (impedance contrast) are indicated for further reference to ages used in this study. This study uses ages defined by the International Commission of Stratigraphy chart of 2018 and Total E&P South Africa. 19

Chapter 1

Introduction

1.1 Introduction

The Southern Outeniqua Basin is an outboard deep-water extension of the shallow-water Bredasdorp, Pletmos, Gamtoos and Algoa sub-basins, that together make up the larger Outeniqua Basin, where the majority of hydrocarbon exploration efforts offshore South Africa have taken place thus far (Fig. 1.1). The basin is bound to the north by the 300m isobath and on its flanks to the west and east by the Agulhas and St.Francis Arches respectively. To the south, the NE-SW trending Diaz Marginal Ridge, a basement promontory, lies along the trace of the Agulhas-Falklands Fracture Zone and defines the southern limit of the basin (Ben-Avraham et al., 1993) Satellite derived bathymetry over the deepwater southern coast shows a clearly defined concave embayment beyond the 300m isobath, that hints at the existence of the underlying Southern Outeniqua Basin. The basin formed during the initial break-up of East and West Gondwana ($\approx$167Ma) with a conjugate basin, the Falklands Plateau Basin, translated to the west by dextral shear motion along the Agulhas-Falklands Fracture Zone which now serves as the basin's northern boundary (Ben-Avraham et al., 1993; Lorenzo and Mutter, 1988; Rabinowitz and Labrecque, 1979). Geophysical and geological study of this conjugate margin has revealed a remarkable symmetry between the Southern Outeniqua

Basin and the Falklands Plateau Basin with both sharing the character of a basin bound on one side by the Agulhas-Falklands Fracture Zone with a sub-parallel, deep sedimentary basin separated from the transform fault by a marginal ridge (Le Pichon and Hayes, 1971; Lorenzo and Mutter, 1988; Platt et al., 1995). DSDP well 330 intersected Devonian-Carboniferous basement, thought to be part of the Cape Supergroup, in the Falklands Plateau Basin providing further evidence as to the position of the Falklands Islands and Maurice Ewing Bank along the south-eastern coastline of South Africa prior to the break-up of West Gondwana (Lorenzo and Mutter, 1988). Although attempts have been made, no drilling had been successfully completed in the Southern Outeniqua Basin due to the effects of the strong Agulhas current that flows along the southern margin of South Africa. Recently, Total E&P has announced a major gas condensate find in the Southern Outeniqua Basin, opening the basin up as a new petroleum province. In contrast to the lack of well control seen in then Southern Outeniqua Basin, the shallow water Outeniqua Basin has seen substantial drilling efforts undertaken over the last 30 years and as such has allowed for confident sequence stratigraphic interpretation of the sub-basins (Broad et al., 2006; Brown et al., 1995; Roux, 1997). Regional second-order unconformities have been defined and mapped across these sub-basins and have been extrapolated from the shelf down into the deeper Southern Outeniqua Basin environment (Brown et al., 1995; Roux, 1997). This thesis aims to constrain the tectono-stratigraphic elements and geometries in the Southern Outeniqua Basin and thereby attempt to add to the understanding of the larger scale plate tectonic stresses and motion as experienced by the region during Gondwana break-up. The fundamental understanding of extension and stretching of continental crust leading to the evolution of passive continental margins, was first proposed by McKenzie (1978). In this pure stretching model, extension of the crust results in the development of conjugate margins whose basins are defined by tilted fault blocks. A second model exists whereby crustal extension is driven primarily by shear stress, resulting in an asymmetric margin profile with one side of the margin defined by rotated

fault blocks (Lister et al., 1986; Wernicke, 1985). Parsiegla et al. (2009) showed that two distinct episodes of continental extension have occurred over the southern margin of South Africa. The first episode (169-155Ma) defined by a stretch (β) value of 1.6, is thought to have affected the entire Outeniqua, whilst the second extensional episode ($\approx$136Ma) with a β value of 1.3, is thought to have only affected the southern portion of the margin. In order to understand the kinematics involved during the tectonic evolution of the basin these two end-member hypotheses, of pure stretching and simple shear, are considered. The first hypothesis is that the Southern Outeniqua Basin developed as a result of rifting during the break-up of Gondwana and existed until a new preferential zone of weakness was developed along which rifting propagated. The second end-member hypothesis is that the Southern Outeniqua Basin developed as a result of trans-tensional extension and is a purely strike slip feature that resulted in a pull-apart basin due to the effects of the proximal and sub-parallel trend of the Agulhas-Falklands Fracture Zone (Fig. 1.1). The true evolution of the basin may, of course, lie somewhere between these two end-members, with for example, early normal faults reactivated in a strike-slip sense or vice versa. In order to accomplish these aims, I have mapped the geometries of basinal faults, which offset the basement significantly, as well as employ the methods of sequence stratigraphy developed by Mitchum, R.M and Vail, P.R (1977) to map major unconformity surfaces and their stratal relations to the depocentres. These methods have ultimately allowed me to infer past motions and comment on the possible tectonic forces responsible for the basin formation, as well as the subsequent provenances for sedimentary in-filling of the basin, in the form of a basin evolution cartoon.

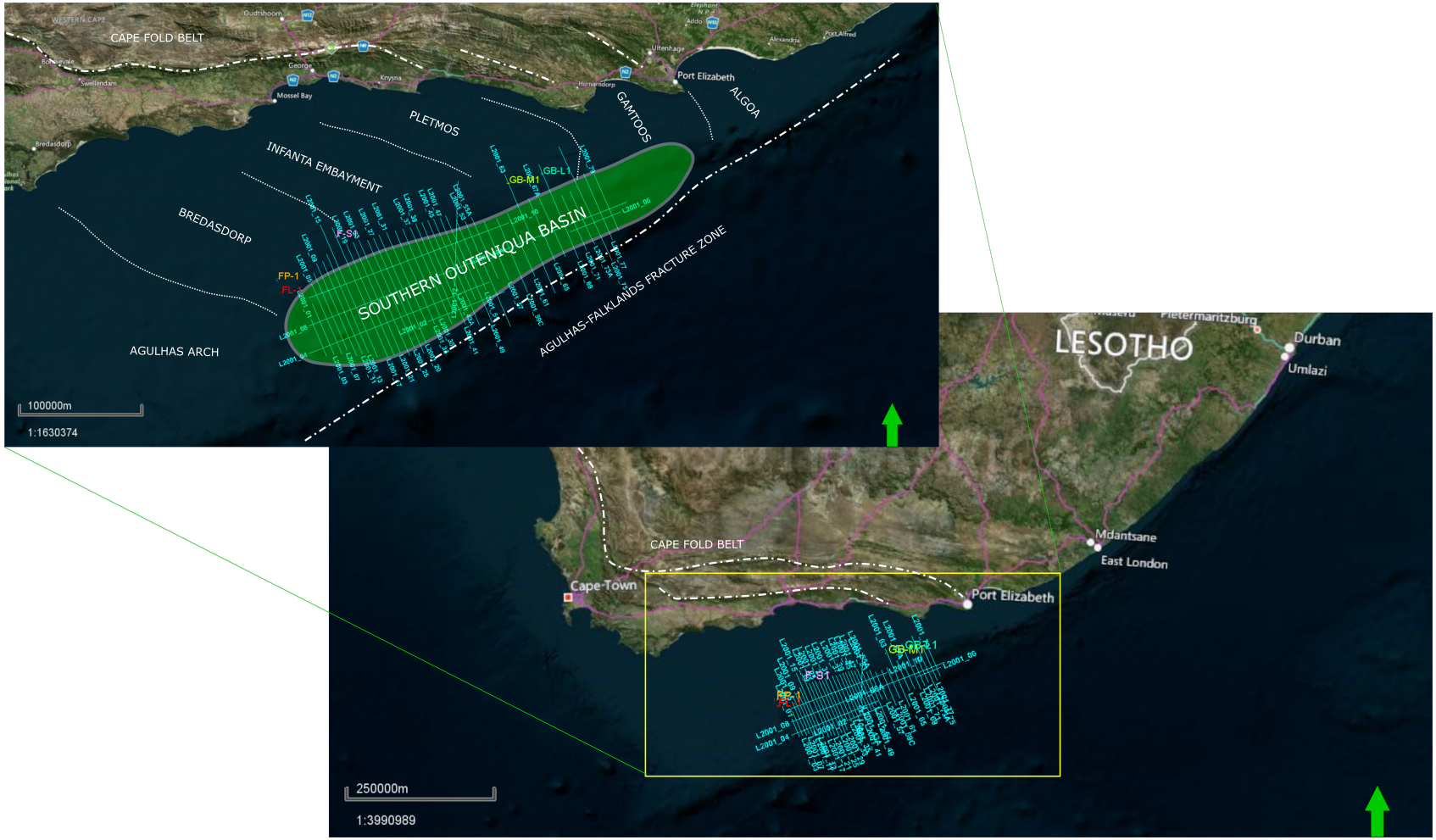


Fig. 1.1 Map showing the position of the 2001 seismic survey (blue lines) used in the study, within the context of the Southern Outeniqua Basin, shown off the southern margin of South Africa. The five exploration wells, FL-1, FP-1, FS-1, GB-M1 and GB-L1 are shown by their names to the north of the survey.

Chapter 2

Geological background

2.1 Plate Tectonic Setting

The present day continental margin of South Africa developed as a result of the break-up of the super continent, Gondwana, that was initiated by lithospheric extension and shear during the early Mesozoic (Rabinowitz and Labrecque, 1979). Mid-late Jurassic extension initially cleaved the super-continent into two portions; West Gondwana, made up of the South American and African plates , and East Gondwana, made up of the Antarctic, Indian and Australian (Fig. 2.1) (Ben-Avraham et al., 1997, 1993; Jungslager, 1999). Continued rifting and extension gave rise to seafloor spreading (≈147Ma) in the incipient Riser-Larsen and Weddell seas (Jokat, 2003; König and Jokat, 2006; Mueller and Jokat, 2017).

The pre-existing planes of weakness within the continental lithosphere, such as the Pan-African suture located sub-parallel to the west coast of South Africa, along the axis of the Orange Basin, and another major crustal weakness oblique to the coast of Durban, situated in the Natal Valley are thought to be the focal points of the resulting continental separation (Booth and Shone, 1999; de Vera et al., 2010; Hirsch et al., 2010; Kuhlmann et al., 2010; Tankard et al., 2009). Rifting of the southern margin is thought to be punctuated by two separate events, the first event initiating during the mid-Oxfordian (≈155Ma) and lasting

till the Valanginian/Hauterivian (≈134Ma) (Jungslager, 1999; McMillan et al., 1997). This first phase of rifting gave rise to the development of a rift basin which is characterised by graben and half-graben structures (Brown et al., 1995). Within this rift basin, known as the Outeniqua Basin, a series of sub-basins, separated from each other by basement arches, display arcuate geometries which generally trend NW-SE (McMillan et al., 1997; Roux, 1997; Broad et al., 2006). These sub-basins from west to east are the Bredasdorp, Pletmos, Gamtoos and Algoa Basins are defined by Brown et al. (1995) and Broad et al. (2006) into their syn-rift and drift depositional sequences respectively (Fig.2.2). The second phase of extension is thought to be driven by the onset of dextral shear along the AFFZ and subsequent transtension of the margin as the African and South American plates slid past each other (Jungslager, 1999).

This movement along the AFFZ is thought to have initiated during the Early Cretaceous at the onset of continental drift and truncates the pre-existing structural trends such as the Permo-Triassic, locally NW-SE trending, Cape Fold Belt and Jurassic to Early Cretaceous failed rift complexes of the Outeniqua Basin (Paton and Underhill, 2004; Sonibare et al., 2014; Thomson, 1999). The dextral shear of the continental lithosphere during this movement along the transform fault heralded the creation of the subsequent conjugate margins of the Falklands Plateau Basin and the greater Outeniqua Basin (Lorenzo and Wessel, 1997). According to Martin and Hartnady (1986) the later drift phase culminated in free connection between the South Atlantic and Indian Oceans during the late Albian when the trailing edge of the Falklands Plateaus is postulated to have cleared the Agulhas Arch. The formation of a marginal fracture ridge on either side of the transform resulted in the Diaz Marginal Ridge (DMR) defining the southern boundary of the Southern Outeniqua Basin and trending parallel to the AFFZ (Fig. 2.3). Ben-Avraham et al. (1993,1997) report that the DMR is a non-magnetic, stratified basement feature of probable continental origin which predates the continental separation and subsequent right-lateral shear along the AFFZ, whilst McMillan

et al. (1997) suggest the development of the DMR is coeval with translation along the AFFZ . Parsiegla (2008) further suggest that the DMR is the product of an uplifted meta-sedimentary block during a transpressional episode along the AFFZ, whilst Parsiegla et al. (2009) prefer the scenario whereby the DMR undergoes thermal uplift due to a temperature contrast between the relatively cold continental crust and a relatively hot spreading ridge as it moved along the AFFZ.

2.2 Sedimentation phases - Outeniqua Basin

The infilling of the Outeniqua Basin and by extension, the Southern Outeniqua Basin, occurred during recurring phases of erosion and sedimentation throughout the Cretaceous and Tertiary (Tinker et al., 2008). These recurring phases of uplift and erosion within the Outeniqua Basin have been defined into five super-cycles which are linked to the global eustatic sea level chart developed in Exxon by Haq et al. (1987) and coincide with enhanced erosion due to local tectonic forcing.

2.2.1 Rift Phase

The Mesozoic basins in the offshore southern margin of South Africa can be sub-divided like other rift basins elsewhere into syn-rift and drift phases of sedimentation (Brown et al., 1995; Jungslager, 1996). Syn-rift sedimentation occurs during extension and stretching of the continental lithosphere during continental break up. The syn-rift sediments lie unconformably onto the basement, made up of Ordovician-Devonian (≈480-360Ma) aged Cape Supergroup meta-sediments, including quartzite and slate (McMillan, 2003). The deposition of these late-Jurassic to early-Cretaceous syn-rift sediments, initially fluvial and lacustrine deposits followed later by shallow marine deposits, are truncated by the Valanginian (≈139Ma) aged Type 1 unconformity, labelled 1At1 in the Petroleum Agency of South Africa (PASA)

nomenclature (Brown et al., 1995). The presence of the 1At1 unconformity announced the end of the rifting and the beginning of transform motion along the AFFZ, leading to marked uplift and changes in the sedimentary source and sink .

2.2.2 Transition Phase

Initial rifting ceased during the early Valanginian (≈136Ma) with basin subsidence resulting in a forced regression but resumed during the initiation of strike-slip motion along the incipient AFFZ. This second phase of extension is represented by the basal unconformity, 1At1, and signifies a transitional phase along the margin (Jungslager, 1996) (Fig2.1). During this phase the first marine shales are deposited onto the underlying 1At1 unconformity as the basin continued to deepen allowing for a restricted marine environment to develop which resulted in the deposition of organic rich shales. The predominantly deep-marine shales of the package drape over tilted fault blocks and indicate rapid subsidence and widespread flooding. Reactivation of faults in a reverse sense of displacement along with local folding are evidences for the tectonic inversion that starts to take place (McMillan et al., 1997) This localised inversion leads to the development of systems tracts in the form of basin-floor fan deposits during the Hauterivian (≈132Ma).

2.2.3 Drift Phase

With the onset of thermal subsidence post-rift, the basin began to subside at a slower rate and allowed for greater sediment input into the deeper basin (Brown et al., 1995).
Stratigraphic correlation between the shelfal sub-basins and their deepwater extension, the Southern Outeniqua basin, is an extrapolation of proximal to distal processes. This correlation means that during regression and subsequently erosional events on the shelf, high energy mass transport deposits would feed the newly sourced sediments into the deeper depocentres of the basin. A number of these regression events occurred during the Hauterivian-Aptian

(≈132-124Ma) and led to the development of large fan complexes within the deeper parts of the basin (Davies, 1997). These regression events, creating Type 1 unconformities, are used as markers in the evaluation of the basin in order to understand the eustatic conditions within the basin through time and thus allow for the qualification of the tectonic derivative of this cycle of relative sea-level rise and fall.

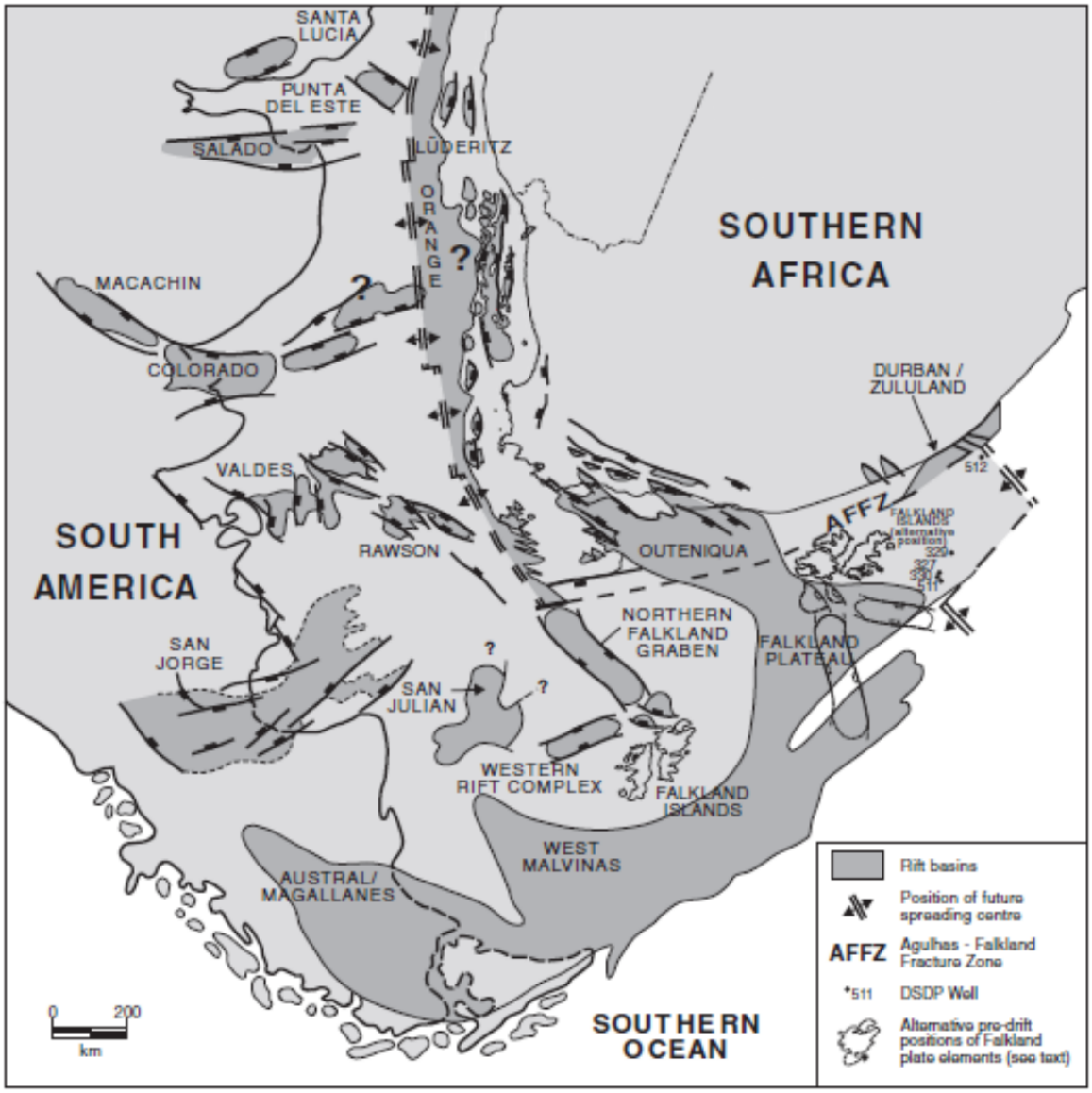


Fig. 2.1 Map showing a plate reconstruction from Jungslager (1999) of Late Jurassic to Early Cretaceous rift basins before the break-up of West Gondwana. An alternative position for the Falklands Islands is proposed, making the Outeniqua Basin conjugate to the North Falklands Basin. This study has a preference for the former position which implies conjugate margins between the Falklands Plateau basin and the Outeniqua Basin.

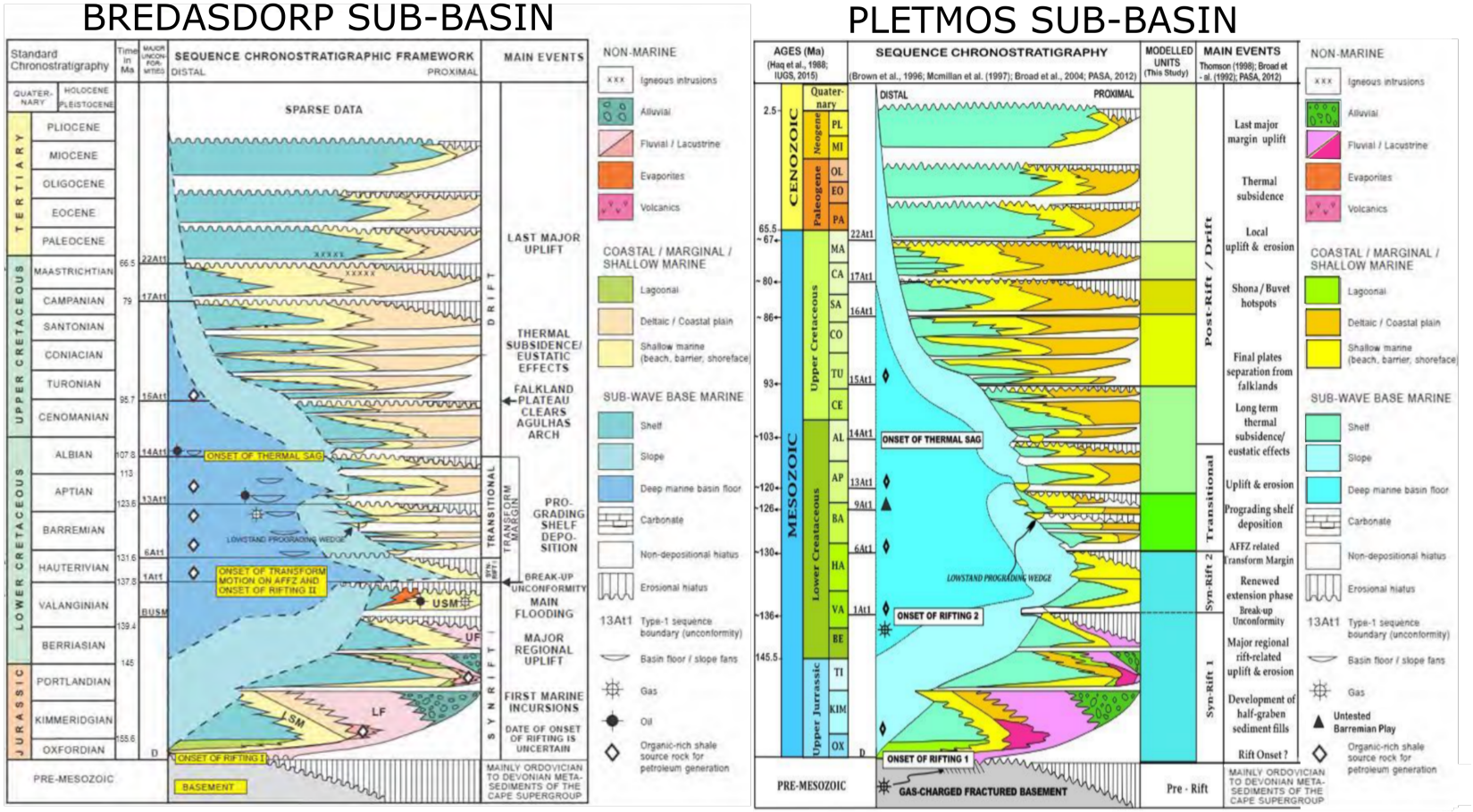


Fig. 2.2 Sequence stratigraphic charts for the Bredasdorp and Pletmos Basins. These two charts are shown in order to elucidate on the stratigraphy of the shelfal basins that bound the western and eastern portions of the Southern Outeniqua Basin (modified after Brown et al. (1995).

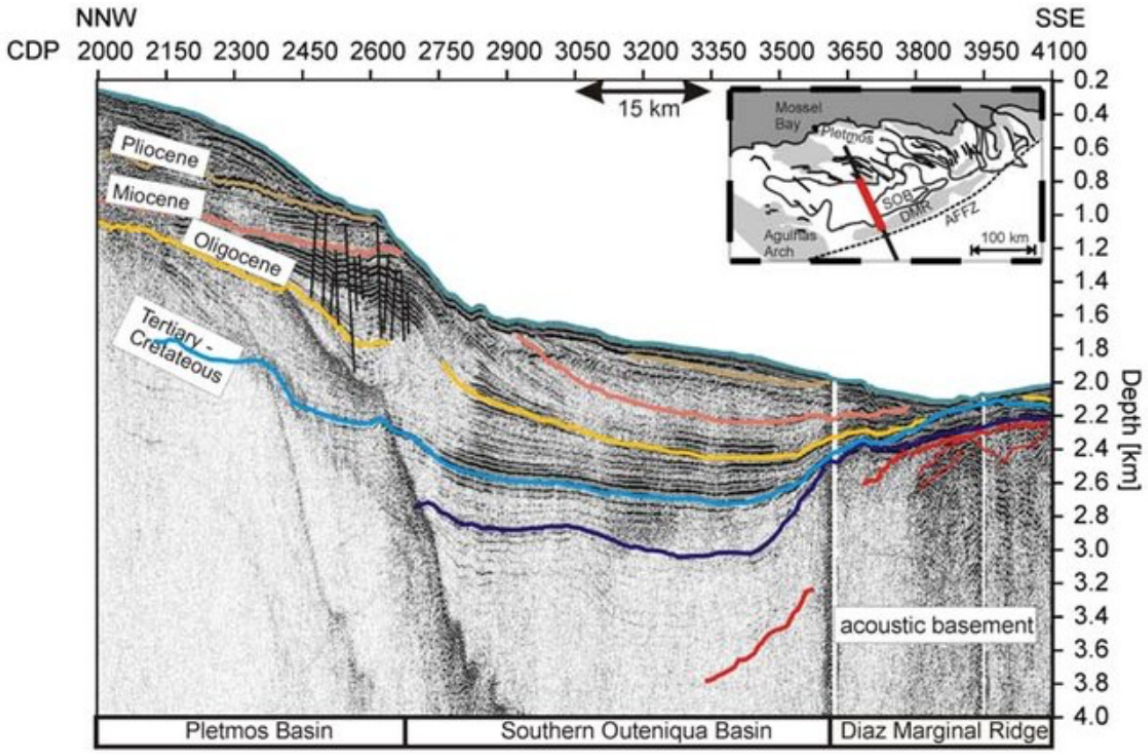


Fig. 2.3 The inset map shows the location of the seismic line across the shallow water Pletmos sub-basin, the Southern Outeniqua Basin and Diaz Marginal Ridge, from north-west to south-east. The seismic image shows the general structure of the Southern Outeniqua Basin in this area with horizon interpretations (Parsiegla et al., 2009).

Chapter 3

Methodology

3.1 Datasets

The datasets supplied for this study were industry acquired seismic and exploration well data as purchased by Total E&P from PASA. The seismic data set includes 43 zero-phase, time-migrated, 2D seismic lines which include 37 inlines (orthogonal to the basinal strike), 5 crosslines shot parallel to the strike of the basin and one oblique line (Fig. 3.1). Additional data came in the form of publicly available satellite derived bathymetry, gravity and magnetics from Smith and Sandwell (1997) used in order to identify present day seafloor morphology and long wavelength crustal features respectively.

3.1.1 Seismic Data

The seismic data provided by Total E&P consists of 43 zero-phased, time-migrated, 2D lines that have a combined 2D coverage of over 3,700km. The polarity of the data was initially received SEGY - Negative, i.e. with an increase in acoustic impedance denoted by a trough. As a matter of personal preference, I subsequently applied a phase rotation to the seismic data of 110 degrees so that an increase in acoustic impedance is represented by a peak in the

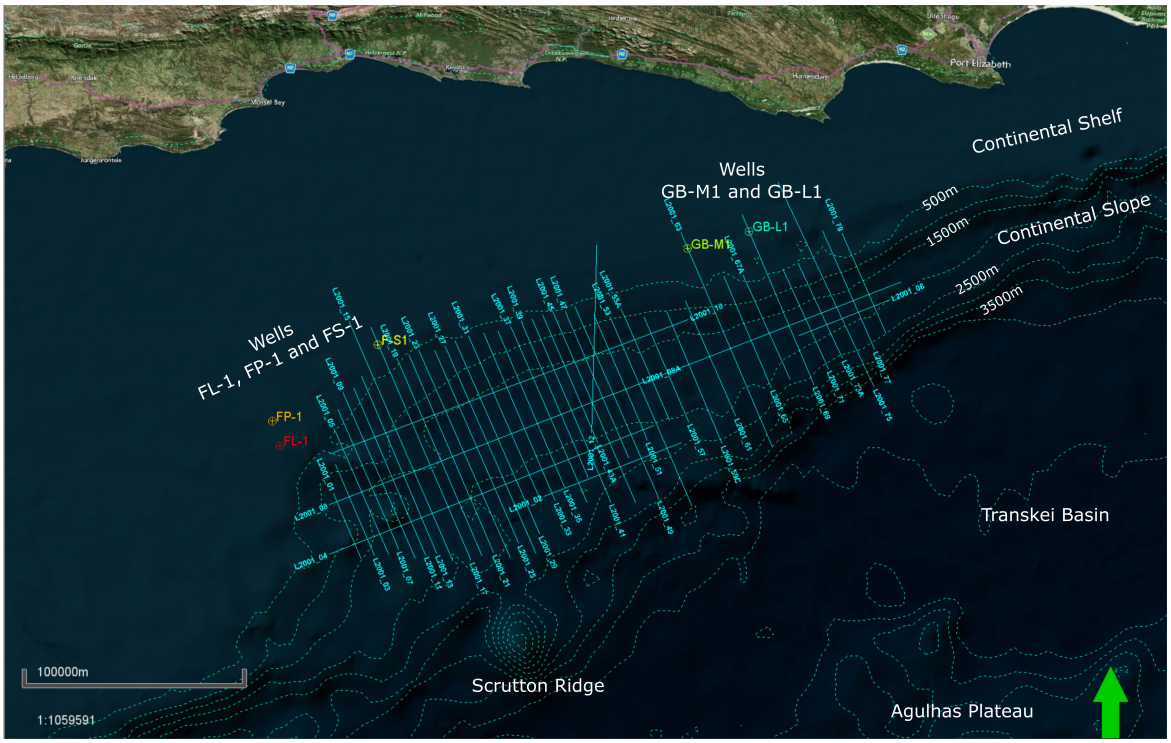


Fig. 3.1 The 2001 survey shown off the southern margin of South Africa with the bathymetry contoured using a 1000m interval. The survey is transposed upon a hybrid map of the southern African coastline and shows the 5 wells used in order to calibrate the seismic and create a time-depth relationship.

seismic wavelet. Acquisition of the seismic was carried out by the Veritas SRV New Venture in a point source / single streamer mode using a 3450 cubic-inch tuned airgun array and a 6000m long streamer, with a nominal group length of 12.5 metres between hydrophones. The seismic was recorded down to 9s Two-Way-Time (TWT) with a sampling rate of 2ms and was completed by the 9th of March 2001 (Veritas Acquisition Report, 2001). Onboard processing of the data by Veritas included Gain Recovery/Spherical Divergence correction, Source Designature, Resampling of the data to 4ms, Veritas' Swell Noise Attentuation Process (SAP) application, Gain Recovery removal and finally output of the data into a SEG-Y format. Processing of the seismic data was then completed in August 2001 by Spectrum Energy and Information Technology, with the main objectives of the processing being to improve structure and fault resolution of the deepwater Southern Outeniqua Basin (Spectrum

Processing Report, 2001). The good signal to noise ratio in the 2001 survey meant that F-x filtering was not necessary in order to remove incoherent background noise prior to migration of the data. For the migration it was found that the Kirchoff-Time (KT) migration algorithm resulted in a particularly high resolution for the imaging of the faults across the slumped shelf zone, whilst no further noise filtering was subsequently applied to the 2001 data.

3.1.2 Well data

Exploration drilling in the deepwater Southern Outeniqua Basin is yet to be completed successfully, however numerous shelfal wells have been drilled in the sub-basins of the shallow-water Outeniqua Basin. Five of these exploration wells were acquired given their proximity to the shelf-break and thus most useful in correlating horizons between the shelf and slope environments. Four of these wells, FP-1,FL-1,FS-1 and GB-L1, provided digital wireline log as well as well-top data, used in the seismic-well tie calibration (Fig.3.1). Distances of more than 50km between the wells means that there is likely significant variation in the lithologies that are encountered given the different sub-basins each well is sampled from. The uncertainty is not quantified in the scope of this study, however the presence of this uncertainty over the large distances was taken into account in the interpretation of the data.

3.1.3 Checkshot data

Well velocity surveys are acquired to asses the variation in seismic velocity around a well bore and increase the reliability of the seismic-well tie derived time-depth conversion. Data from wells FP-1, FL-1, FS-1 and GB-L1 were made available to me for analysis and conditioning. Quality control of the checkshot data was performed in Petrel (2014) with all data points plotted on a graph with a regression function generated in order to illustrate the expected increase in velocity with depth trend. Anomalous data points that did not approximately fit

the regression function were deleted in order to get the data in the best possible condition for calibration with the sonic logs in the wells.

3.1.4 Potential Field Data

Publicly available regional gravity and magnetic digital datasets accessed from the National Oceanic and Atmospherics Administration (NOAA), were processed using Generic Mapping Tools (GMT) software in order to highlight key aspects of the datasets. Processing of the gravity data from Smith and Sandwell (1997) was done in order to generate both Free-Air and Bouguer anomaly maps. The Free-Air anomaly was generated to more precisely map the gravitational responses of the different lithologies and thereby accurately delineate the outlines of the sedimentary basins. The Bouguer anomaly was generated in order to understand the margin-scale gravity responses and thereby help with the later plate tectonic reconstructions (see section 5.1.1). Directional gridding and extrapolation of the raw EMAG2 data compiled by Maus et al. (2009) was done using GMT to better image oceanic lineaments (striping) in the region. The interpretation and calibration of the observed magnetic striping to magnetochrons defined by König and Jokat (2006), allowed for relative timings of oceanic crust formation to be mapped, assisting in the chronological interpretation of plate tectonic events during the evolution of the margin and in the particular, the Southern Outeniqua Basin.

3.2 Data Analysis

The multiple geophysical and geological datasets that were analysed necessitated a thorough review of methodologies employed to understand and draw conclusions from the data provided. Extensive literature reviews of seismic amplitude analysis, sequence stratigraphy, fault mechanics, rift evolution and passive margin formation, thermodynamics and plate

tectonics were performed in order to observe and correctly qualify the impacts of each on the evolution of the Southern Outeniqua Basin.

3.2.1 Seismic-well tie

A seismic to well tie was generated in order to calibrate the seismic data with the supplied data of four of the shelf-based exploration wells by PASA using Schlumberger's Petrel software (e.g. Fig 3.12). In order to achieve the tie a synthetic seismogram was generated using sonic and density logs from the wells and integrated with additional checkshot data received from Total E&P. A standard zero-phased Ricker wavelet, with a frequency of 25Hz, was chosen for the dataset after which the Integration Method was applied. This method was preferred as it uses a single process to integrate the multiple datatypes (checkshot data, sonic and density logs, a seismic survey as reference and a seismic wavelet) in order to generate the synthetic and tie the well. Initially the seismic did not tie very well and resulted in too much stretching and squeezing of the data in order to make it fit. A renewed approach of simply flipping the polarity of the wavelet led to a very good match within the tie and resulted in an average bulk shift of 20 milliseconds. The resulting time-depth-relationship (TDR) generated was then applied in order for the tie to be active. Given the basin-scale nature of the horizon mapping, an accuracy of a few cycles was considered sufficient to tie unconformity surfaces on the shelf to their correlative conformities in the deeper portion of the Southern Outeniqua Basin. The tie to the PASA supplied well data indicates that the oldest mapped horizon (BR), appears to correlate with the basal second order unconformity designated 1At1 without any initial stretching or squeezing of the data (Fig.3.2). Horizons were picked following a standard approach of starting with the sea-bed reflector in order to understand the polarity of the data, in this case the standard SEG positive format was applicable, whereby the hard event of the interface between the water column and the sea-bed is denoted by a positive, high amplitude blue (black) seismic response in the default (black-grey-white) seismic colour

spectra. Thereafter Type 1 unconformities were identified, labelled BR to G, mapped and matched with the horizons 1At1 to 22At1 following the PASA nomenclature (Fig.3.3 and Table 3.1).

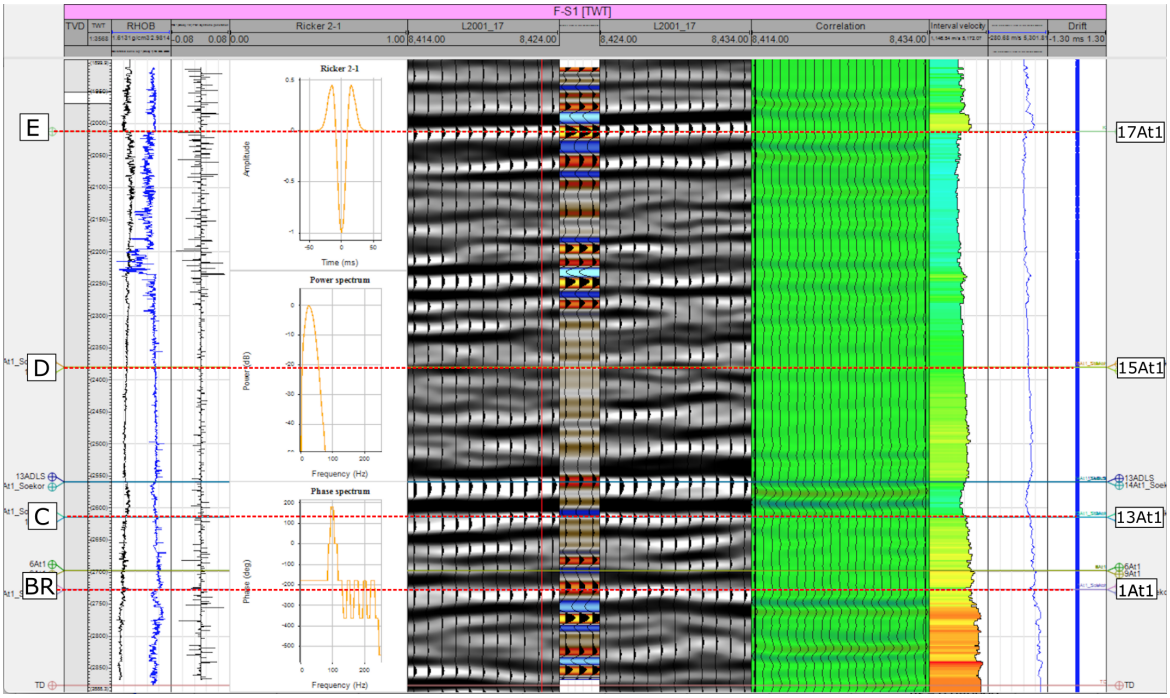


Fig. 3.2 Well FS-1 location shown in Fig. 3.1. The seismic well-tie was generated using calibrated sonic and density logs of the supplied well data. Reflectors shown are those which were interpreted by the precursor to PASA with their relevant polarity interpretations shown. A good correlation was found between the synthetic seismogram and the seismic from which a time-depth relation was calculated and run through the survey area.

3.2.2 Sequence Stratigraphy

The use of sequence stratigraphy models outlined by Vail et al. (1977) were employed in order to define sequences and extrapolate sequence boundaries across from the shelf into the deepwater slope environment of the Southern Outeniqua basin (Fig.3.2). Second order unconformity surfaces, labelled BR, B, C, D, E, F and G, corresponding to eustatic sea level fall and subsequent erosion were identified, mapped and correlated with the At1 second order unconformities defined by Brown et al. (1995) and the PASA using the available well log

Horizon (this study)	PASA nomenclature	Age	Seismic Response
BR	1At1	Valanginian (≈134Ma)	Peak
B	≈6At1	Hauterivian (≈130Ma)	Trough
C	13At1	Aptian (120Ma)	Peak
D	15At1	Cenomanian/Turonian (93Ma)	Peak
E	17At1	Campanian (80Ma)	Peak
F	20At1	late Campanian (≈76Ma)	Peak
G	22At1	Maastrichtian (≈66Ma)	Peak
Seabed	Seabed	Present Day	Peak

Table 3.1 Horizons mapped and informally named in this study have been correlated with Type-1, second-order unconformities as defined by Brown et al. (1995) and in use at the Petroleum Agency of South Africa. Horizons with their corresponding ages and seismic response (impedance contrast) are indicated for further reference to ages used in this study. This study uses ages defined by the International Commission of Stratigraphy chart of 2018 and Total E&P South Africa.

information. The base unconformity, BR or 1At1, represents the unconformity surface which developed after rifting had ceased and movement along the AFFZ had begun. The mapping of BR proved challenging across the basin as the unconformity truncates heterogeneous basal lithologies, including the typical "noisy" basement signature of meta-sedimentary units in addition to the tops of divergent reflector geometries which are inferred to represent syn-rift sediments (Fig. 3.3).

3.2.3 Fault interpretation and mapping

The picking of faults was carried out by a number of methods; namely by identifying reflectors which intersect zones of seismic discontinuity, the correlation of similar reflectors which seem to be offset and the observation of increased sediment package thickness in the hanging walls of proposed faults. Faults that produced large basement offsets or significant sedimentary deformation were mapped whilst smaller faults that did not offset the stratigraphy significantly were observed and described but not mapped in this study. In addition to seismic discontinuity mapping for faults, coherence and variance attributes were run on the data in order to better delineate the local variation in the seismic signal. These attributes measure the dissimilarity of the data in adjacent traces and allow for the enhanced imaging of faults by producing more defined vertical changes in seismic signal.

3.2.4 Velocity analysis and depth conversion

Checkshot velocity data taken from the wells on the shelf, allowed for the calculation of a time-depth regression function which gave an expression of $y=0.000189x^2 + 0.961164x$, where x is representative of the twt (in seconds) down to each surface and y is the corresponding depth to the surface (in metres)(Fig.3.4). Additional stacking velocities generated during the processing phase have also been made available and have been imported into the software and processed using the Dix Formula $V^2=\frac{(T_2V_2^2)-(T_1V_1^2)}{T_2-T_1}$ in order to obtain the interval velocities.

Cross-plots generated in Petrel were used in order to QC the interval velocities derived from the stacking velocities, for each of the horizons, with anomalous data points being removed from the resulting interval (Fig. 3.5)

3.2.5 Seismic artefacts

A seismic artefact is a reflection contained within the seismic data which does not represent an actual geological feature. Interpreting reflections that are not actually primary signals is one of the most challenging tasks set for an interpreter. Artefacts such as diffraction patterns originating from faults, multiples derived from high amplitude reflectors, axial planes creating seismic shadows and interpreting noise as discontinuous signal, thereby inferring a fault, have all been seen within the data set and have with a high degree of certainty been accounted for. The quality of the seismic dataset is generally good. Some lines however do still contain processing artefacts and not all diffraction hyperbole have been collapsed back to the point source. These artefacts however can be useful in terms of identifying faults that lie in a similar plane to that of the line, helping to illuminate faults which may otherwise go by unnoticed (Fig. 3.6).

3.2.6 Isochron maps

In order to qualify the conclusions drawn from the mapping of the key second order unconformity surfaces throughout the basin, isochron maps were generated between specific horizon intervals. Isochron maps give the interpreter the ability to produce a Two-Way-Time (TWT) thickness map between different horizon surfaces and as such provide data with which to observe sediment thickness variations through time. Isochron maps between unconformities B-E and B-F were generated as they were interpreted to represent the period of greatest deposition within the basin and therefore allow the observation of the overall thickness variation across the basin through time. Isochron thickness maps were also generated between

unconformity intervals C-D, D-E and E-F in order to observe subtle changes in sedimentary deposition on a shorter time scale, with the intention of providing evidence for possible transient periods of uplift and erosion across the basin.

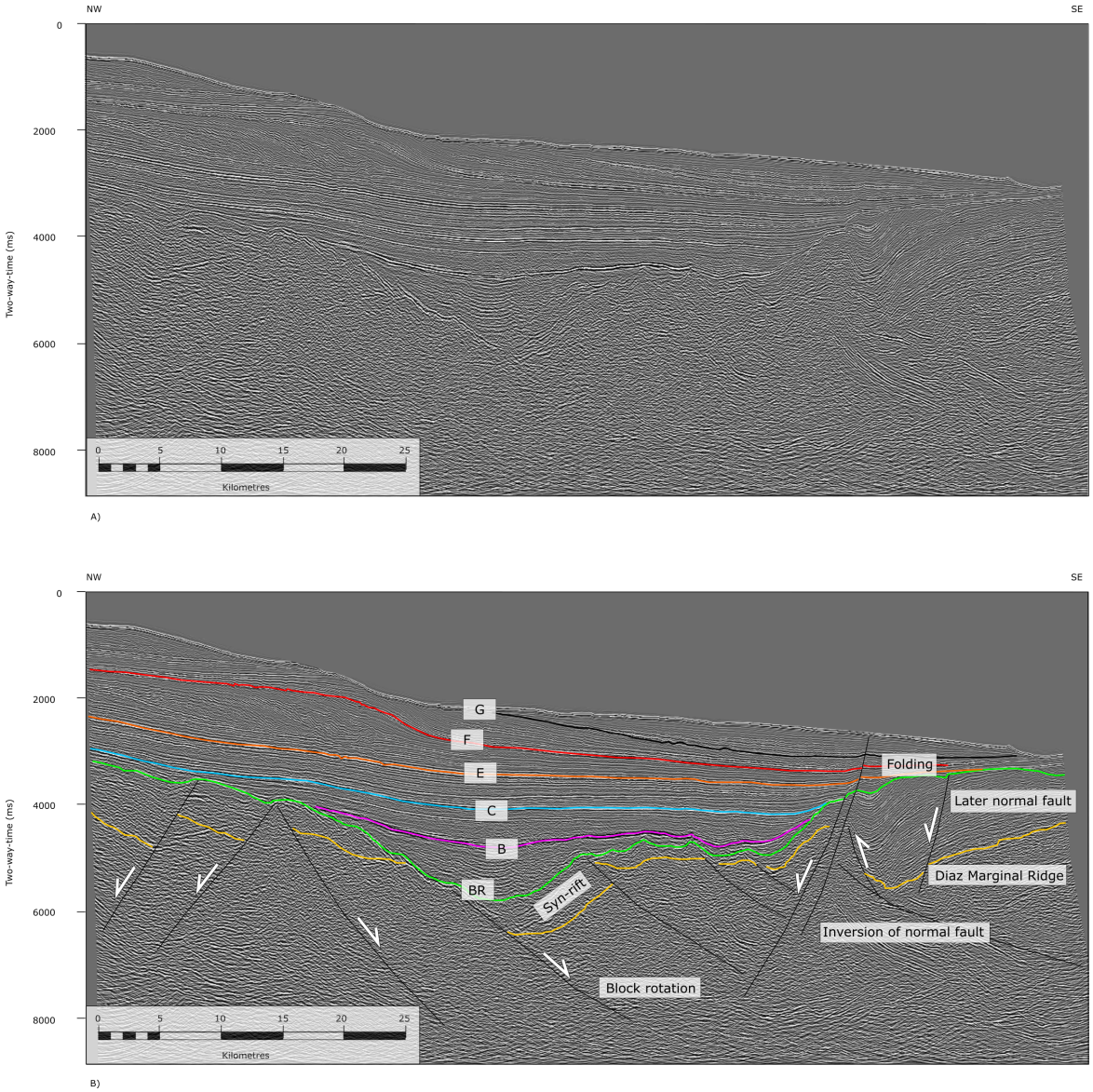


Fig. 3.3 Seismic line 2001-33, location shown in Fig.3.1. The interpreted seismic section shows the key second order unconformity surfaces, BR-G,that were mapped across the basin. Fault planes and sense of slip are annotated to show the normal and reverse faulting.

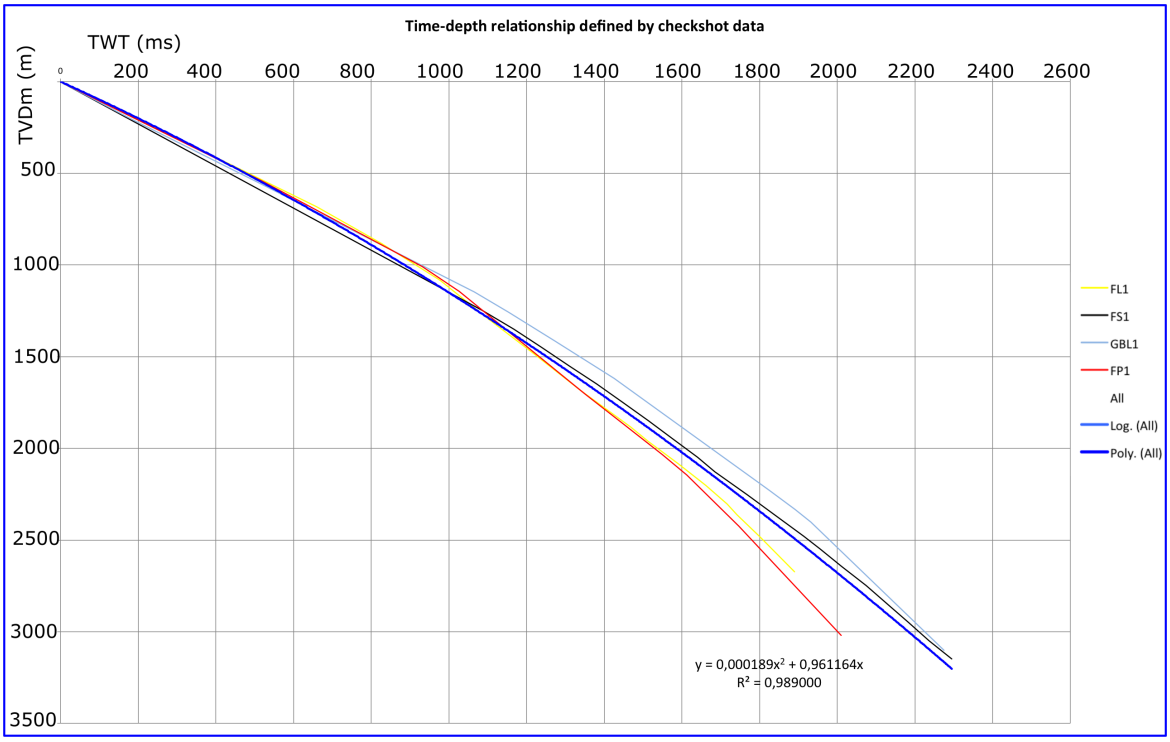


Fig. 3.4 The graph shows the polynomial functions of check-shot velocities for each of the 4 wells that were used (see Fig. 3.1. for location). A regression function is then generated showing a correlation coefficient of 98,9 percent, with the function being used as a means of depth converting specific reflection horizons.

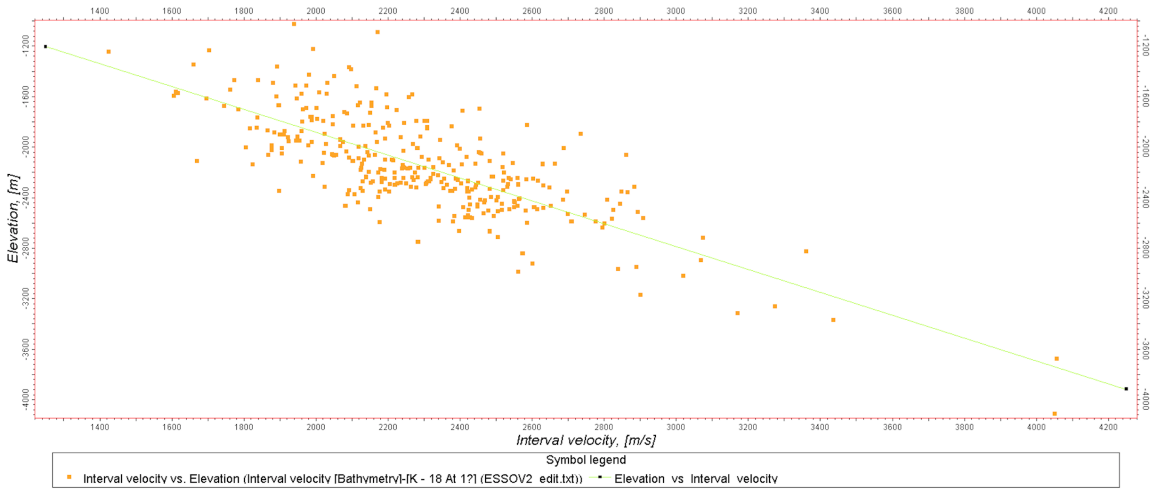


Fig. 3.5 A crossplot showing the datapoints of the interval velocities as derived from a stacking velocity cube using the Dix equation.

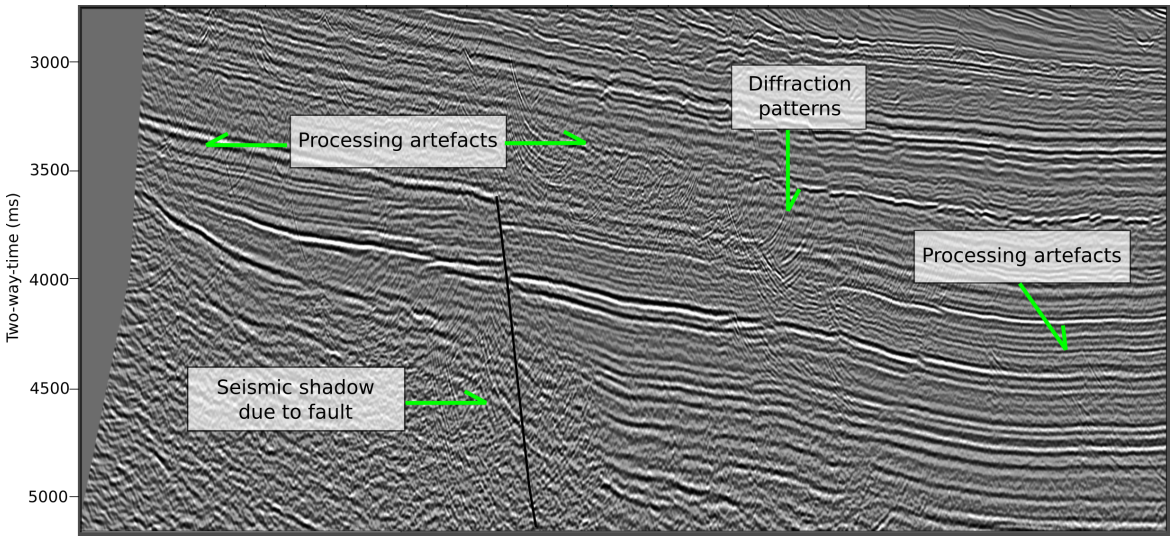


Fig. 3.6 Seismic line 63. The quality of the seismic is generally good. Some lines however do still contain processing artefacts and not all diffraction hyperbole have been collapsed back to the point source. These artefacts however can be useful in terms of identifying faults that lie in a similar plane to that of the line, helping to illuminate faults which may otherwise go by unnoticed.

Chapter 4

Sequence Stratigraphy

4.1 Introduction

In this chapter, I will describe the evolution of basin-fill as far as can be determined from the 2D seismic lines. The first part of my interpretation involved identifying the most obvious seismic reflectors and mapping these throughout the basin (Section 3.2.2). When these horizons had been mapped, they could be correlated with previously recognised unconformity surfaces by carrying out a seismic-to-well tie (Section 3.2.1). After carrying this out successfully, a time history of depocentre migration was then established. An important objective was also to describe the packages, or sequences, between these reflectors to understand the evolution of sedimentation. To this end, units that were inferred to be genetically-related were classified into depositional sequences, following the definition of Mitchum, R.M and Vail, P.R (1977) who stated," a depositional sequence is a genetically related unit bound by unconformities and/or their correlative conformities". These packages are described in detail later in Section 4.3. The basic method of delineating depositional sequence boundaries is known as the 'reflection termination mapping' technique (Vail et al., 1977). This technique looks for the ending of a reflection where the geometry of the termination defines the position of the unconformity. A distinction is made between sedimentary related terminations, such

as pinch outs, and those caused by tectonic fault disturbances or artefacts in the data. The sequences are known to be bound by surfaces which represent significant events in the depositional history of the basin and as such mark variation in the sedimentation and provenance in time.

In total, five major depositional packages were interpreted from the seismic data and their associated unconformity reflections, labelled Package (P) 1-5 and BR to G respectively, are present across the basin with varying amounts of continuity along seismic lines. If my interpretation of the packages is correct, then these may be comparable to megasequences and as such provide relative timing for deposition and erosion across the basin. Gridded surfaces were generated for each of the reflectors, although the line-spacing is relatively wide (6-10km). This imposes a limit on the resolution of the grids in one dimension. Experiments were carried out with various gridding parameters (e.g tension) to ensure that the grids are representative of the data. The large areal extent and varied morphology of the basin along its strike, necessitated that the study area has been segmented into four regions; far-west, west, central and east for easier frame of reference (Fig. 4.1).

4.2 Mapped seismic horizons

Across the basin, the unconformities are defined as hard events as the erosion of underlying more cemented strata by coarser, more porous and subsequently less dense sediments, typically lends to an increase in acoustic impedance and thus a positive seismic peak. The horizons mapped within the study area followed a basic nomenclature which is reasonably tied to the At1 unconformity surfaces picked within the wells in order to get a relative timing of sequence deposition (refer to Ch. 3, Table 3.1.). The horizons mapped include,from oldest to youngest, BR, B, C, D, E, F, G and the seabed (Fig. 4.2).

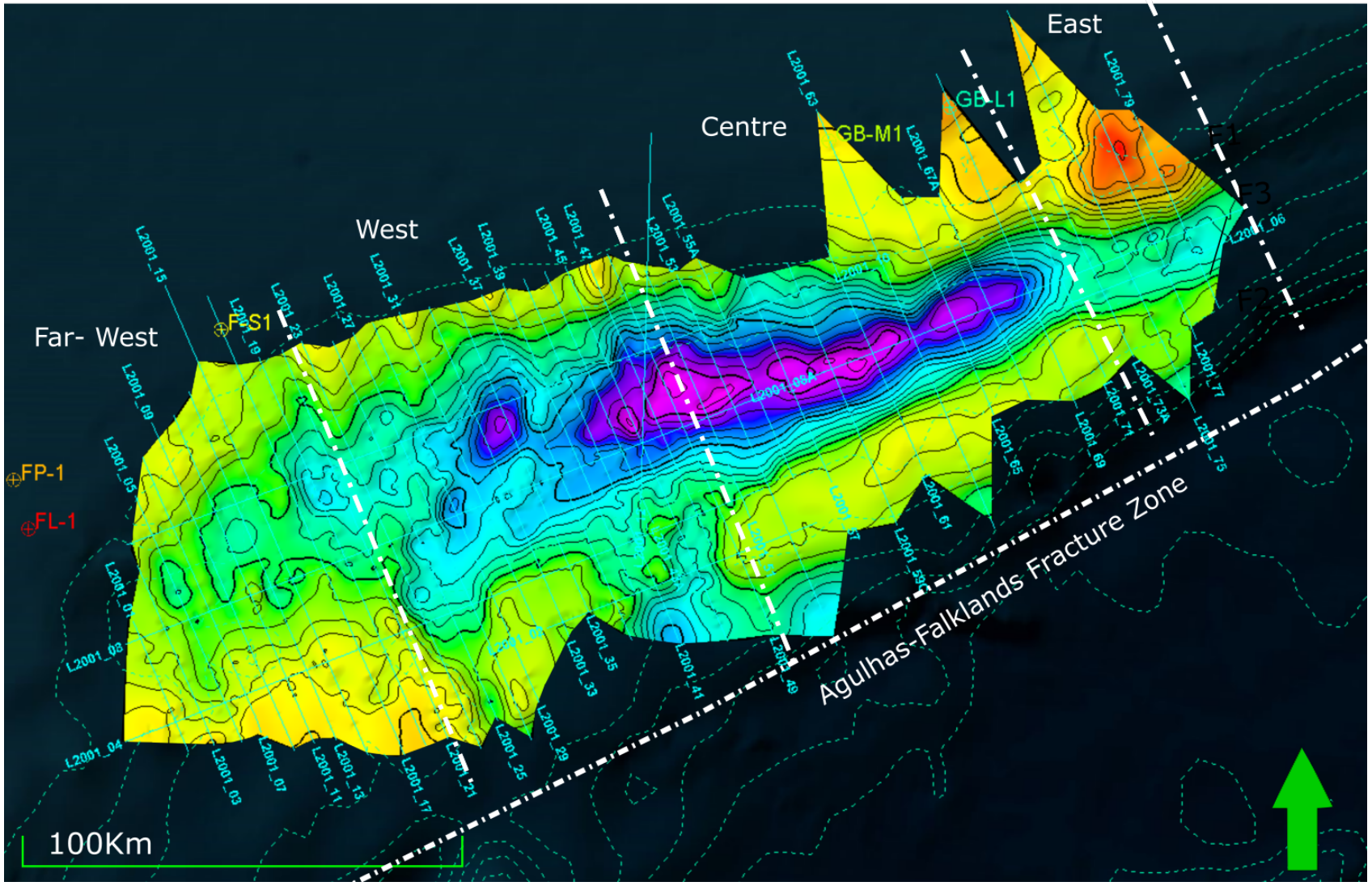


Fig. 4.1 A time structure map of the oldest mapped unconformity surface, BR (refer to Section 3.2.2), used to illustrate the sub-division of the basin into four regions based on morphological variation seen along strike. The regions are labelled Far-West, West, Central and East from the SW to NE along the strike of the basin

4.2.1 Horizon BR - Valanginian [134Ma]

The BR or 1At1 reflector (refer to section 3.2.2) was picked by identifying the oldest (deepest) unconformity surface truncating both the basement, identifiable by the lack of clearly stratified reflectors, as well as the divergent reflectors of syn-rift sediments. The time structure map, ranging from 1750ms to 6500ms, indicates that the morphology of the BR surface is varied across the basin (Fig. 4.1). The BR reflector has a predominantly semi-continuos, medium to high amplitude seismic response and is typically a "peak" (increase in acoustic impedance) event. Due to the lateral variation in lithologies, basement versus syn-rift sediments, the picking of the BR unconformity is often challenging. Over the basement the seismic response of the unconformity is typically a strong peak amplitude response, whereas when the unconformity truncates the syn-rift sediments, the polarity of the response can change depending on the lithology the horizon truncates (Fig. 4.2). The picking of this reflector was important as a topographic marker in highlighting accommodation areas within the basin, developed after lithospheric extension and prior to major transform motion, where sediments would be channeled and deposited. In the far-west sector of the basin the topography is elevated with the unconformity bounding a basement high in the northern part of the sector (Fig. 4.3). The unconformity in this sector is deformed by basement derived faults and becomes chaotic/discontinuous towards the south where it defines the northern shoulder of the Diaz Marginal Ridge. Planation and truncation of the syn-rift strata within the DMR, forms a distinct bevelled surface on the top of the structure where the BR reflector can be characterised as an angular unconformity (Fig. 4.3). Within the western sector, the BR surface undulates over an elevated basement high in the northern part of the basin. A strong amplitude response in this part of the sector decreases towards the middle of the basin, where the reflector becomes medium-low amplitude as it erodes the top of the syn-rift strata. The reflector in the southern part of the western sector is highly deformed with numerous faults offsetting the reflector as it passes over the DMR (Fig. 4.3). The BR surface in the

central sector of the basin defines a deep (≈5500ms TWT) NE-SW trending depression, bound to the south and north by basement highs (Fig. 4.4). In the southern part of the eastern sector of the basin, the BR reflector is characterised as an angular unconformity, truncating the underlying folded syn-rift sediments of the DMR, whilst in the northern part (north of the St. Francis Arch) the reflector is itself inclined and truncated (Fig. 4.5). The top of the DMR structure is bevelled by the BR unconformity after which the reflector decreases in elevation on the southern side of the marginal ridge (Fig. 4.4). The paleo-slope shown in the BR surface is shallowest in the south-west (far-western and western sectors) and gets progressively steeper towards the north-east (central and eastern sectors) (Fig. 4.7A). The high gradient of the slope in this sector suggests a potential pathway along which future gravity-driven sediments (in the form of fans) would flow during subsequent infilling of the basin.

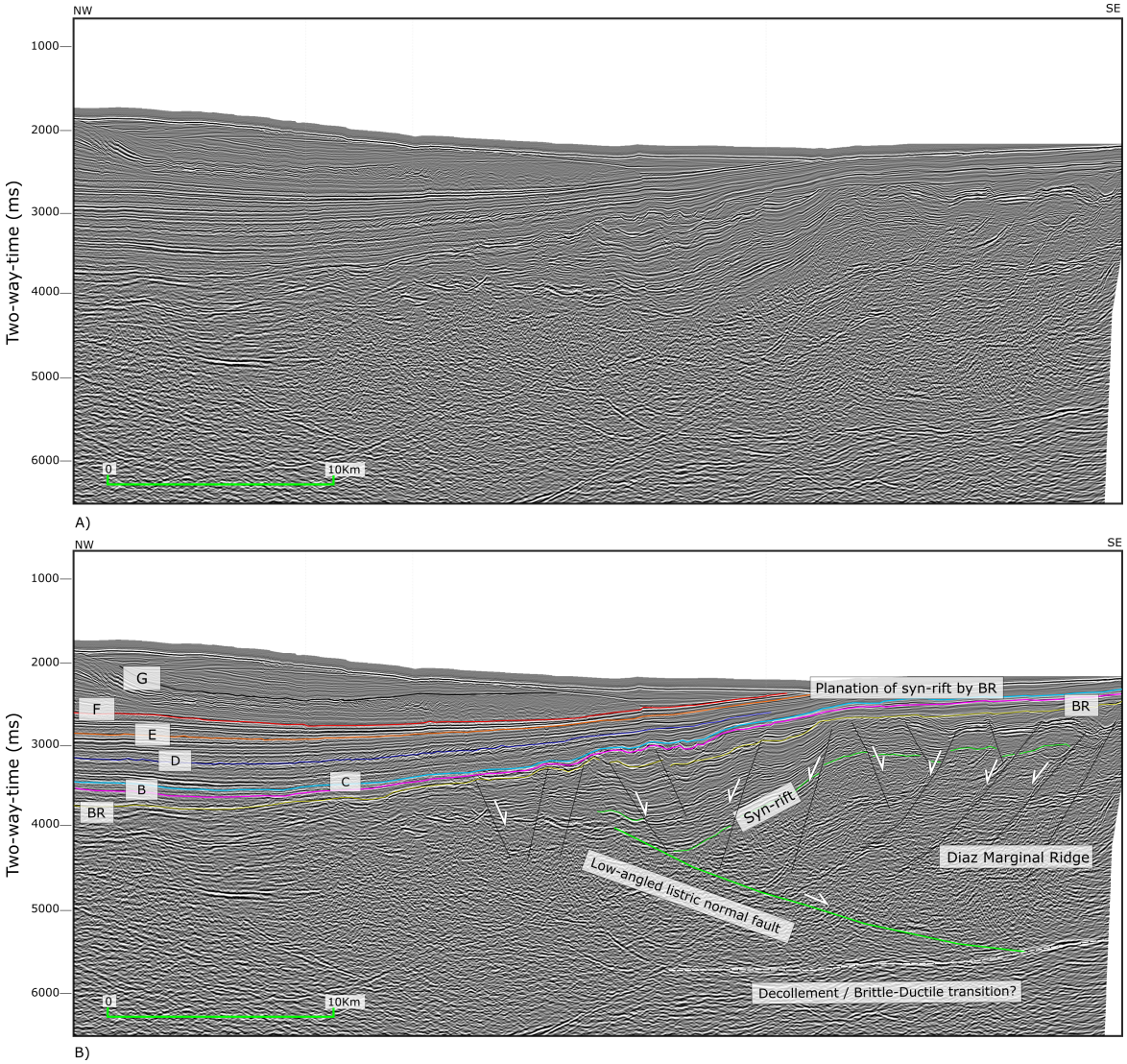


Fig. 4.2 Seismic line L2001-9, located in the far-western sector, location shown in Fig. 4.1. The BR reflector truncates the deformed syn-rift sediment that form part of the Diaz Marginal Ridge in the far-western sector. Horizon B is only present in the northern part of the far-western sector where it onlaps onto the BR horizon towards the south.

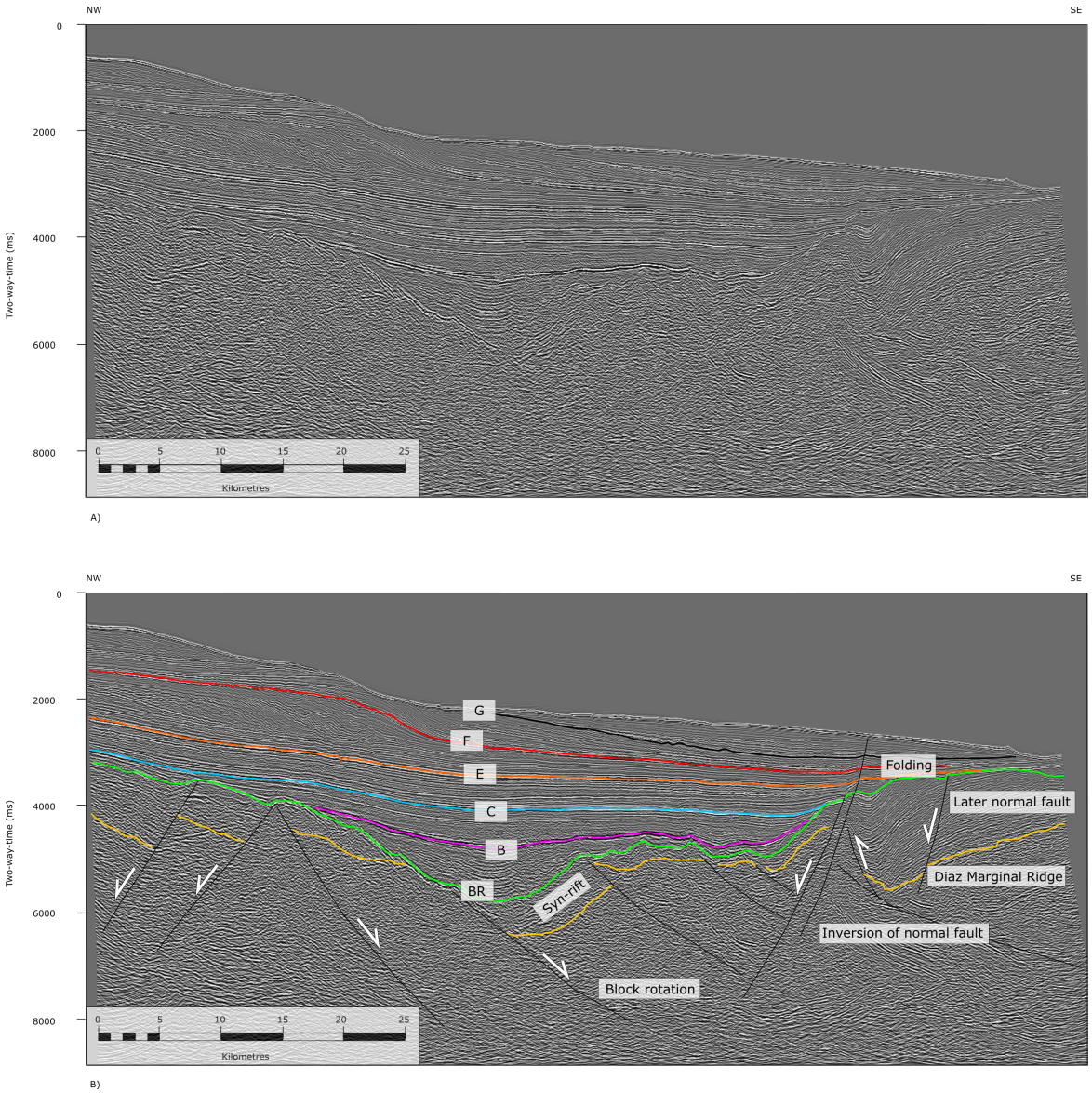


Fig. 4.3 Seismic line 2001-33, in the western sector, location shown in Fig. 4.1. The interpreted seismic section shows the key second order unconformity surfaces. Horizon BR truncates the syn-rift strata within the rotated fault blocks in the centre of the basin as well as the top of the DMR. Later faulting over the DMR displaces the BR reflector that forms the top of the structure; horizon E onlaps the surface, which is tilted to the north

4.2.2 Horizon B - Hauterivian [130Ma]

The seismic response of reflector B is a medium-high amplitude trough that is continuous across the central, western and far-western sectors and is not present in the eastern sector of the basin. The reflector onlaps against the elevated topography of the underlying BR horizon in the far-western sector of the basin and is present only in the northern part of the sector (Fig. 4.2). Within the western sector of the basin, a high amplitude broad response of the reflector is visible and is easily mapped across the middle of the basin before on-lapping the basement high to the north; in the southern part of this sector the reflector onlaps the northern shoulder of the DMR with the geometry of the reflector becoming inclined towards the ridge (Fig. 4.3). A deepening of the horizon B surface (≈4900ms TWT) occurs in the southern part of the boundary between the western and central sectors of the basin (Fig. 4.4). Within the central sector of the basin the reflector is confined by and onlaps the basement highs to the south and north. The horizon B time structure surface ranges in elevation from 2500ms to 4900ms TWT and indicates depressions orientated in NNE-SSW and NE-SW had developed in the western and central sectors of the basin during this time (Fig. 4.7b).

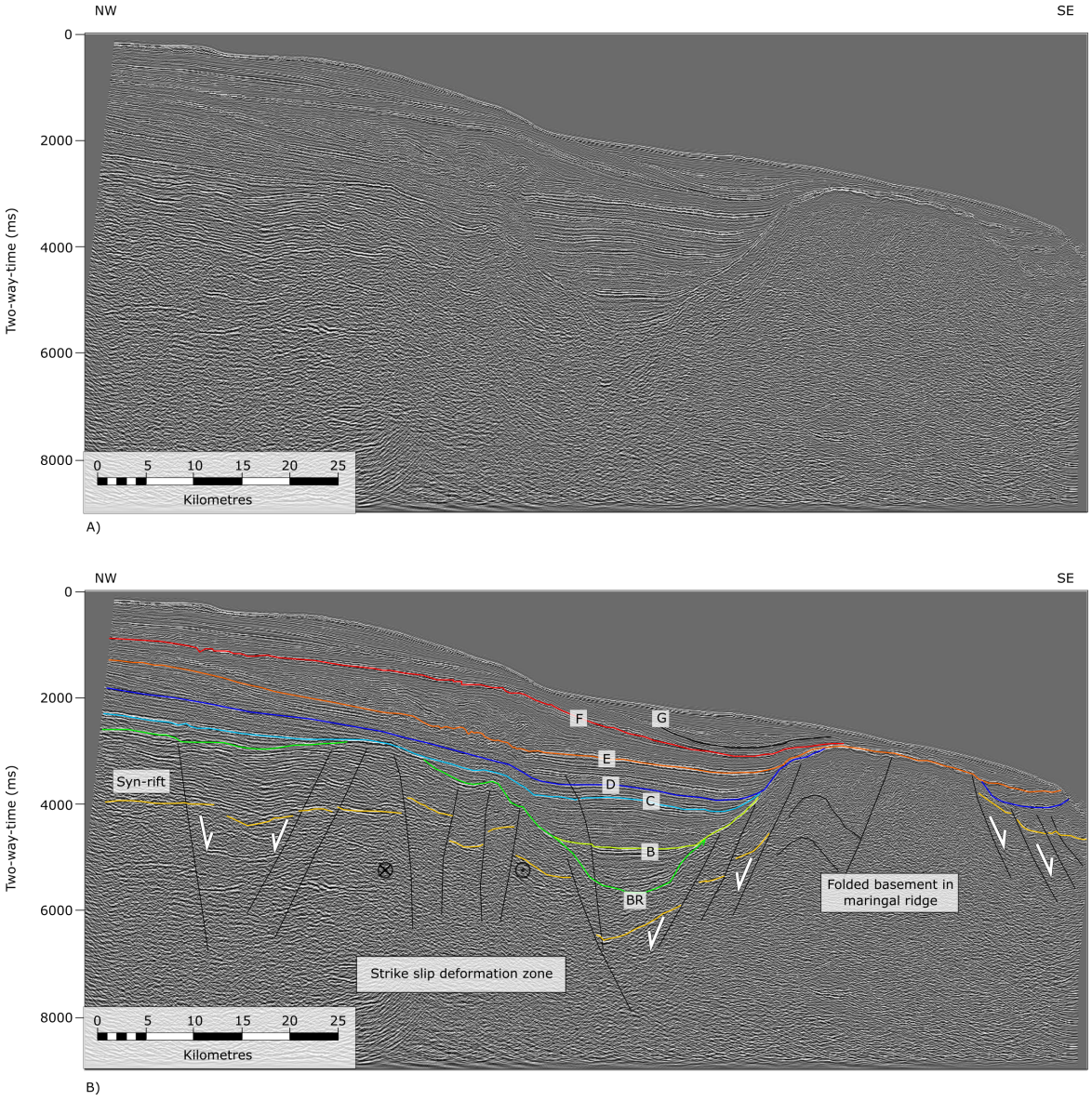


Fig. 4.4 Seismic line 2001-63, in the central sector, location shown in Fig. 4.1. The interpreted seismic section shows the unconformity surface B on-lapping the basin-bounding faults in this central sector of the basin.

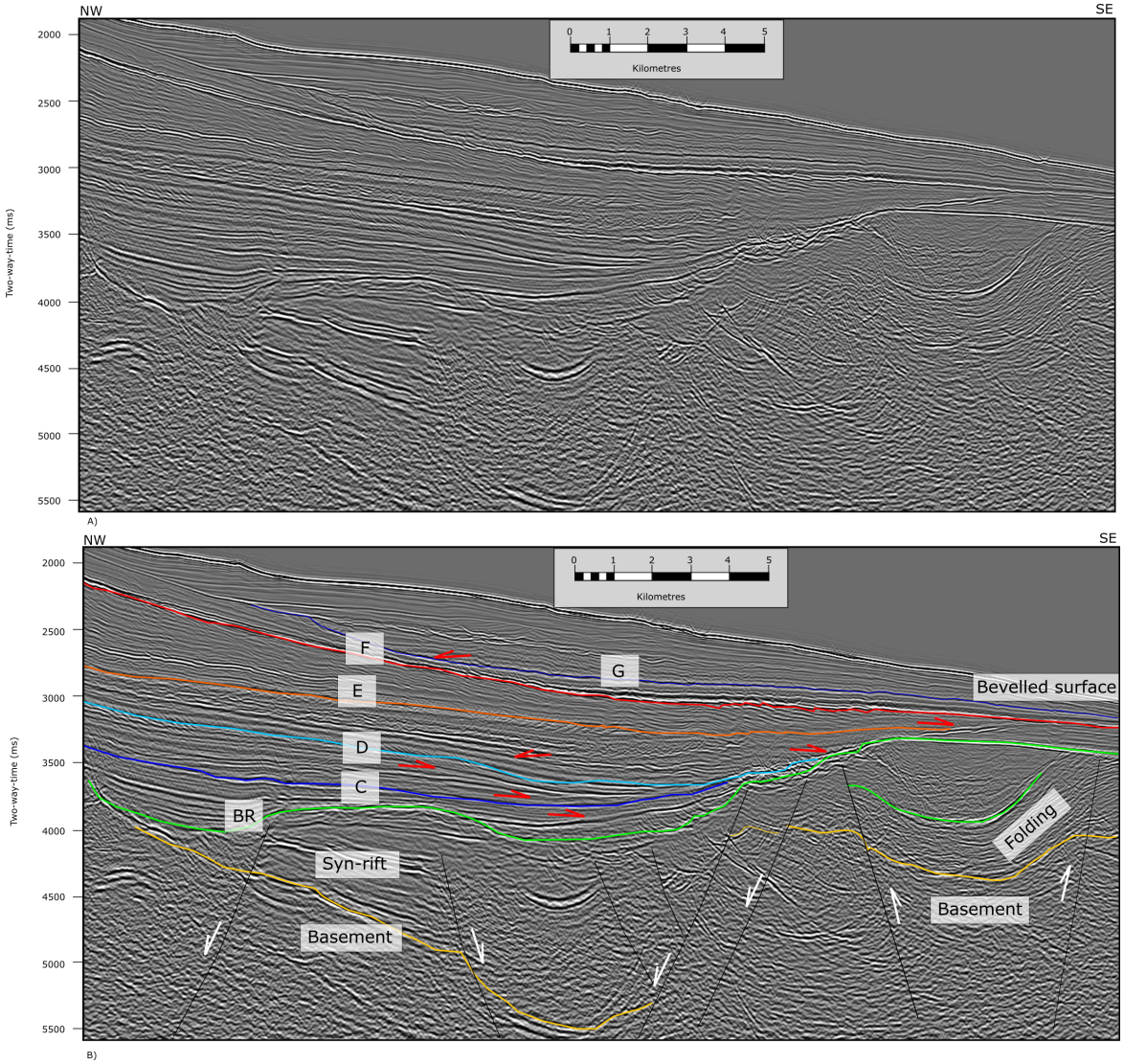


Fig. 4.5 Seismic line 2001-75, in the eastern sector, location shown in Fig. 4.1. The interpreted seismic section shows the unconformity surface C on-lapping the basin-bounding faults of the basement highs to the south of the basin.

4.2.3 Horizon C - Aptian (120Ma)

The reflector corresponding to horizon C is medium-high amplitude peak and continuous across all of the sectors of the basin. In the far-western sector of the basin the unconformity extends across the basin from the south to the north and overlies the Diaz Marginal ridge in the southern part of the sector (Fig. 4.2). In the western sector the unconformity is continuous from the Outeniqua sub-basins into the middle of the Southern Outeniqua Basin but onlaps against the northern shoulder of the DMR in the southern part of the sector (Fig. 4.3). The horizon separates the conformable, concordant reflectors of the underlying package from the down-lapping and on-lapping reflectors above, indicating a significant erosional event which was followed by the deposition of basin floor fans, as is seen in the western sector of the basin (Fig. 4.6). In the central sector, the unconformity is a strong amplitude peak that truncates a basement high on the northern part of the basin before onlapping against the basement promontory of the DMR in the south (Fig. 4.4).The time structure map ranges in elevation between 1100ms and 3900ms TWT (Fig. 4.7C) with topographic highs in the central, eastern and southern part of the far-western sectors of the basin. The unconformity is present within the middle of the basin but is interpreted to onlap against the St.Francis Arch and DMR to the north and south, respectively (Fig. 4.5). The time structure map of this surface indicates an embayment in the far-western sector and a main depression in the western sector of the basin (Figs. 4.6 & 4.7c). Topographic highs to the northern and southern parts of the far-western sector likely acted as sediment sources for the subsequent fans downlapping onto the sediments above this surface. An anomalous intra-basinal high in the western sector could be evidence for early Aptian inversion of the surface (Fig. 4.7C). An elevated topography in the eastern sector of the time structure map indicates that the unconformity surface likely eroded sediments from this part of the basin into the deeper central and western sectors.

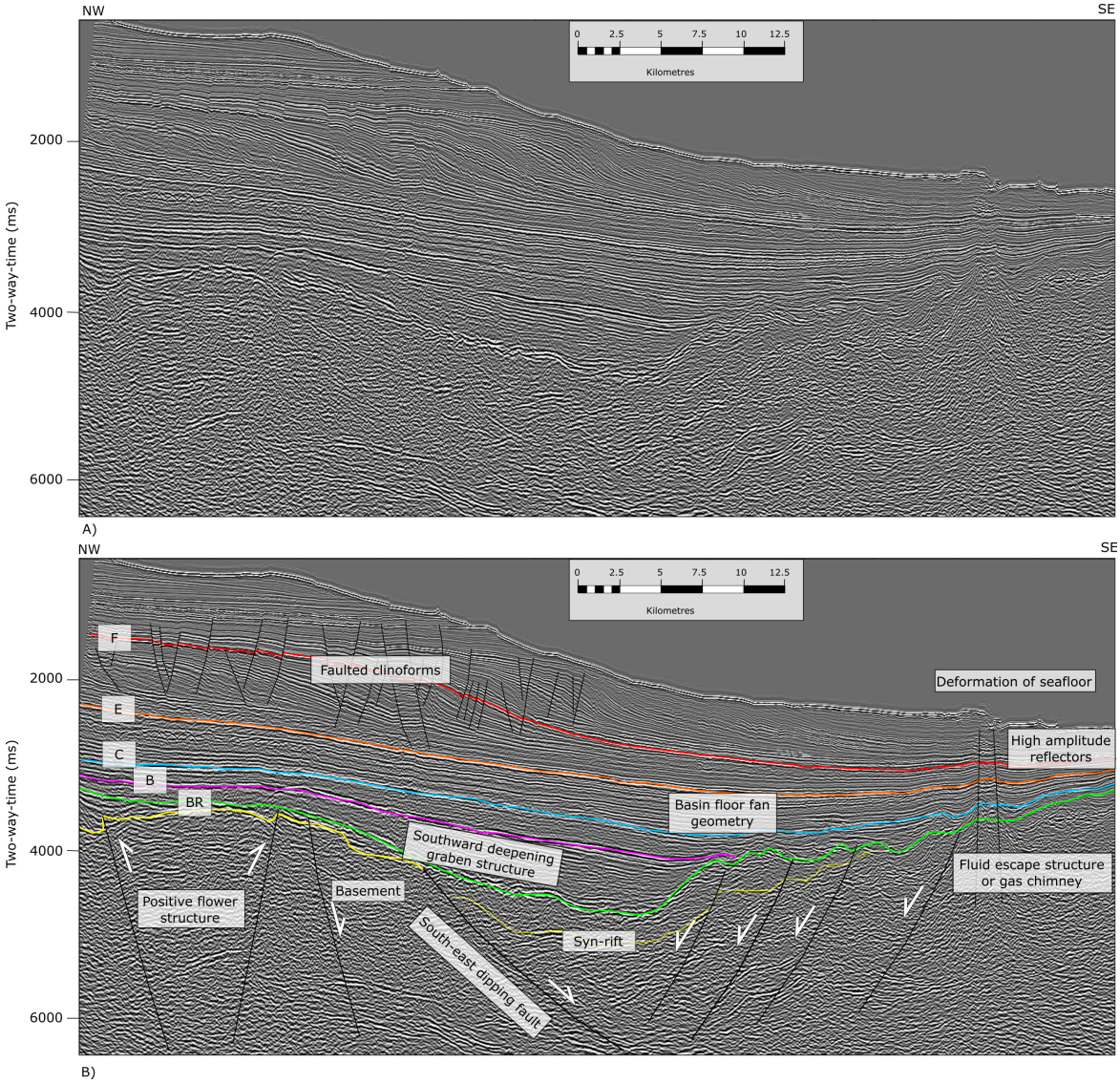


Fig. 4.6 Seismic line 2001-19, in the western sector, location shown in Fig. 4.1. The interpreted seismic section shows the unconformity surface C mapped across the basin, with overlying sediments displaying down-lapping reflector geometries onto the surface. These down-lapping geometries are characteristic of basin-floor fan deposits onto underlying sequence boundaries (Vail et al., 1977)

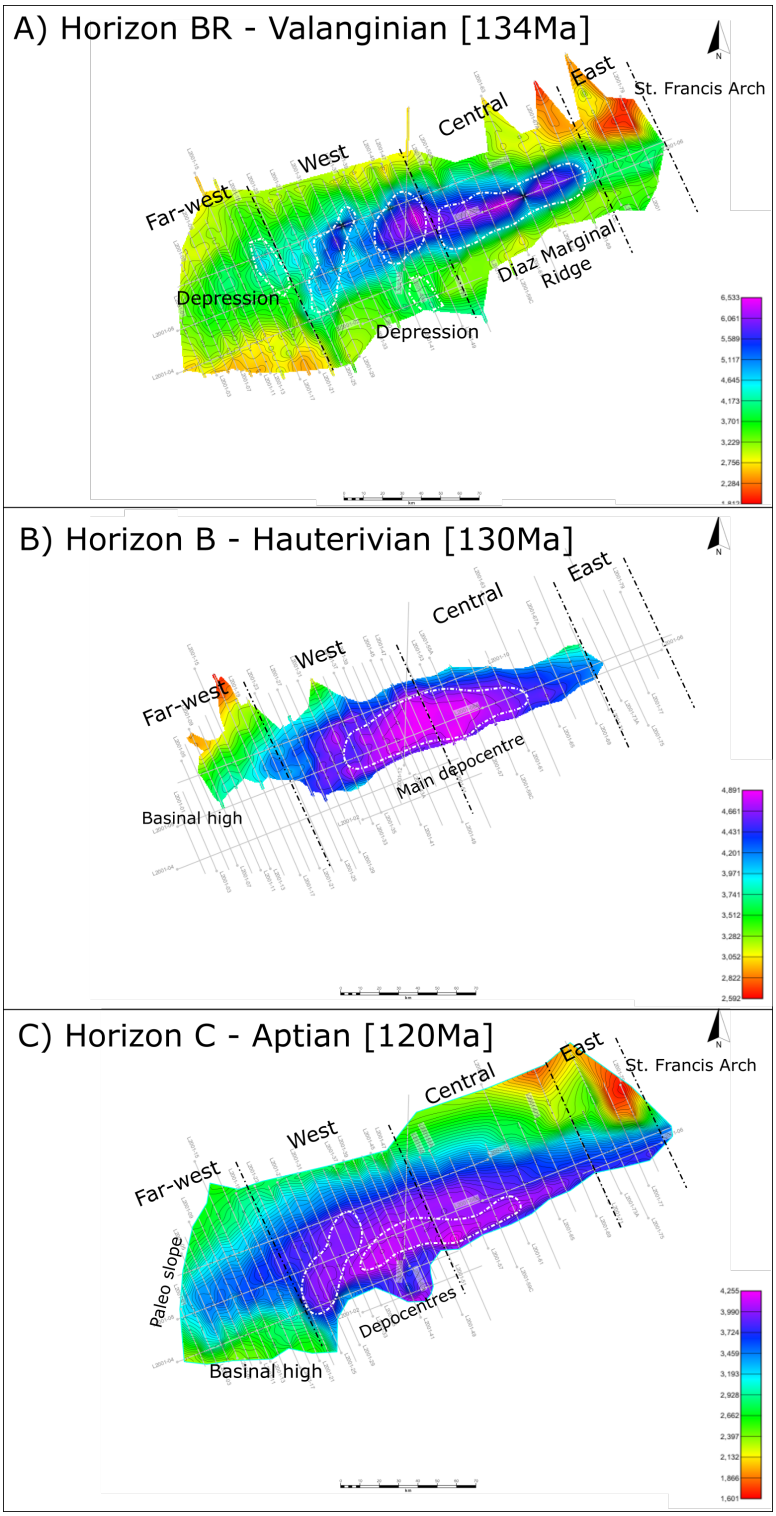


Fig. 4.7 a) Time structure maps within the context of the four sectors of the basin. A) Horizon BR - Valanginian (134Ma). The white ellipses on the structure map show three main depocentre geometries (NNE-SSW, NE-SW and NW-SE) at the beginning of transform motion along the AFFZ. B) Horizon B - Hauterivian (130Ma). The white ellipses show the change in depocentres relative to horizon BR; the horizon B surface is limited in areal extent when compared to the BR surface. C) Horizon C - Aptian (120Ma). The time structure map demonstrates a NE-SW trending depocentre in the western and central sectors and the development of an embayment in the far-western sector. The southern part of the far-western sector is elevated in the time structure map indicating a basinal high during the development of the unconformity.

4.2.4 Horizon D - Cenomanian (93Ma)

The horizon D reflector is a medium-amplitude peak that is continuous across all sectors of the basin. In the far-western sector of the basin, the reflector onlaps against sediments deposited above the DMR indicating that the structure had been uplifted before the development of this surface during the Cenomanian (Fig. 4.2). In the western sector of the basin, the unconformity onlaps the northern shoulder of the DMR and has a medium-high amplitude seismic response as a result of the large impedance contrast between the underlying and overlying layers (Fig. 4.4). In the central part of the basin the reflector is affected by small-scale polygonal faults and may be interpreted as being caused by the dewatering of the underlying shales (Fig. 4.8) . Horizon D shows a much more pronounced erosional character in the eastern sector of the basin where it truncates the sediments above horizon C and also the top of the DMR (Fig. 4.5). The time structure map of horizon D has an elevation range of 1000ms to 4400ms TWT with the darker blue to purple colours indicating the deepest parts of the horizon. A noticeable change in slope seems to have occurred between horizons C and D with the gradient of the slope in horizon D visibly shallower in the far-western sector of the basin (Figs. 4.7c and 4.13a) . The concave shape to the contour lines in this sector may hint at a paleo shelf-break with a deep depocentres within the southern part of the western sector. An elongated NE-SW depression continuous from the western to central sectors is aligns with the trend of the Diaz Marginal Ridge, which has an acoustically transparent seismic facies in these sectors (Fig. 4.10).

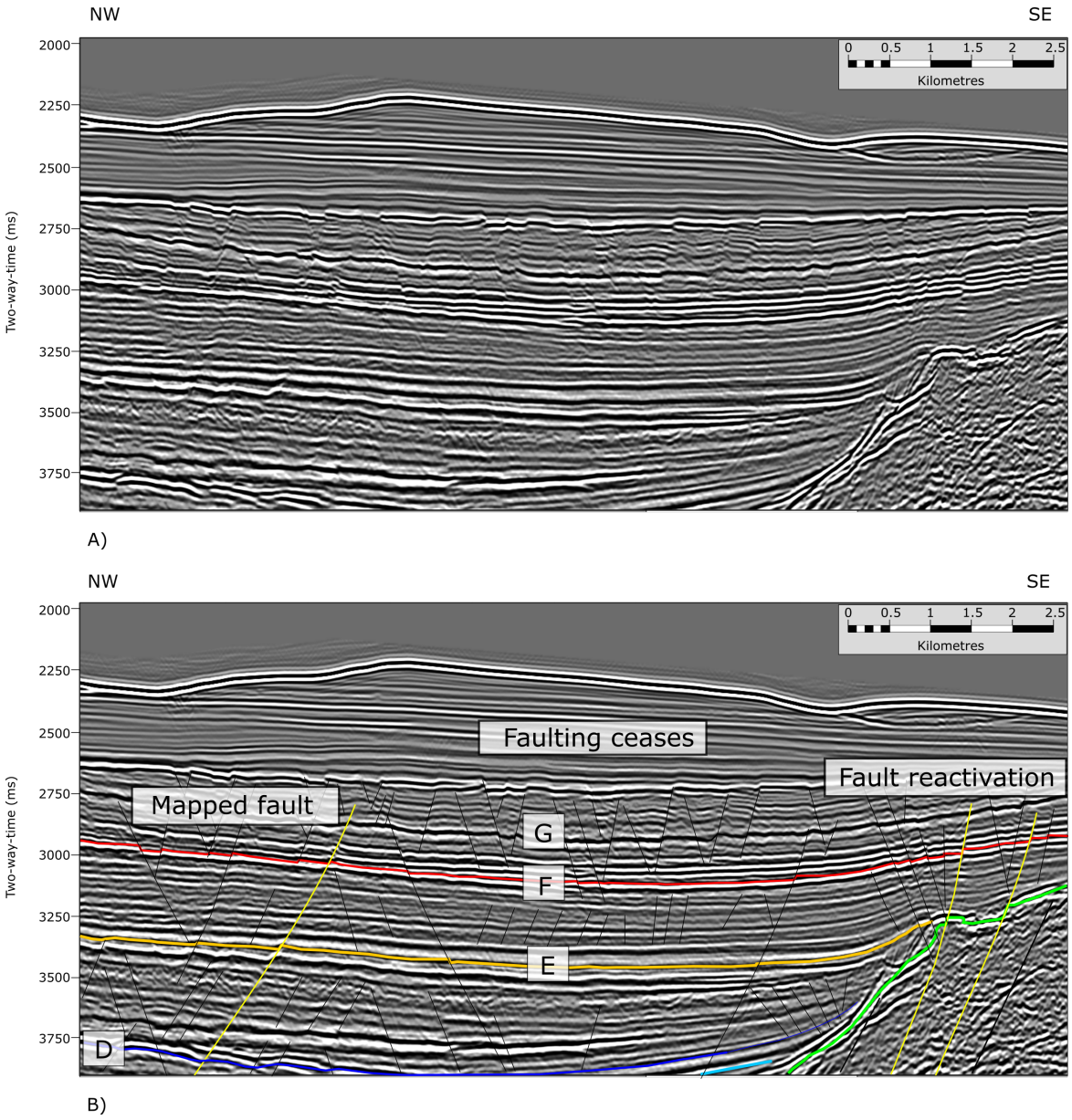


Fig. 4.8 Seismic line 2001-61, in the central sector, location shown in Fig.4.1. The seismic section shows polygonal faulting, due to the de-watering of shale sediments, between reflectors D-G within the middle of the basin.

4.2.5 Horizon E - Campanian (80Ma)

Seismic horizon E is characterised by a high-amplitude peak that is continuous through all sectors of the basin. In the far-western sector of the basin, this unconformity surface separates underlying concordant reflectors, from overlying sigmoidal and oblique clinoforms geometries (Fig. 4.9). In the western sector of the basin, the unconformity progressively decreases in amplitude towards the southern part of the sector. Significant deformation by underlying faults across the northern shoulder of the DMR break the continuity of the reflector as it onlaps the marginal ridge (Fig. 4.12). In the central sector of the basin, the horizon loses the high-amplitude peak response as the reflectors tracks from north to south, where it reaches the shoulder of the DMR (Fig. 4.10). In the northern part of the eastern sector the horizon is a high-amplitude seismic peak but loses its character southward where it onlaps sediments overlying the top of the DMR (Fig. 4.11). The 1200ms to 3800ms TWT time structure map indicates that an embayment is more developed in the far-western sector during the Campanian when compared to the Cenomanian time structure map of (Figs. 4.13a & 4.13b). The contours in the southern part of the far-western sector extend further to the north-east than during the Cenomanian (93Ma) and suggest a deepening of the basin in the western sector of the basin. The contours of the paleo-slope in the western and far-western sectors are wider relative to those of the central and eastern sectors of the basin suggesting that the eastern and central sectors remained elevated until the Santonian (Figs. 4.13b). An intra-basinal high is evident in the time structure contours at the transition form the central to eastern sectors of the basin.

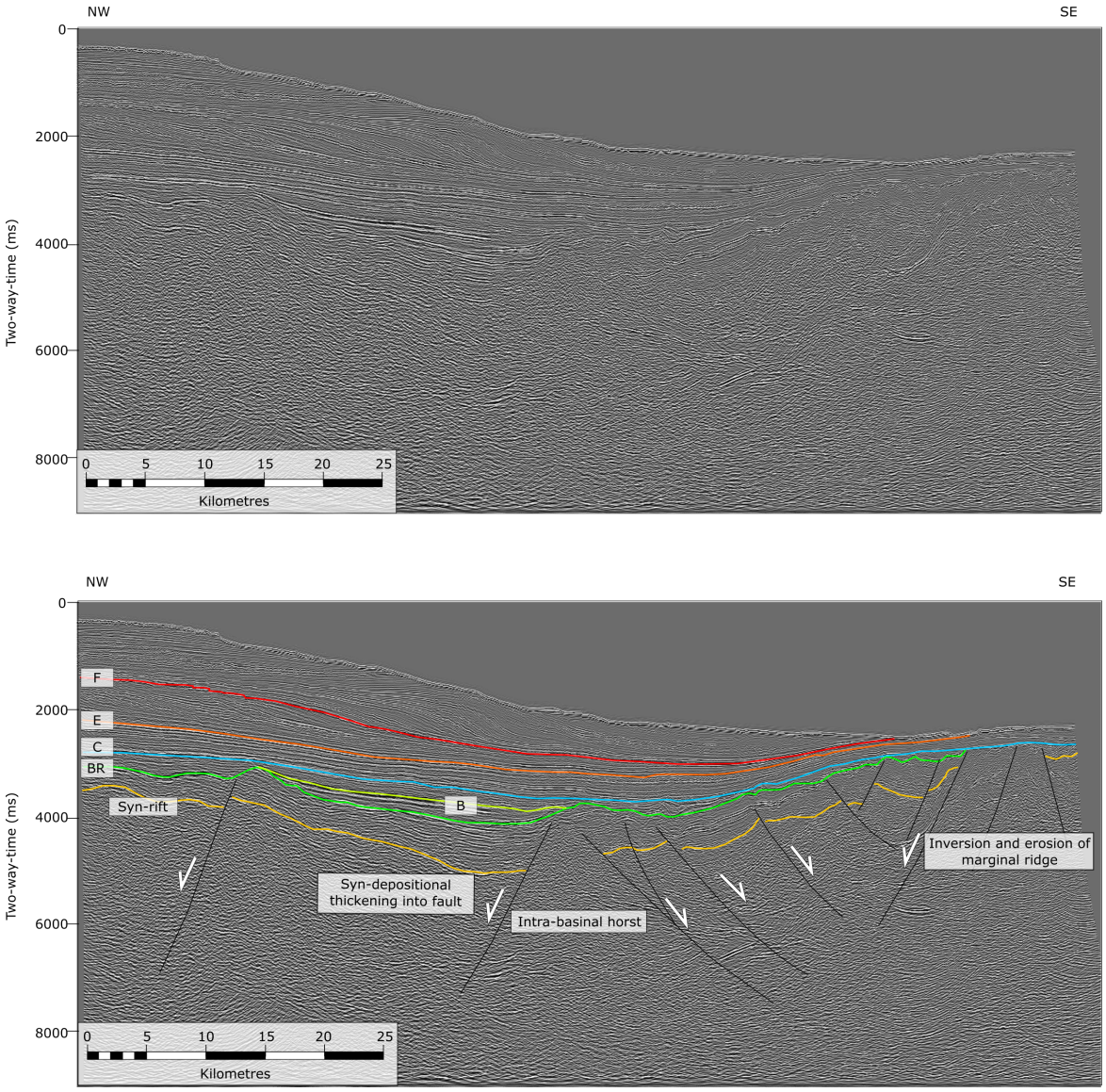


Fig. 4.9 Seismic line 2001-13, in the far-western sector, location shown in Fig. 4.1. The seismic section shows unconformity horizon E gaining elevation from north to south as the reflector passes over the Diaz Marginal Ridge and is eventually truncated by the seafloor.

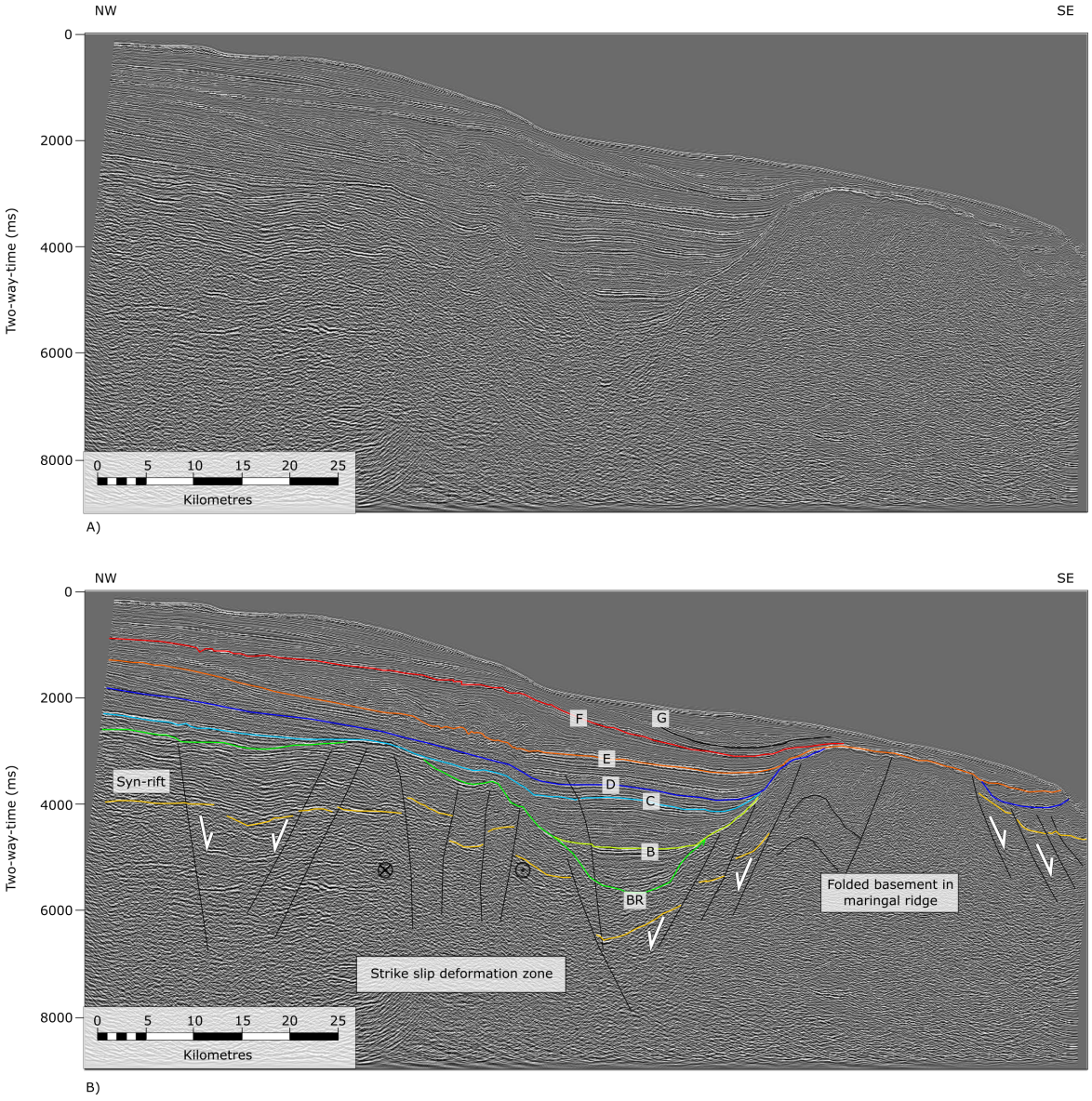


Fig. 4.10 Seismic line 2001-63, in the central sector, location shown in Fig. 4.1. The interpreted seismic section shows the unconformity surface B on-lapping the basin-bounding faults in this central sector of the basin.

4.2.6 Horizon F - late Campanian (76Ma)

The horizon F reflector is a high-amplitude seismic peak that is continuous throughout all of the sectors in the basin. In the far-western sector the unconformity is deformed by growth faults within a prograding clinoform package and is challenging to track across the slope (Fig. 4.6). Towards the southern end of the far-western sector, the horizon becomes eroded by mass transport complexes and temporarily loses continuity before regaining its character over the northern part of the DMR where it is truncated by the seafloor (Fig. 4.9). In the western sector of the basin, the horizon is easily mapped and maintains a high amplitude seismic peak across the shelf-break into the middle of the basin. In the southern part of the sector the horizon onlaps the top of the DMR, which is tilted basin-ward in this sector (Fig. 4.12). The time structure map has an elevation range of 850ms to 3800ms TWT with the highest elevation present along the northern part of all of the basin sectors (Fig. 4.13c). A steeper gradient in the far-western and western sectors compared to the time structure map of horizon E, indicate that the shelf-break has prograded southwards from the Campanian (80Ma) to the late Campanian (76Ma). The surface shows that the depocentre has centred in the western sector of the basin with concave contours in the far-western sector indicating a gentle paleo-slope developing in the south-western part of the basin. The time structure map shows a higher elevation in the central sector, corresponding to the northern shoulder of the DMR and suggests that the underlying structure has had an effect on the horizon after it had been deposited, e.g. as a shallow drape anticline (Fig. 4.10).

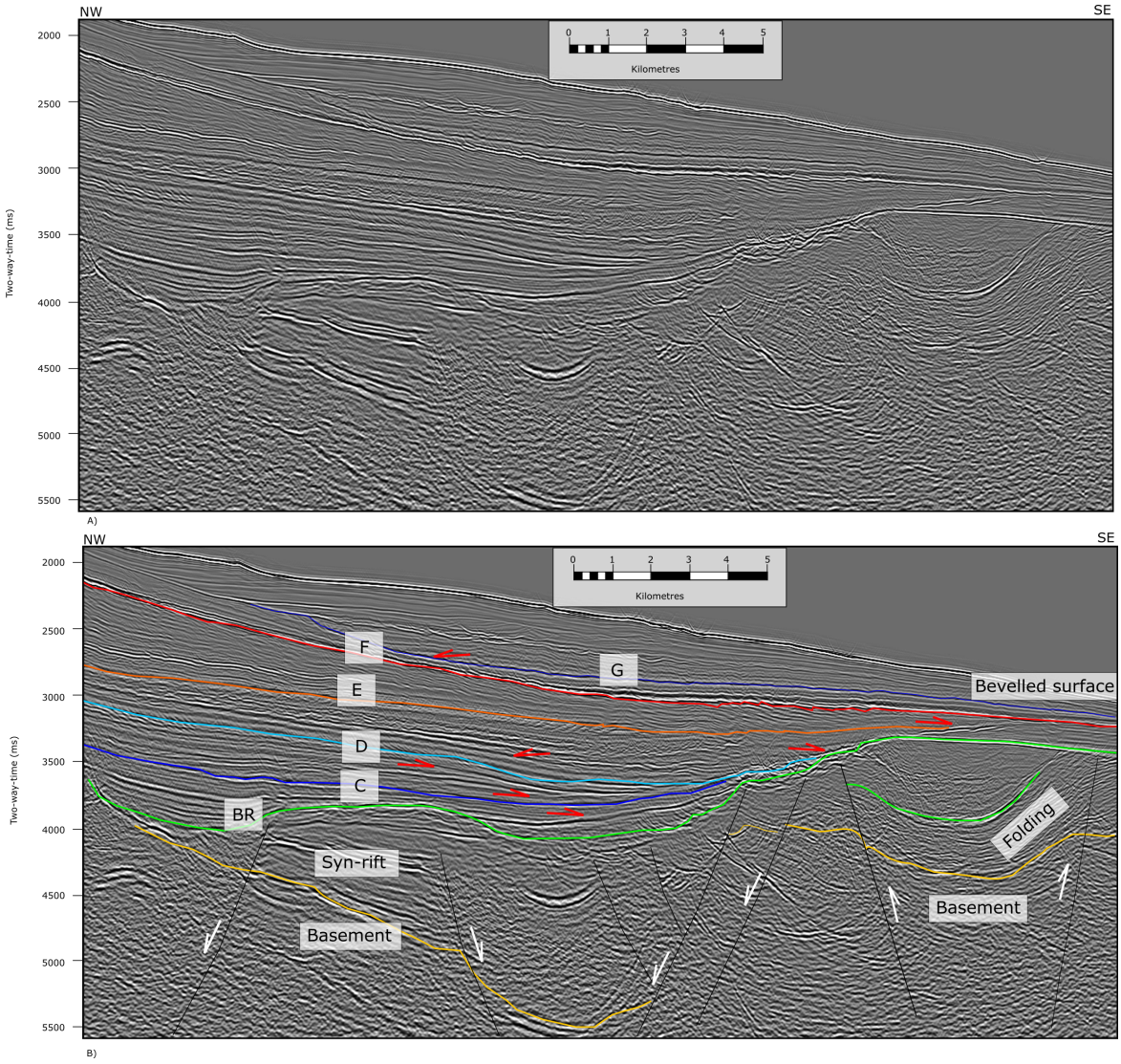


Fig. 4.11 Seismic line 2001-75, in the eastern sector, location shown in Fig. 4.1. The interpreted seismic section shows the key first order unconformity surfaces, BR truncating the syn-rift strata within the rotated fault blocks in the centre of the basin. The BR surface in this part of the basin is also observed to be a part of and folded along the shoulder of the Diaz Marginal Ridge.

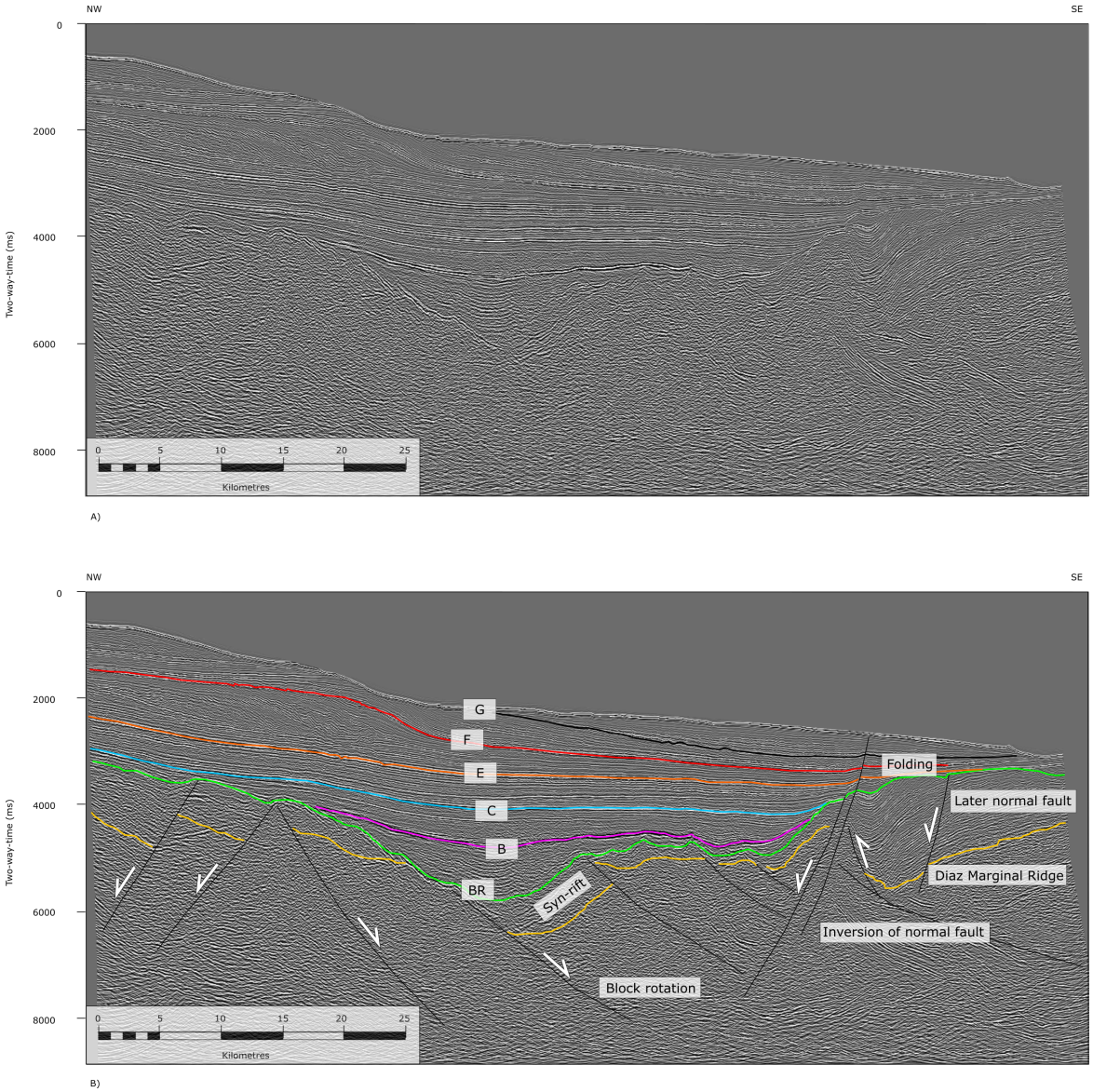


Fig. 4.12 A) Seismic line 2001-33, in the western sector, location shown in Fig. 4.1. Interpreted sections shows Horizon F on-lapping older reflectors over the northern shoulder of the Diaz Marginal Ridge.

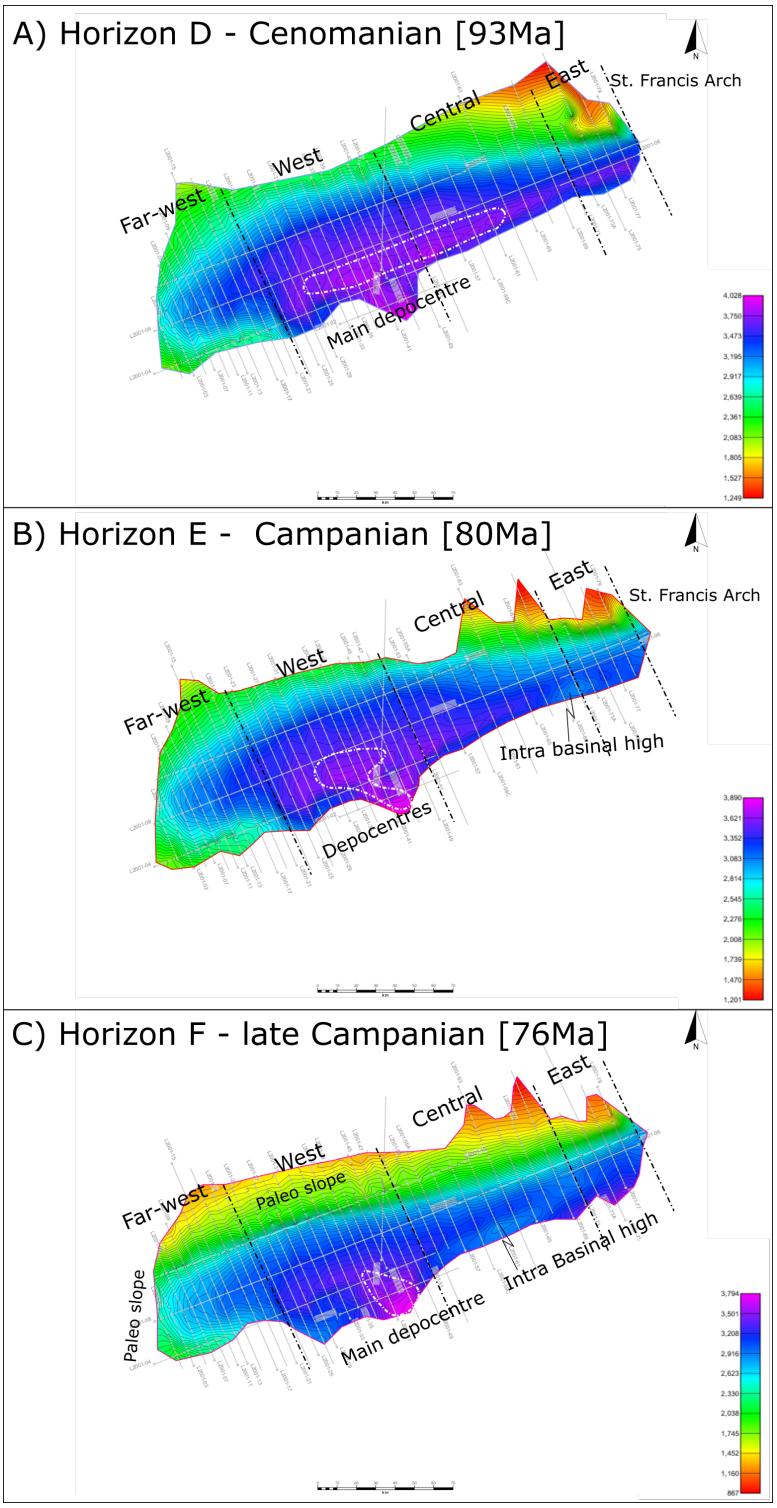


Fig. 4.13 Time structure maps within the context of the four sectors of the basin. a) Horizon D - Cenomanian (93Ma). The white ellipse on the structure map shows the main depocentre straddling the central and western sectors of the basin. The wide contour space between contours suggests that the northern and south-western parts of the basin were characterised by a slope environment during the Cenomanian. b) Horizon E - Campanian (80Ma). The white ellipses shows a south-westward change the position of the depocentre relative to horizon D. The time structure map demonstrates a more defined embayment developing in the south-western part of the far-western sector. c) Horizon F - late Campanian (76Ma) showing the progradation of the shelf.

4.2.7 Horizon G - Maastrichtian (66Ma)

The seismic response of horizon G is characterised by a continuous, medium amplitude peak that is mappable across all of the sectors of the basin (Fig. 4.11). In the eastern sector of the basin, the reflector is elevated on the northern part of the basin where it is eroded over the paleo shelf-break and has a gentle concave geometry to the south where it overlies the DMR (Fig. 4.12). In the central sector of the basin the concave geometry becomes more pronounced and seems to be controlled by the adjacent basinal high of the DMR where it does not extend over the structure (Fig. 4.14) This is in contrast to the western sectors of the basin where the reflector deepens to ≈3600ms TWT and is more planar in geometry, becoming part of the sediment package which overlies the deeper basin (Fig. 4.12). The time structure map of the horizon within the basin ranges in elevation from 760ms to 3688ms TWT and contours demonstrate the gentle concave geometry of the reflector in the eastern sectors, the deeply concave geometry in the central and far-western sectors of the basin and the wide planar geometry of the surface in the western sectors of the basin (Fig. 4.15).

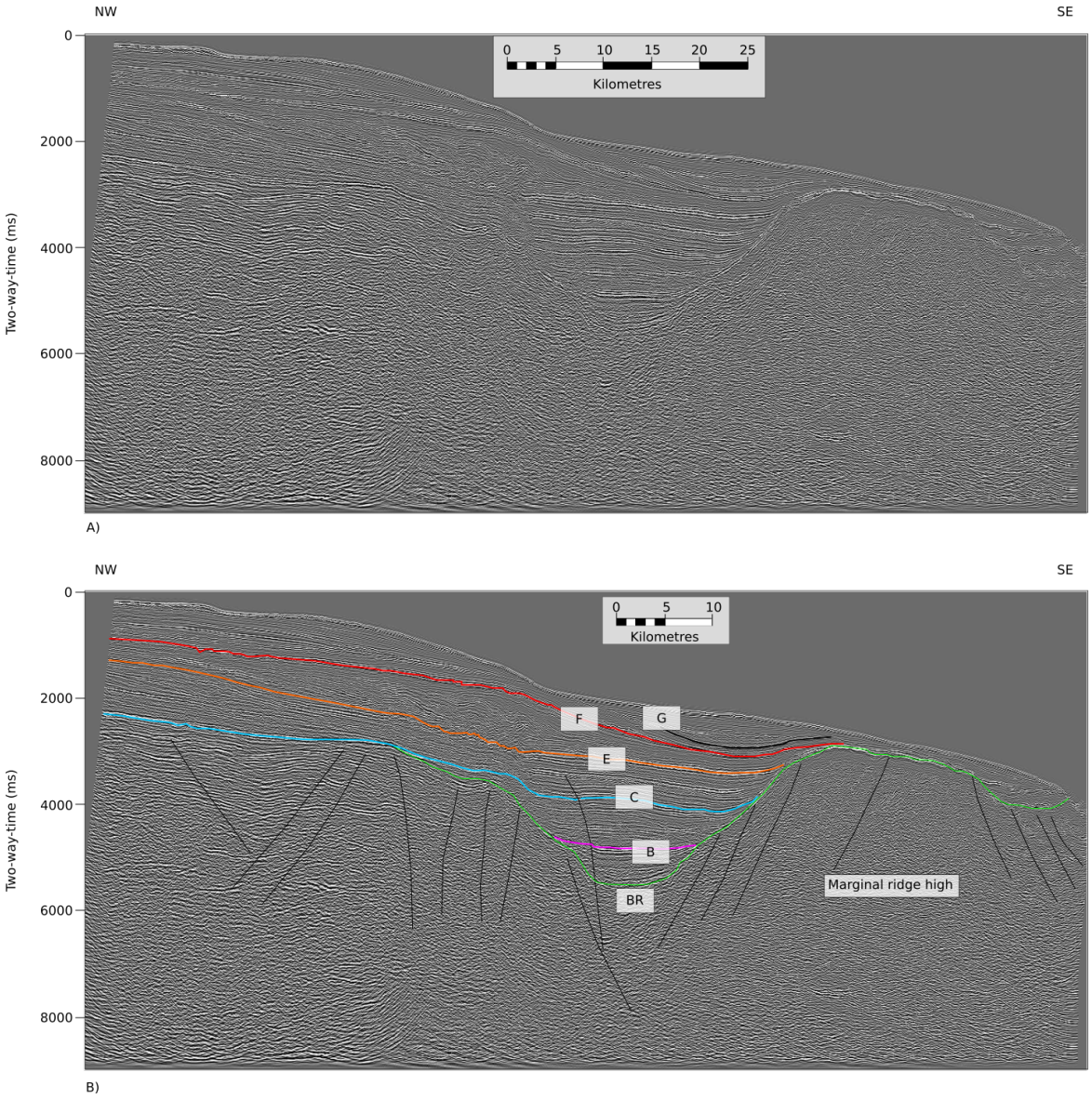


Fig. 4.14 Seismic line 2001-63, in the central sector, location shown in Fig. 4.1. Interpreted seismic section shows the tight concave geometry of reflector G as it approaches the DMR high.

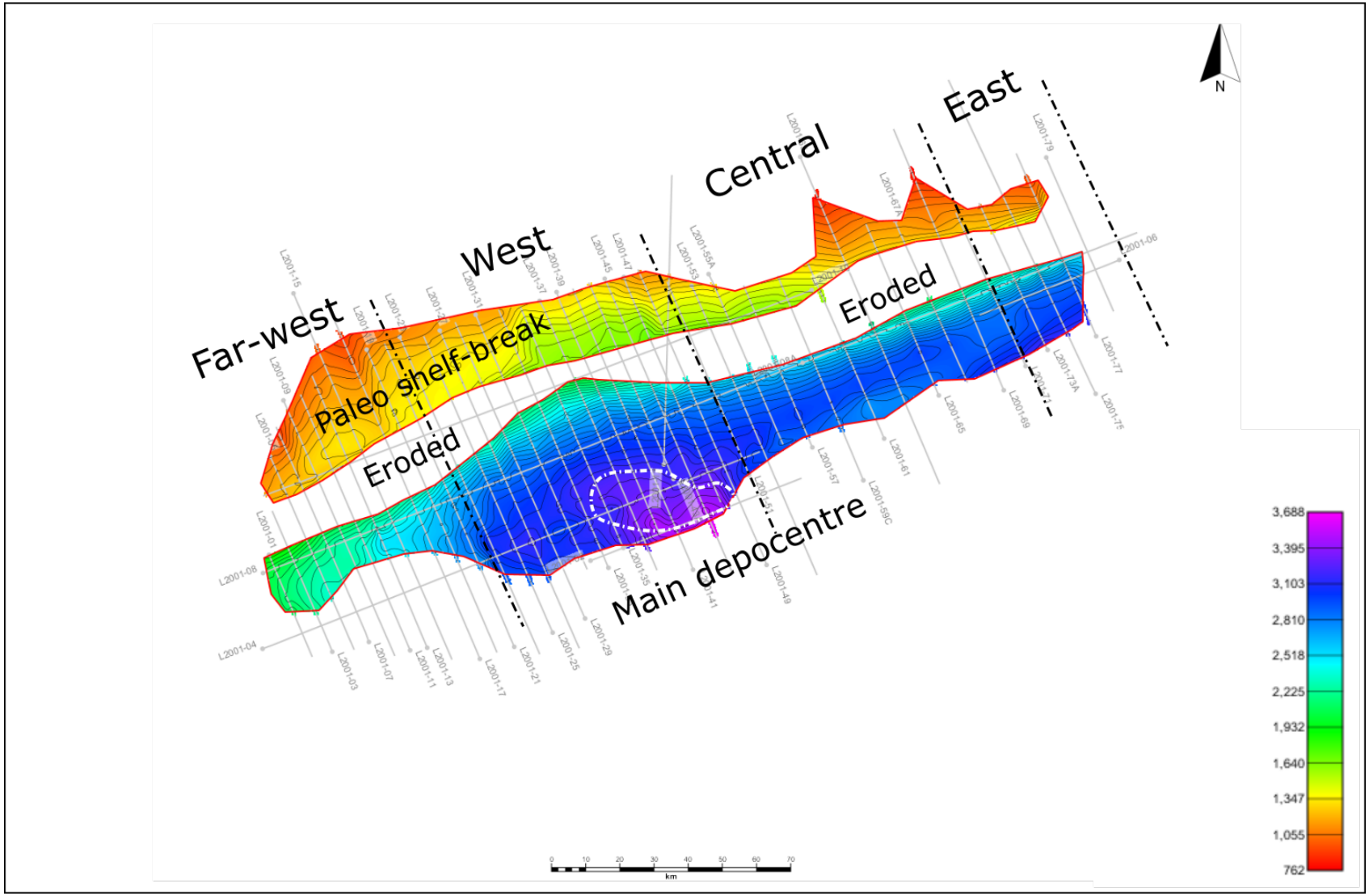


Fig. 4.15 Time structure map of horizon G over the study area of the Southern Outeniqua Basin. The reflector is eroded along the northern part of all sectors in the basin and shows a concave geometry in the eastern sector, becoming more concave in the central and far-western sectors where it seems to be defined by the Diaz Marginal Ridge. The surface in the western sector deepens to the south and is more planar in geometry where it overlies the marginal ridge structure.

4.2.8 Seabed

In Chapter 3, I explained that the polarity of the data initially resulted in the seismic response of the seafloor being a trough, but that after a 110 degree phase rotation it has been adjusted to display a peak. The reflector was picked across the survey area in an attempt to detect the tectonic signature, both early and late stage, within the basin. The mapped horizon (Fig. 4.16) shows an embayment of the continental slope which hints at the existence of the underlying basin. The surface elevation ranges from 600ms to 4400ms which corresponds to a water-depth of ≈450 - 3300m. The observation of several faults, especially present over the DMR, offsetting the seabed reflector is evidence of neo-tectonic activity along the margin, which is corroborated by Ben-Avraham et al. (1995)(Fig. 4.17). Ambiguous vertical faults that terminate at the sea floor and generate near-surface sediment slumping, could be interpreted as gas chimneys although the present 2D survey is unable to definitively map these anomalies (Fig. 4.17).

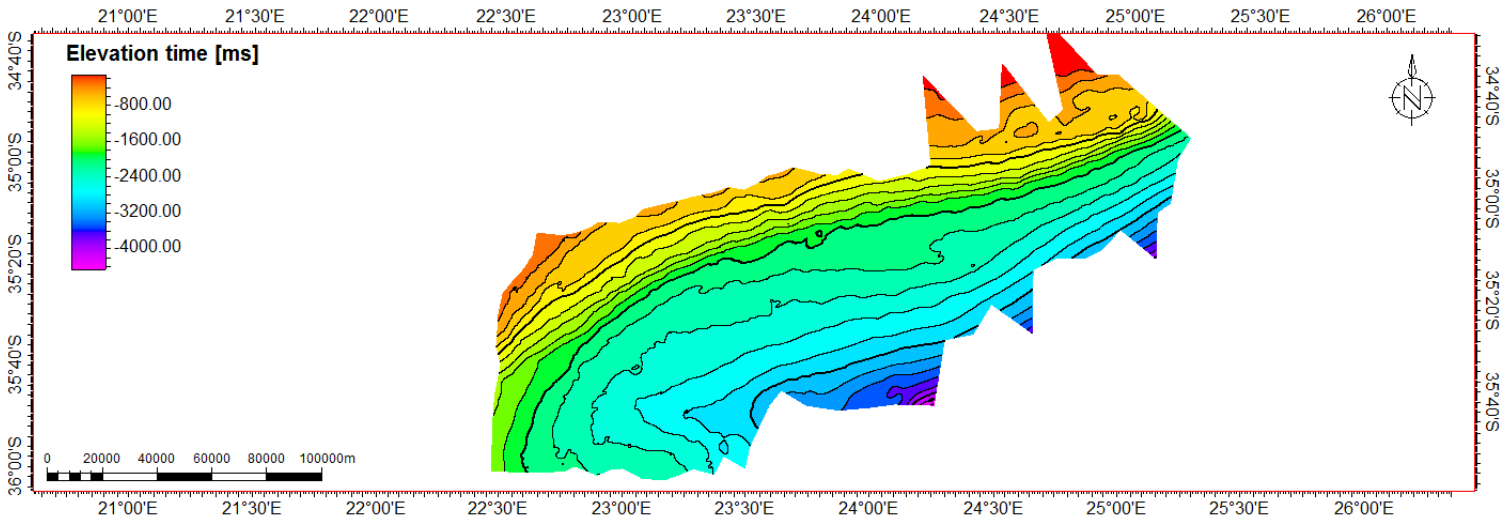


Fig. 4.16 Time structure map of the seabed in the study area of the Southern Outeniqua Basin.

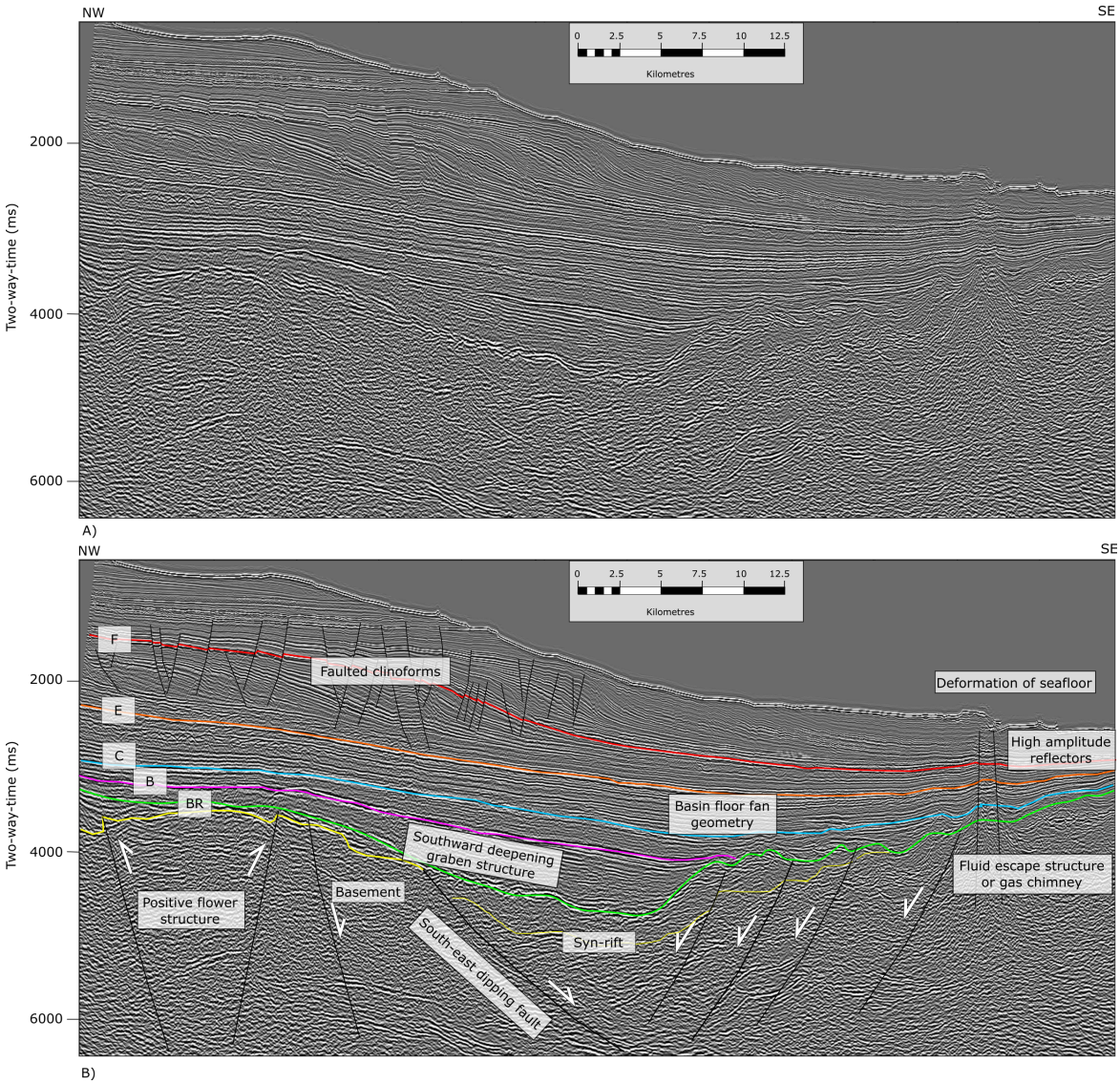


Fig. 4.17 Seismic line 2001-19, in the western sector, location shown in Fig. 4.1. Interpreted seismic section shows faults originating over the Diaz Marginal Ridge displacing the seabed.

4.3 Seismic packages

The sedimentary packages bound by the second-order unconformity surfaces BR-G have been sub-divided into five main packages based on similar reflector geometries and seismic signature. The grouping of these packages allows for specific intervals of sedimentation to be analysed within a broader structural context which can then be related to the overall plate tectonic evolution of the margin. Ages of unconformity surfaces are discussed in section 3.2.2. and shown in Table 3.1.

4.3.1 Pre-rift package

Although not penetrated by wells in this area the reflection character of the pre-rift basement, proposed to be meta-sedimentary units belonging to the Cape Supergroup, is recognisable (Broad et al 2006). The reflections are clearer in the south-western and north-eastern portions of the basin with semi-continuous, concordant, high amplitude reflections visible beneath both the shelf and slope parts of the basin (Fig. 4.17). These strata can be distinguished from the overlying divergent reflections that are indicative of syn-rift deposits (Fig. 4.19). The well imaged reflections beneath the shelf and slope parts of the basin are contrasted with a transparent acoustic basement which shows almost no internal reflectivity or character beneath the outer part of the basin (Fig. 4.19). This transparent acoustic basement forms an approximately 30km wide feature that trends sub-parallel to the AFFZ in a NE-SW orientation, known as the Diaz Marginal Ridge (DMR) (Ben-Avraham et al., 1993). Anomalous mid-sequence, high-amplitude, cross-cutting reflections, observed in the central and northern parts of the basin, seem to generate a distinctive seismic shadow beneath the reflectors and are thought to be igneous intrusions. Similar observations of igneous-like features beneath the marginal ridge in the Falklands Plateau Basin have been reported by Lorenzo and Mutter (1988).

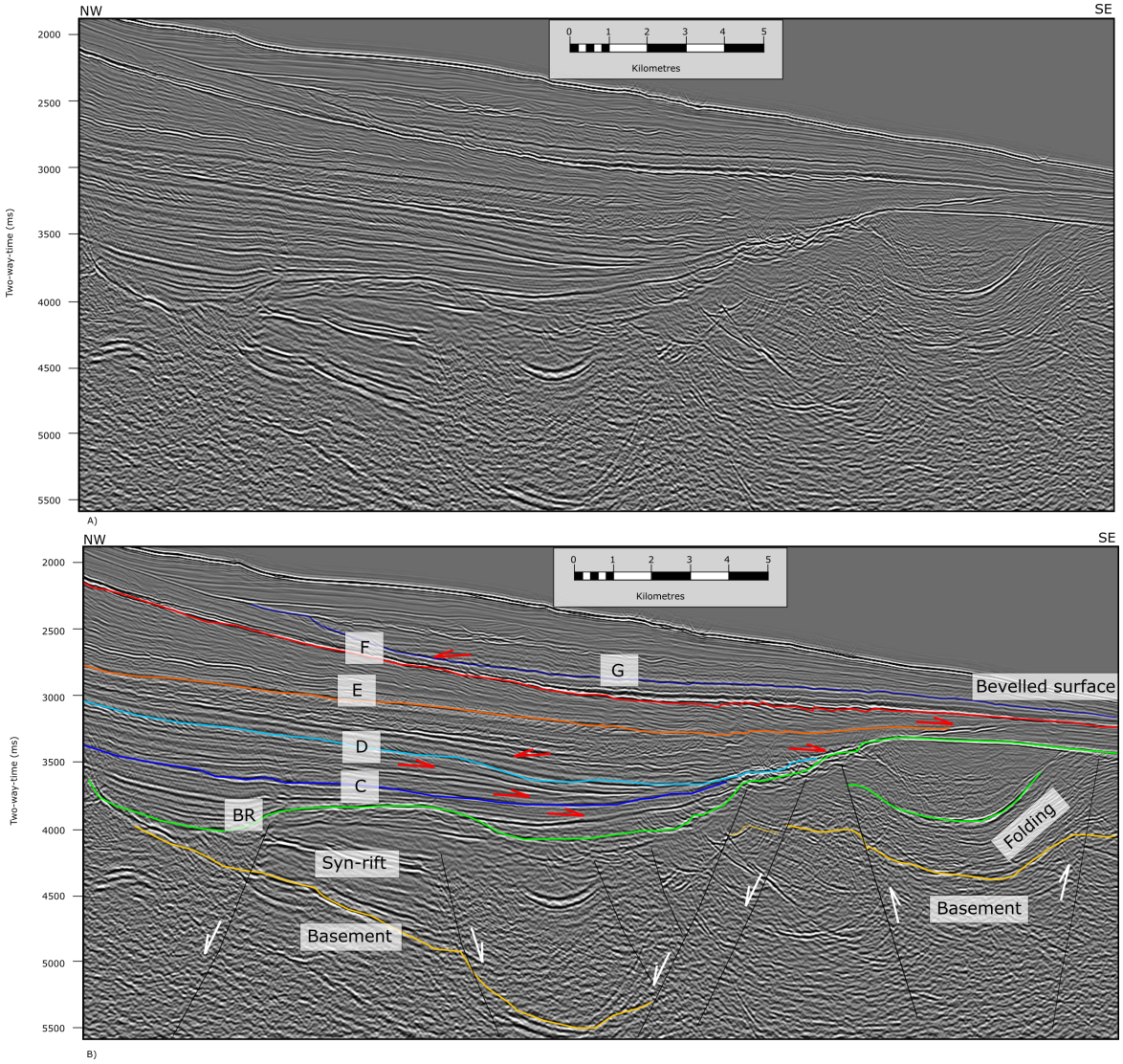


Fig. 4.18 A) Seismic line 2001-75, in the eastern sector, location shown in Fig. 4.1. Interpreted seismic section shows the clear syn-rift strata overlying the acoustically chaotic basement.

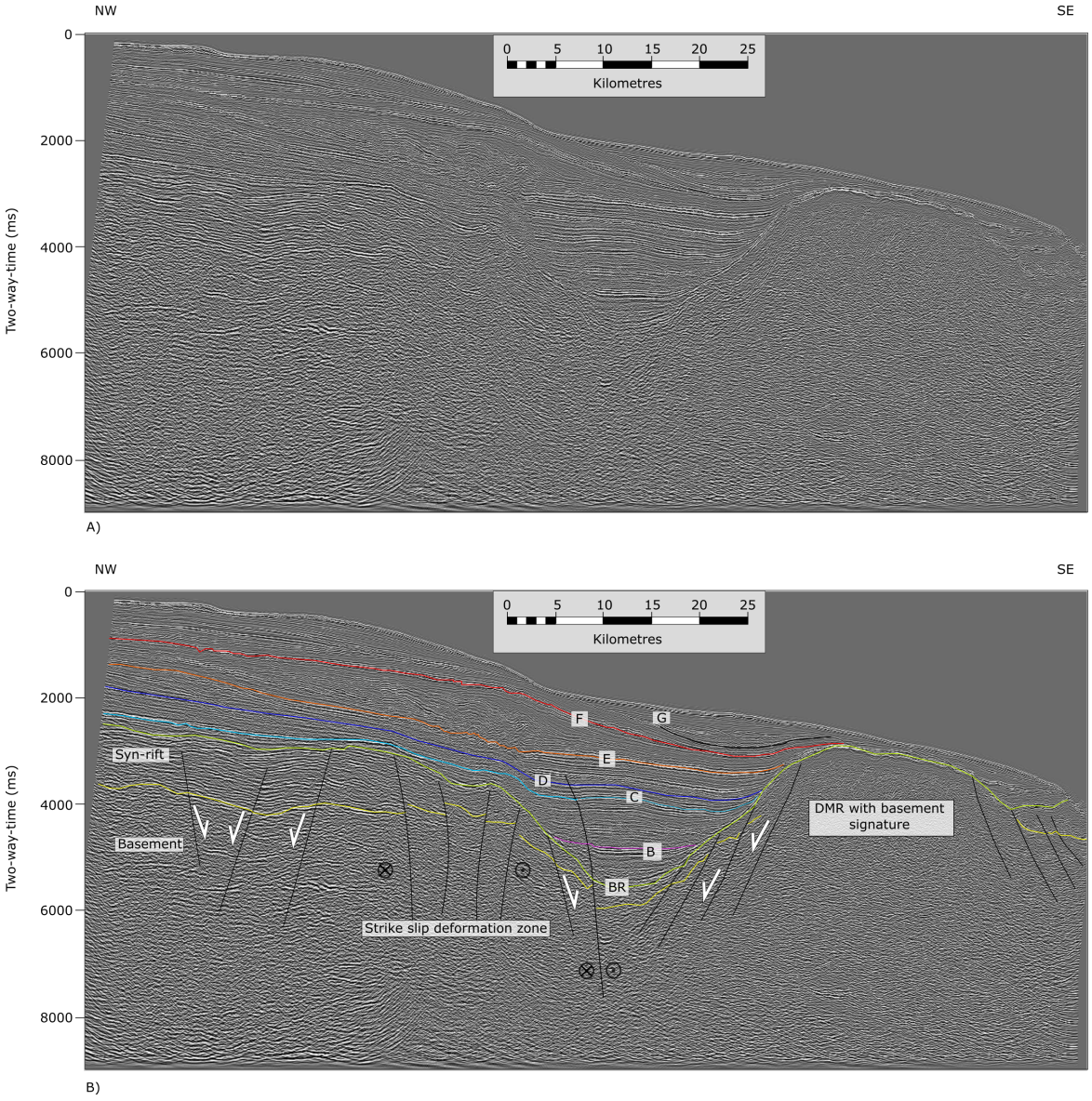


Fig. 4.19 A) Seismic line 2001-63, in the eastern sector, location in Fig. 4.1. Interpreted seismic section shows syn-rift strata in the northern part of the basin but very little on the southern part of the basin.

4.3.2 Syn-rift package

The syn-rift package was not mapped given the ambiguity of identifying syn-rift from basement on this vintage of seismic data, however observations of the syn-rift package were made where the package was clearly distinct from the underlying basement. In the southern part of the eastern sector of the basin, the syn-rift is easily recognised by its high amplitude, high frequency character thickening into the basin bounding faults where the strata is highly faulted both in a normal and reverse sense (Fig.4.18). En-echelon folding of the syn-rift strata within the Diaz Marginal Ridge, is readily identifiably on the seismic and was extensive enough to map the fold axes of the strata (Fig. 4.18). In the northern part of the central sector, the syn-rift strata are not easily distinguished from the stratified basement of Cape Supergroup meta-sediments and thus the actual base of syn-rift is subjective. The syn-rift sediments in northern part of the basin are thicker than the strata in the southern part of the basin, defined by the northern shoulder of the DMR (Fig. 4.19). In the south-western part of the central sector, a marked change in the seismic facies of the marginal ridge occurs from acoustic basement to syn-rift sediments along the strike of the DMR (Fig. 4.20). In the western sector of the basin the package is thickest and is present in both the northern and southern parts of the basin. The strata here thicken into normal faults that verge to the south-east and show pronounced folding and inversion of the reflector geometries (Fig. 4.20.). In the northern part of the far-western sector of the basin, syn-rift strata packages have a more chaotic seismic facies compared to the package in the southern part which forms part of the DMR in this sector (Fig. 4.21)

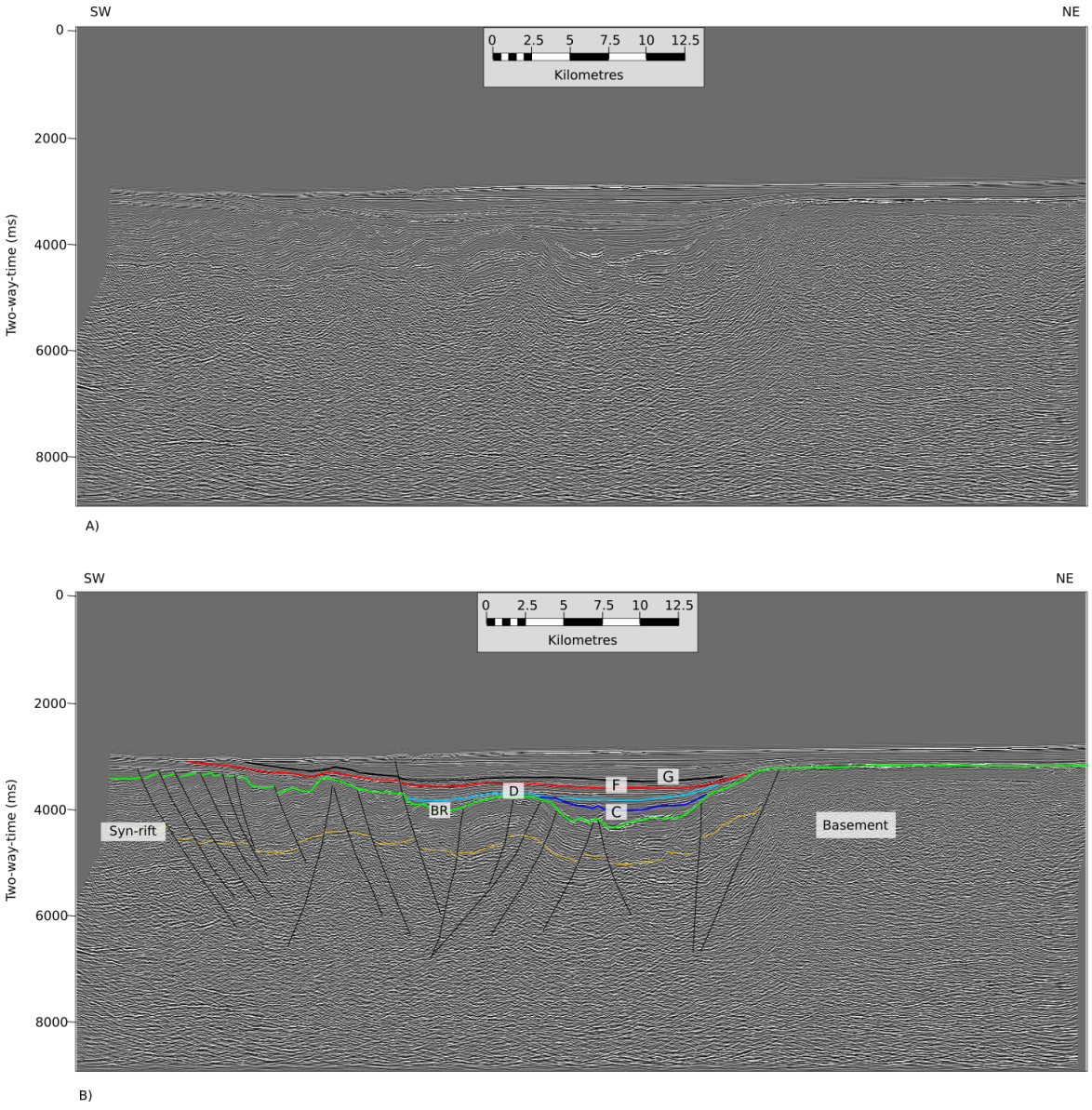


Fig. 4.20 A) Seismic line 2001-2, in the western sector, location in Fig. 4.1. Shows the variation in lithology that makes up the Diaz Marginal Ridge in the western sector of the basin. Syn-rift strata with divergent and parallel reflector geometries are identifiable and contrast with the acoustic chaotic basement that makes up portions of the ridge

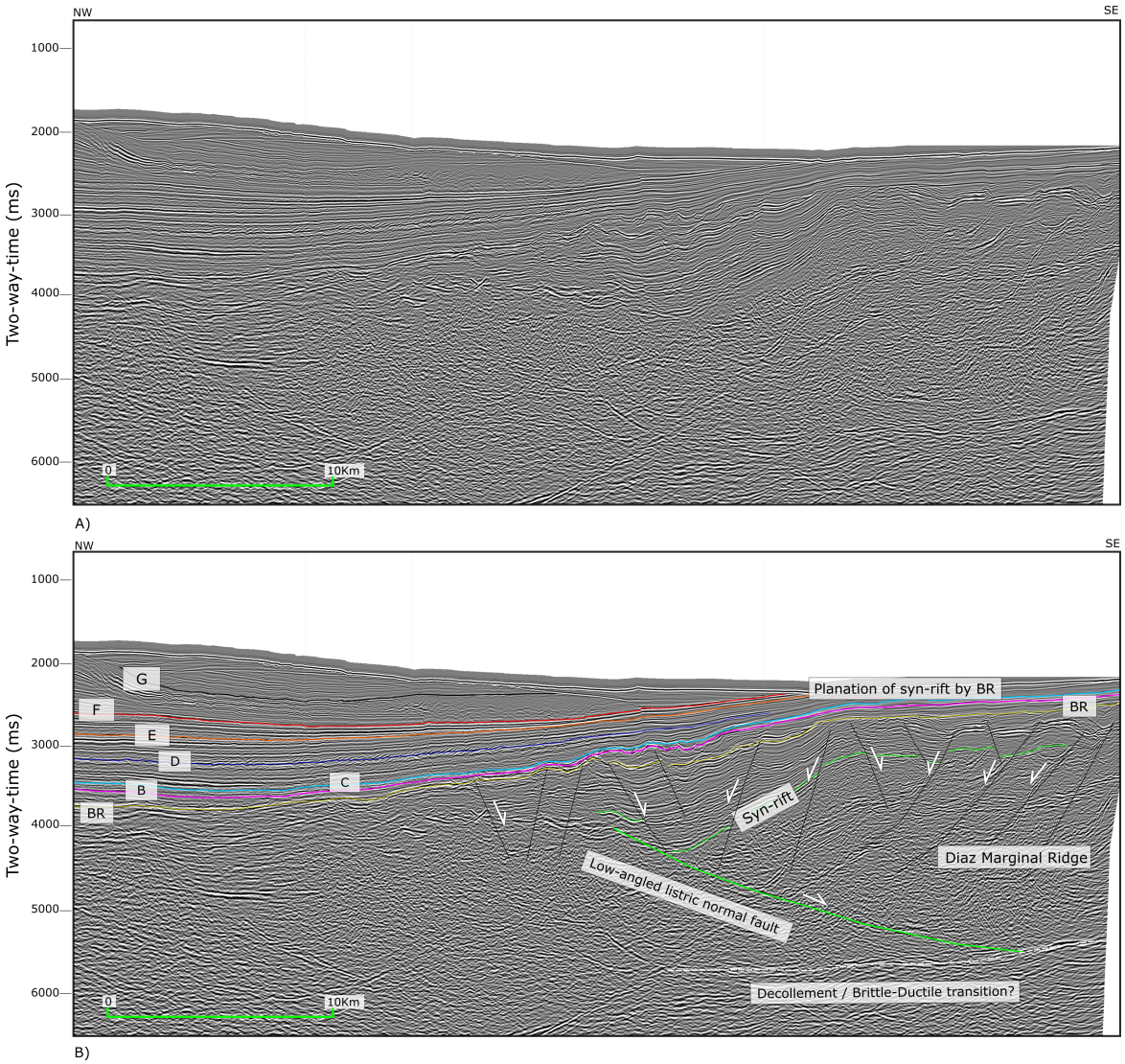


Fig. 4.21 Seismic line L2001-9, located in the far-western sector, location shown in Fig. 4.1.

4.3.3 Reflector BR to B: Package 1 (P1)

Seismic sequence P1, Valangian - Hauterivian (134-130Ma), is defined at the base by reflector BR and the top by reflector B (Fig. 4.22). North of the St. Francis Arch in the eastern sector, the package is low amplitude and low frequency with parallel reflectors that are deformed by faults. On the southern side of the arch, the package is defined by divergent reflector geometries that thicken and become parallel towards the south where they onlap onto onto an intra-basinal high and the northern shoulder of the DMR (Fig. 4.18). In the northern part of the central sector, the package has largely been eroded by the overlying unconformity horizon C, Aptian (120Ma), with the seismic facies of the strata defined by high amplitude, medium-frequency semi-parallel reflectors. In the southern part of the central sector the internal reflections are medium-high amplitude and divergent on the northern and southern shoulders of the respective basement highs, thickening and becoming semi-parallel and continuous in the middle of the basin (Fig. 4.19). In the western sector of the basin the package is wedge shaped with a southward thickening and onlapping of the reflectors onto the hanging-wall of the syn-rift package (Fig. 4.23). The seismic facies is characterised by medium amplitude, semi-continuous reflectors at the base of the package becoming lower frequency, semi-parallel and continuous towards the top of the package (Fig. 4.21). In the far-western sector, the internal reflection pattern is high-amplitude and low frequency, with semi-continuous reflections onlapping the basement fault surfaces to the north and south. In the southern part of the far-western sector, the seismic facies of the lower section of the package is relatively transparent with low-amplitude, high frequency internal reflections that are deformed by faulting over the northern shoulder of the DMR. The upper section of the package in this area is higher amplitude and seems to be prograding towards the north, possibly indicating the presence of fans (Fig. 4.21).

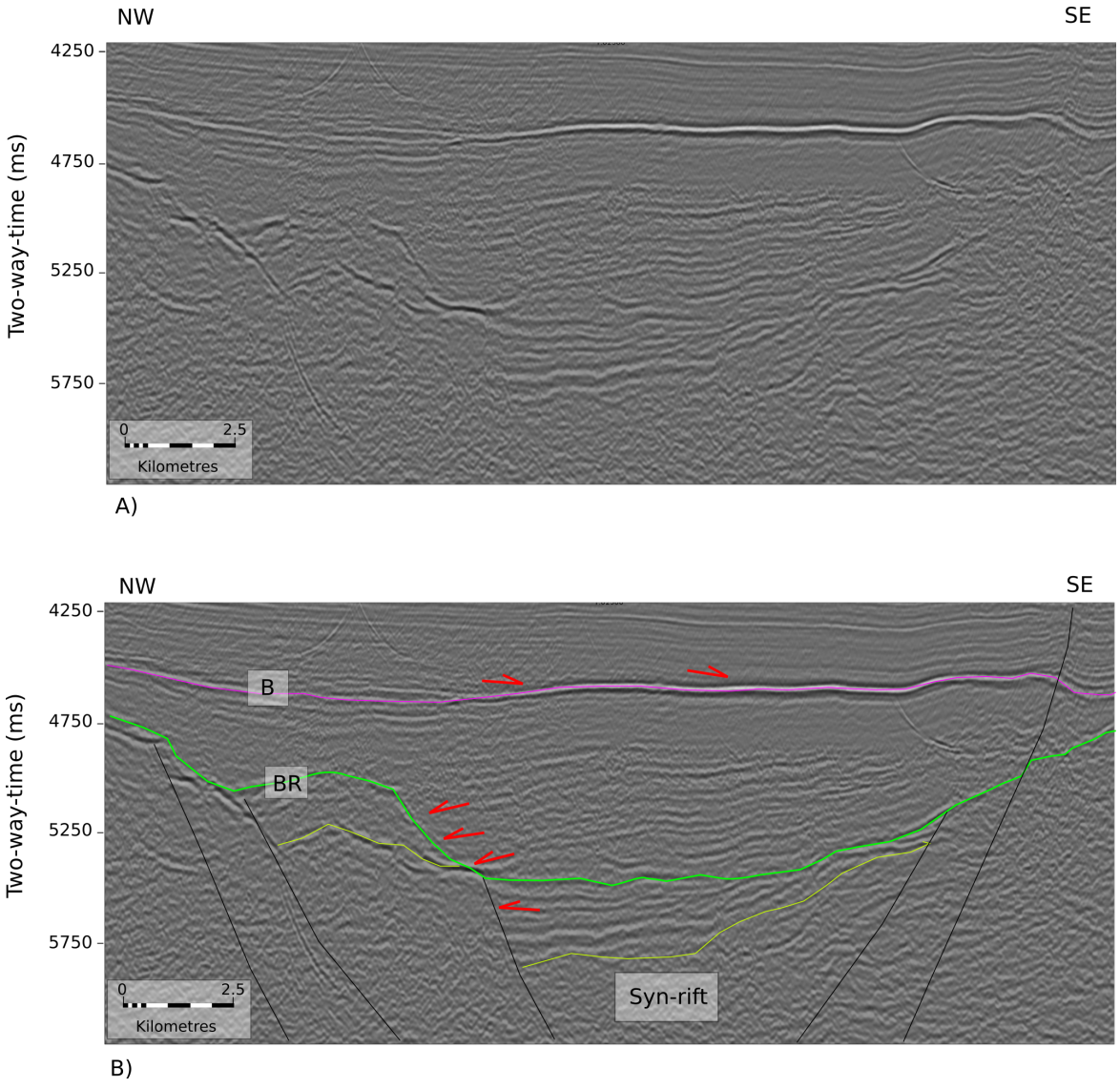


Fig. 4.22 A) Seismic line 2001-31, in the western sector, location shown in Fig. 4.1. Shows the thickening of the on-lapping reflectors of Package 1 towards the north.

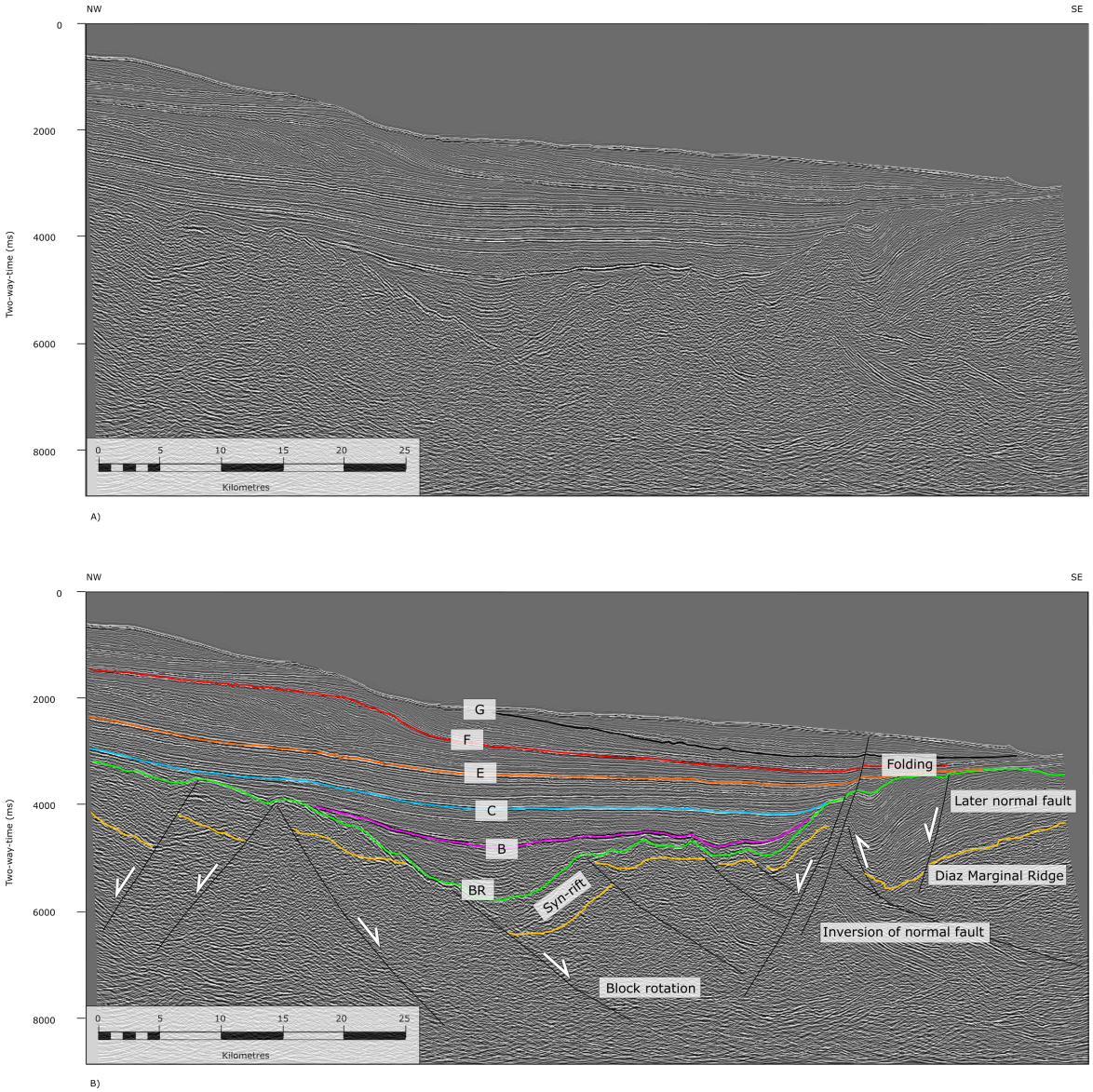


Fig. 4.23 A) Seismic line 2001-33, in the western sector, location shown in Fig. 4.1. Interpreted section shows deformation within the P1 (horizons BR - B) over the Diaz Marginal Ridge segment.

4.3.4 Reflector B to C: Package 2 (P2)

Seismic sequence P2, Hauterivian - Aptian (130-120Ma), is bound at its base by the regional unconformity horizon B, Hauterivian (130Ma) and by unconformity horizon C, Aptian(120Ma) at the top of the package. To the north of the St. Francis arch, in the eastern sector of the basin, the medium-high amplitude, continuous reflectors downlap onto horizon B, in a prograding configuration. South of the arch the sediments are wedge shapes, thickening toward the middle of the basin with internal reflections low-amplitude, medium frequency in the lower part of the package becoming progressively higher amplitude, higher frequency in the upper part of the package from the north towards the south (Fig 4.24). To the north of the basement high in the northern part of the central sector, the internal reflection of the package is continuous, medium-low amplitude and medium frequency (Fig. 4.25). The package is markedly thinner in the northern part of the sector than middle of the Southern Outeniqua Basin where it is defined by medium-amplitude, medium-frequency, continuos reflectors that onlap the northern shoulder of the DMR. A wedge shaped geometry of reflectors on the northern shoulder, prograding into the middle of the basin, within the upper part of the package could indicate fans being sourced form the DMR (Fig. 4.25). In the northern part of western sector, the P2 sequence is very thin and indistinguishable over the basement high (Fig. 4.26). In the middle of the basin, the internal pattern is characterised by medium-low amplitude, medium-high frequency and continuous reflections which onlap the northern shoulder of the DMR in the lower section of the package. In the upper section of the package, the reflections are wedge shaped, high-amplitude, discontinuous and truncate the underlying reflectors on the northern shoulder of the DMR. This reflector configuration could be explained as fans emanating from the Diaz Marginal Ridge and prograding into the middle of the basin (Fig. 4.26). In the far-western sector, the P2 package is thin ($\approx$100ms TWT) with a low-amplitude, medium frequency internal reflection pattern that onlaps the

northern shoulder of the DMR; the reflections are inclined as they reach the DMR suggesting inversion of the original reflection geometries (Fig. 4.21).

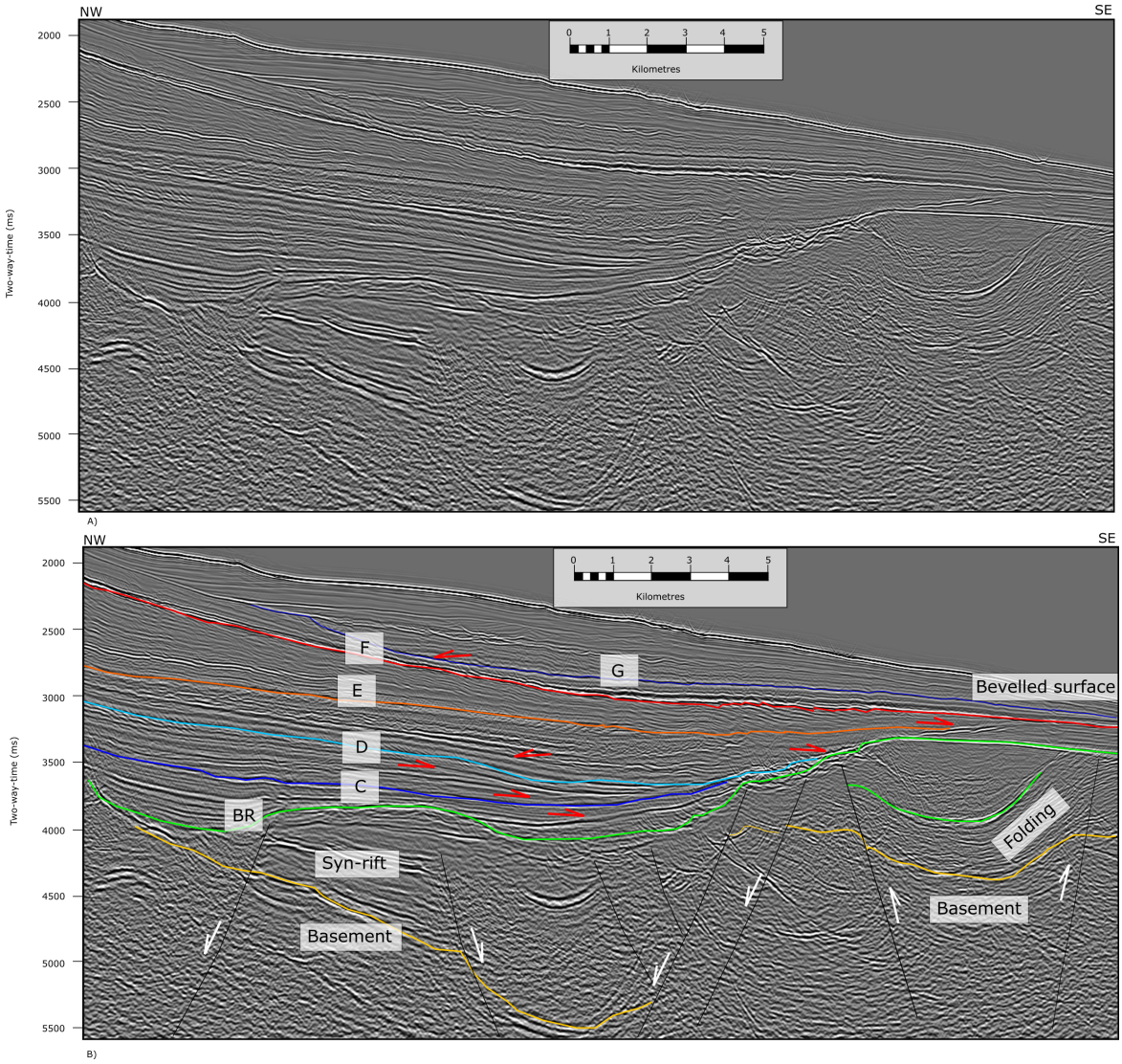


Fig. 4.24 A) Seismic line 2001-75, in the eastern sector, location shown in Fig. 4.1. Interpreted seismic section shows the clear folding of the syn-rift strata overlying the acoustically chaotic basement.

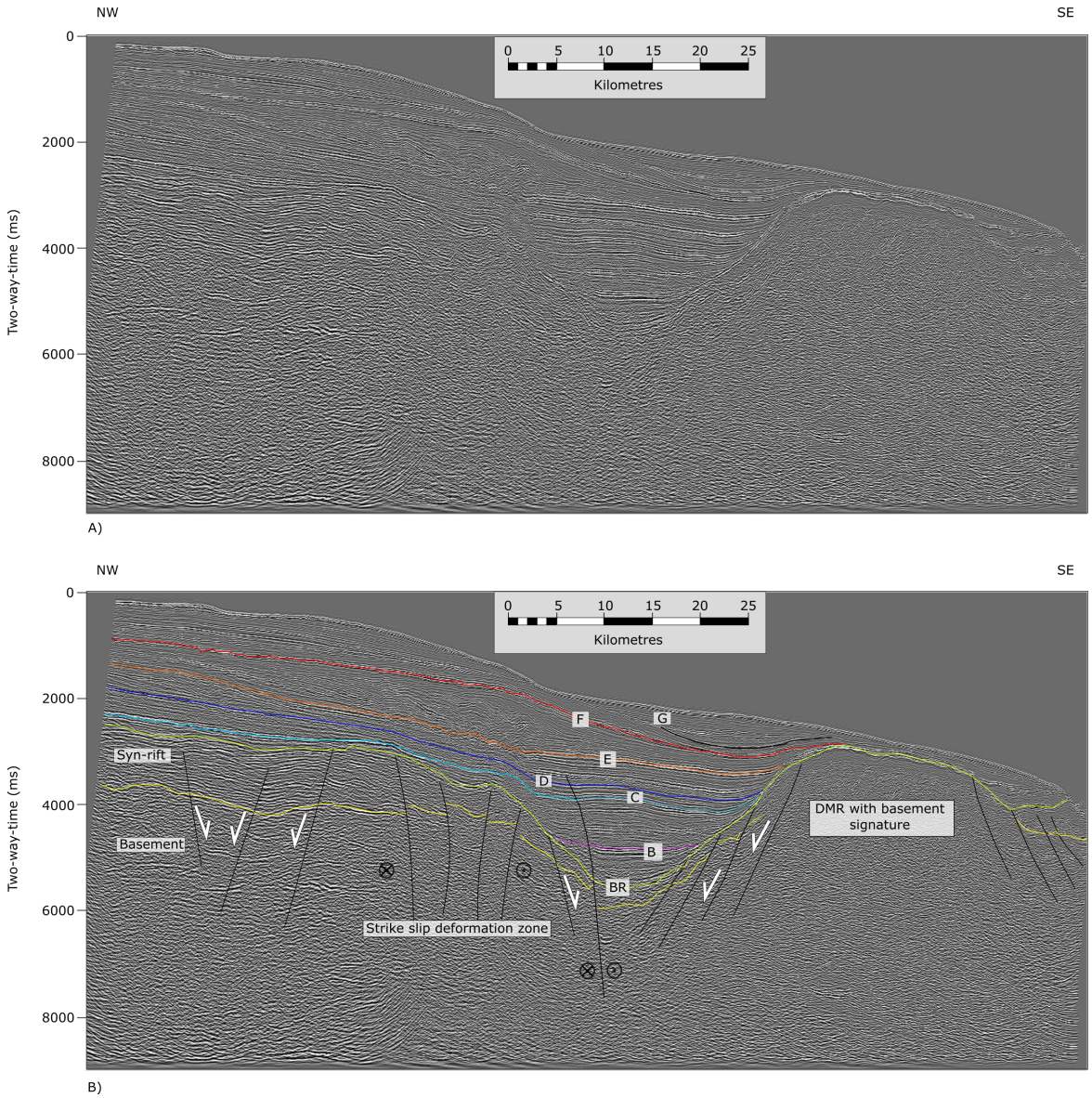


Fig. 4.25 A) Seismic line 2001-63, in the eastern sector, location shown in Fig. 4.1. Interpreted seismic section demonstrating the thin package of P2 over the northern part of the sector relative to the thicker package in the middle of the basin with reflections onlapping the DMR to the south

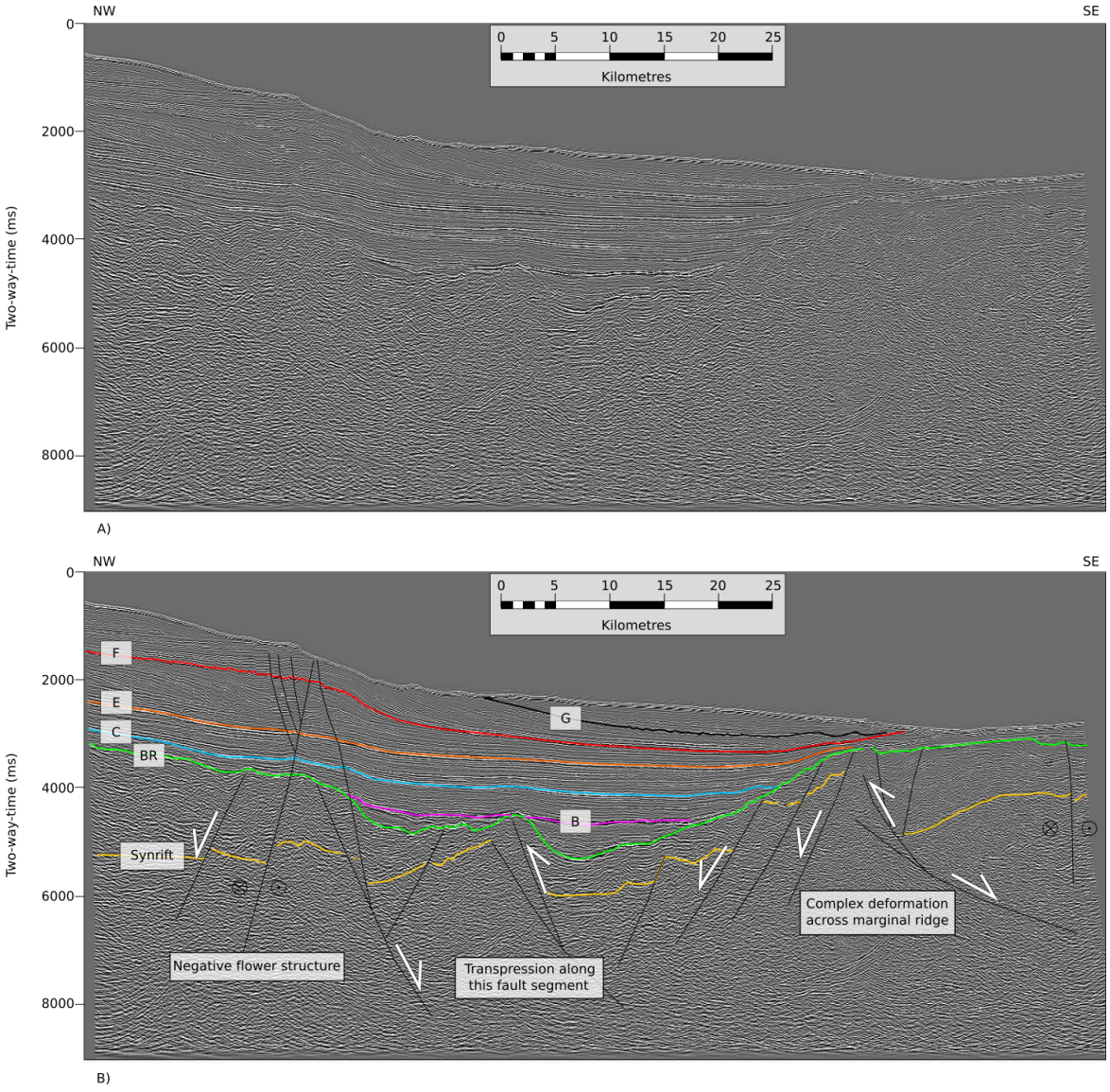


Fig. 4.26 Interpreted line L2001-29, in the western sector, location shown in Fig. 4.1. In the north the sequence of P2 is very thin and indistinguishable from sediments onlapping onto unconformity BR, while the package thickens towards the DMR in the south.

4.3.5 Reflector C to D - Package 3 (P3)

Seismic sequence P3, Aptian - Early Turonian (120 - 93Ma), is bound by the base unconformity horizon C, Aptian (120Ma) and the unconformity horizon D, Cenomanian (93Ma) at the top of the package. To the north of the St. Francis Arch, in the the eastern sector, the package is thickest to the north but thins towards the south. The reflectors are high-amplitude, discontinuous and downlap onto horizon C in a prograding geometry. Third order high-stand and low-stand system tracts are visible in this package to the north of the arch. To the south of the arch, the package is roughly lens-shaped with the thinnest part of the package towards the St. Francis Arch and DMR topographical highs respectively. The lower section onlaps onto horizon C in the northern part of the Southern Outeniqua Basin but is truncated by high amplitude, low frequency reflectors on the northern shoulder of the DMR (Fig. 4.24). The upper section along the northern shoulder of the DMR has concave, high-amplitude reflectors that become medium-amplitude, semi-parallel and continuos from south to north, into the middle of the basin (Fig. 4.24). In the central sector, the internal pattern of the reflectors is predominantly medium-high amplitude, continuous and parallel from north to south, where the lower section of the package onlaps against the northern shoulder of the DMR. The upper section of the package however is a wedge shaped unit, thickest along the northern shoulder of the Diaz Marginal Ridge, truncating the underlying sediments and thinning towards the middle of the basin (Fig. 4.27). In the western sector, the lower section of the package onlaps the underlying horizon C to the north and thickens towards the DMR in the south. In the upper section of the package, mound shaped basin floor fan geometries downlap underlying reflectors along the trend of the northern shoulder of the Diaz Marginal Ridge, suggesting the structure controlled the sediment pathway (Fig. 4.28). In the far-western sector of the basin the internal reflection pattern of the package is medium-high amplitude in the lower section and low-amplitude in the upper section. The package thins towards the south towards

the northern shoulder of the DMR where the top reflector of the package, horizon D, pinches out against sediments of the lower section of the package.

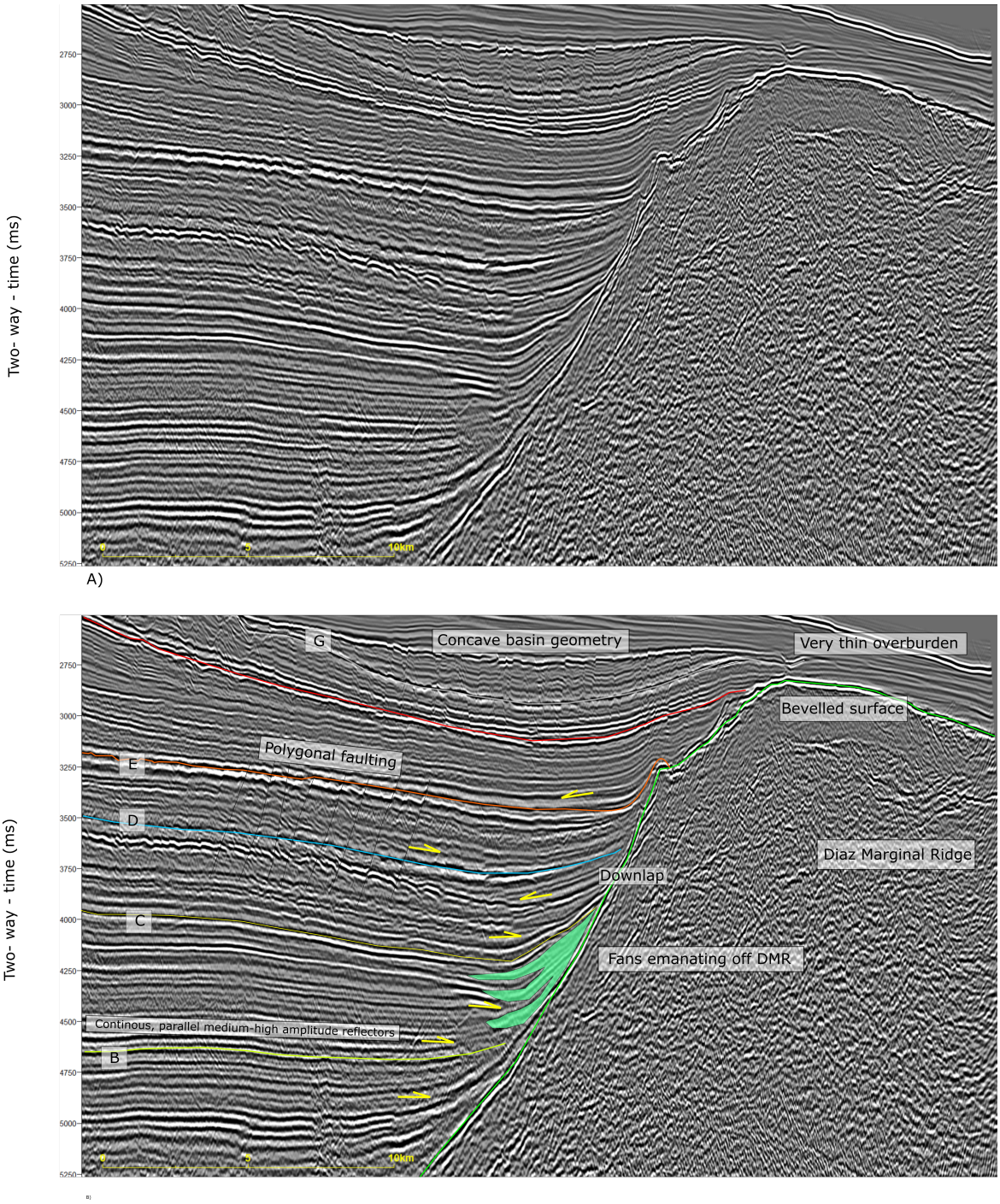


Fig. 4.27 A) Seismic line 2001-61, in the eastern sector, location shown in Fig. 4.1. Interpreted seismic section demonstrating the continuous, parallel, medium-high amplitude reflectors of P3 being truncated by wedge-shaped reflectors which appear to emanate from the northern shoulder of the DMR

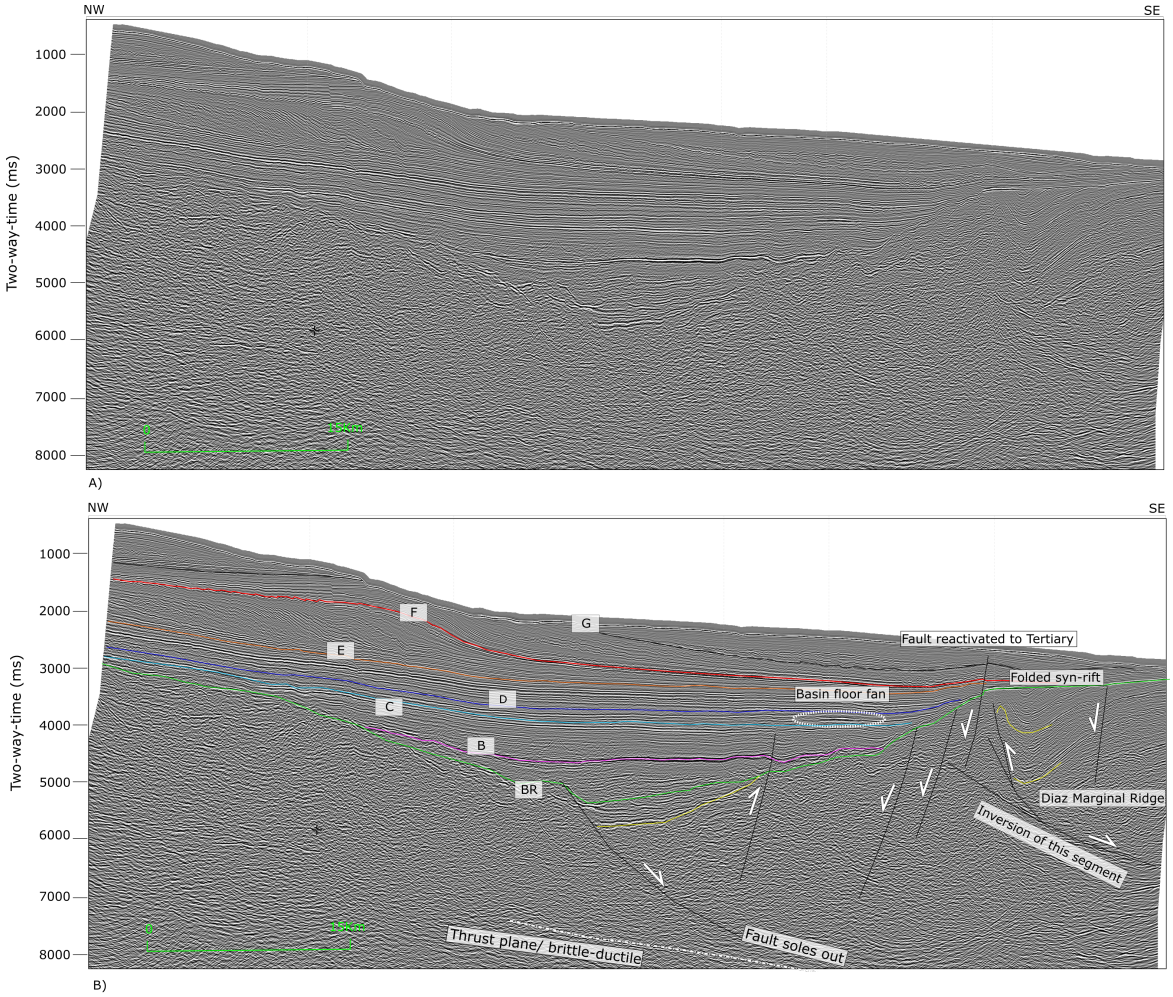


Fig. 4.28 A) Seismic line 2001-31, in the western sector, location shown in Fig. 4.1. Interpreted section shows deformation within the BR-B package over the Diaz Marginal Ridge segment.

4.3.6 Reflector D to E - Package 4 (P4)

Seismic sequence P4, Early Turonian - Campanian (93 - 80Ma), is bound by the base unconformity horizon D (Early Turonian) and the top by unconformity E (Late Santonian). In the eastern sector of the basin the package is thin over the St. Francis Arch <100ms and gets thicker into the middle of the basin, reaching its greatest thickness of ≈500ms TWT, before wedging out against the DMR (Fig. 4.29). The internal reflection pattern is low-amplitude, low frequency and continuous in the lower part of the package. A noticeable change in reflection patter occurs in the upper part of the package is markedly different with high-amplitude, high-frequency discontinuous reflectors becoming separated from the lower part of the package by a wedge shaped unit emanating from the DMR (Fig. 4.29). In the northern part of the central sector, the reflectors remain low frequency in the lower part of the package and transition into higher-amplitude, higher frequency, semi-continuous in the upper part of the package towards the south before onlapping against the DMR (Fig. 4.27). Deformation of the package in the southern part of the sector is suggested to be attributed to the de-watering of shale lithologies as the faulting appears to correlate with the part of the package that hosts continuous, low-medium amplitude, medium frequency internal reflectors, typical of shale deposition (Fig. 4.27). In the western sector of the basin, the package is thinner than in the central and eastern sectors and is characterised by medium-amplitude, medium-frequency internal reflector patterns. Towards the southern part of the sector, the package thins against the northern shoulder of the DMR where the reflectors onlap the structure and were later faulted. (Fig. 4.28). In the far-western sector the package is thinnest, ≈100ms TWT, with low amplitude, low frequency internal reflection patterns in the northern part of the sector, becoming high-amplitude, high frequency in the southern part of the sector before pinching out against the DMR (Fig. 4.30).

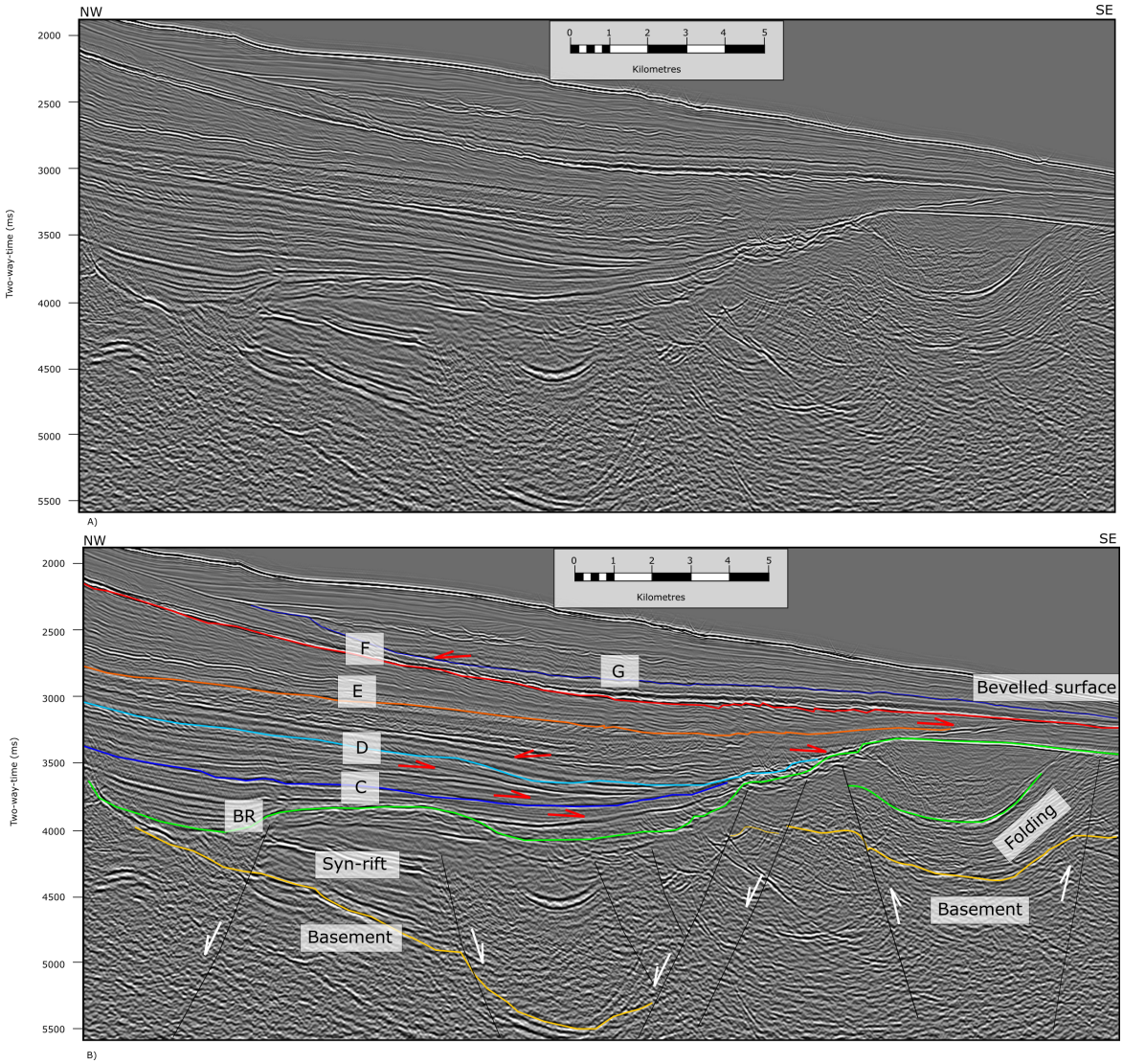


Fig. 4.29 Seismic line 2001-75, in the eastern sector, location shown in Fig. 4.1. Interpreted seismic section demonstrates the low-amplitude, low frequency, continuous reflection pattern of the lower part of P4, horizons D - E. The upper part of the package is markedly different with high-amplitude, high-frequency discontinuous reflectors onlapping the shoulder of the DMR.

4.3.7 Reflector E to Seabed - Package 5 (P5)

Seismic sequence P5, Campanian - Cenozoic (80-0Ma), is the largest of the packages and is further subdivided into a lower unit P5a, Campanian - Late Campanian (80-76Ma) and an upper unit P5b, Late Campanian - Cenozoic (76-0Ma). The two sub units P5a and P5b, both are characterised by prograding and aggrading clinoforms packages present

across the northern parts of all sectors of the basin. The lower unit P5a, is bound at the base by unconformity horizon E and at the top by unconformity horizon F (Fig. 4.31). Internal reflector patterns within P5a are high-amplitude, semi-continuous with reflectors downlapping and prograding onto unconformity horizon E in the eastern and central sectors of the basin. The reflection pattern in the eastern and central sectors is sigmoidal in the lower unit becoming oblique and finally aggradational in the upper part of unit P5a (Fig. 4.25). In the western and far-western sectors, the reflectors in the lower part of the unit remain medium-amplitude, semi-continuous and parallel before the reflection pattern changes to sigmoidal in the upper part of the unit (Figure 4.26). The upper unit P5b, is defined at the base by unconformity F and the top by the seafloor. In the far-western sector of the basin, downlapping reflector geometries onto horizon F prograde from the south-west towards the north-east (Fig. 4.31). Erosional scarps in the lower part of sub-unit P5b, step towards the north-east and truncate the sediments overlying horizon F almost truncating reflector F. Reflector patterns in the lower part of the unit are typically low-amplitude, medium-frequency except where these sediments are eroded by high-amplitude, high-frequency. In the upper part of the unit reflectors are semi-continuous and deformed by faulting.

4.4 Isochron maps

In order to quantify the variation in accommodation space and subsequent sedimentary supply into the basin during its evolution, isochron maps were generated for packages 1- 5. These maps illustrate the net thickness of each sedimentary package in two-way-time (ms), between the bounding surfaces and as such allow for a temporal frame of reference for controls on sedimentation throughout the basin. The isochron map for sedimentary package P1 indicates that the thickest accumulation of sediment occurred in the central and western sectors of the basin in depocentres orientated NNE-SSW and NE-SW during the Valangian-Hauterivian (134-130Ma) (Fig. 4.32). Thinning of the surface appears to be confined to the northern part

of the far-western sector and into the western sector. A subtle NW-SE trending depression is visible in the far-western sector where limited accumulation of sediment took place.
The isochron thickness map for package P2 defines sedimentary erosion/deposition between horizon B, Hauterivian (130Ma) and horizon C, Aptian (120Ma). Thickening of the package is centred in the central and western sectors of the basin with a smaller accumulation of sediment in the NE-SW trending depression mentioned previously. Thinning of the package over the basement promontories of the St. Francis Arch in the northern the DMR in the south is evident in the eastern and far-western sectors. the isochron thickness map for Package 3 indicates general thinning in the eastern and far-western sectors of the basin with thickening occurring in a NE-SW trending depression in the central and western sectors of the basin. The isochron map for seismic package 4 suggests a general thinning of the package in the far-western and western sectors of the basin. Thickening is localised to an elongated NE-SW trending depression with the greatest amount of thickening (>500ms TWT) occurring in the southern part of the eastern sector of the basin. The isochron thickness maps of the sub-units belonging to P5 indicate a substantial change in sediment thickness across the basin. The isochron map of P5a, the lower unit of the package, indicates that accumulation and thickening of the package occurred in a north-easterly direction in the northern parts of the far-western ,western and central sectors; thinning of the sediment package is evident in the southern parts of the sectors. The isochron thickness map fro sub-unit P5b indicates that the sedimentary package is thinner in the areas where sediments part of the lower sub-unit used to accumulation during the Campanian - Late Campanian (80-76Ma). The P5b map shows thickening of the sedimentary package in the northern part of the far-western sector and a subtle thickening of the package in a NE-SW trending geometry.

4.5 Summary

The mapping of second order unconformities, labelled Horizon BR - G, has allowed the distinction of five super-sequences, designated Package 1-5, present within the basin. The BR reflector surface represents the basal unconformity produced during the transition from orthogonal rifting to transform motion associated with movement along the incipient Agulhas-Falklands Fracture Zone. The mapped surface allowed for the visual interpretation of accommodation areas that reveal the three distinct geometries, NW-SE, NE-SW and ENE-WSW, and therefore areas of strain localisation along the normal faults initiated during the transition from rifting to shear motion. The NE-SW trending depocentres (≈5000ms TWT deep) concentrated in the central and western sectors of the basin are much deeper than depocentres (≈1500ms TWT deep) on the flanks of the basin in the eastern and far-western sectors. Subsequent uplift and erosion lead to the development of the Horizon B unconformity which truncates the underlying transitional sedimentary infill, presumed to be marine shale, and caps the first super-sequence designated Package 1. Minor displacement occurs in the subsequent time after deposition of Package 3 with on-lapping geometries interpreted to indicate thermal subsidence and traditional passive margin conditions starting to prevail along the margin. This however is abruptly altered during the basin-wide uplift and erosion, most clearly seen in the central and eastern sectors, of sediments leading to the development of an unconformity surface labelled horizon D. This unconformity surface truncates the underlying P3 reflectors as well as the Diaz Marginal Ridge with the greatest erosion occurring in the central and eastern sectors of the basin on the northern shoulder of the marginal ridge. Sedimentary infilling, bevelling of the marginal ridge top and down-lapping reflector geometries coming off the ridge high, suggest that transient uplift in this area was caused by either transpression associated with a change in plate velocity or by some other thermal perturbation along the southern boundary of the basin. Deposition of sediments overlying package P3, in a stacked series of parallel to sub-parallel reflectors

indicates further basin subsidence and infill in a more traditional passive margin setting and show a cyclical depositional character resulting from eustatic sea level rise and fall. Sedimentary provenance in this time period seems to be predominantly from the north-east with prograding, aggrading and retrograding reflector forms indicative of the eustatic cycling suggested above. A marked transition in the provenance direction occurs after the development of the second order unconformity horizon F, Late Campananian (76Ma) across the basin. Following the development of this unconformity, sediments are predominantly supplied into the basin from the south-west of the area, rather than from the north-east as had been in the underlying packages.

The interpretation of the isochron thickness maps as well as individual unconformity surfaces has indicated a complex history of stratal geometry variance through time. The conclusions that can be drawn suggest a complex interplay between tectonic controls and sediment supply into the basin, with tectonic forcing playing a greater role in accumulating and altering the provenance of the sediments filing the basin through its evolution.

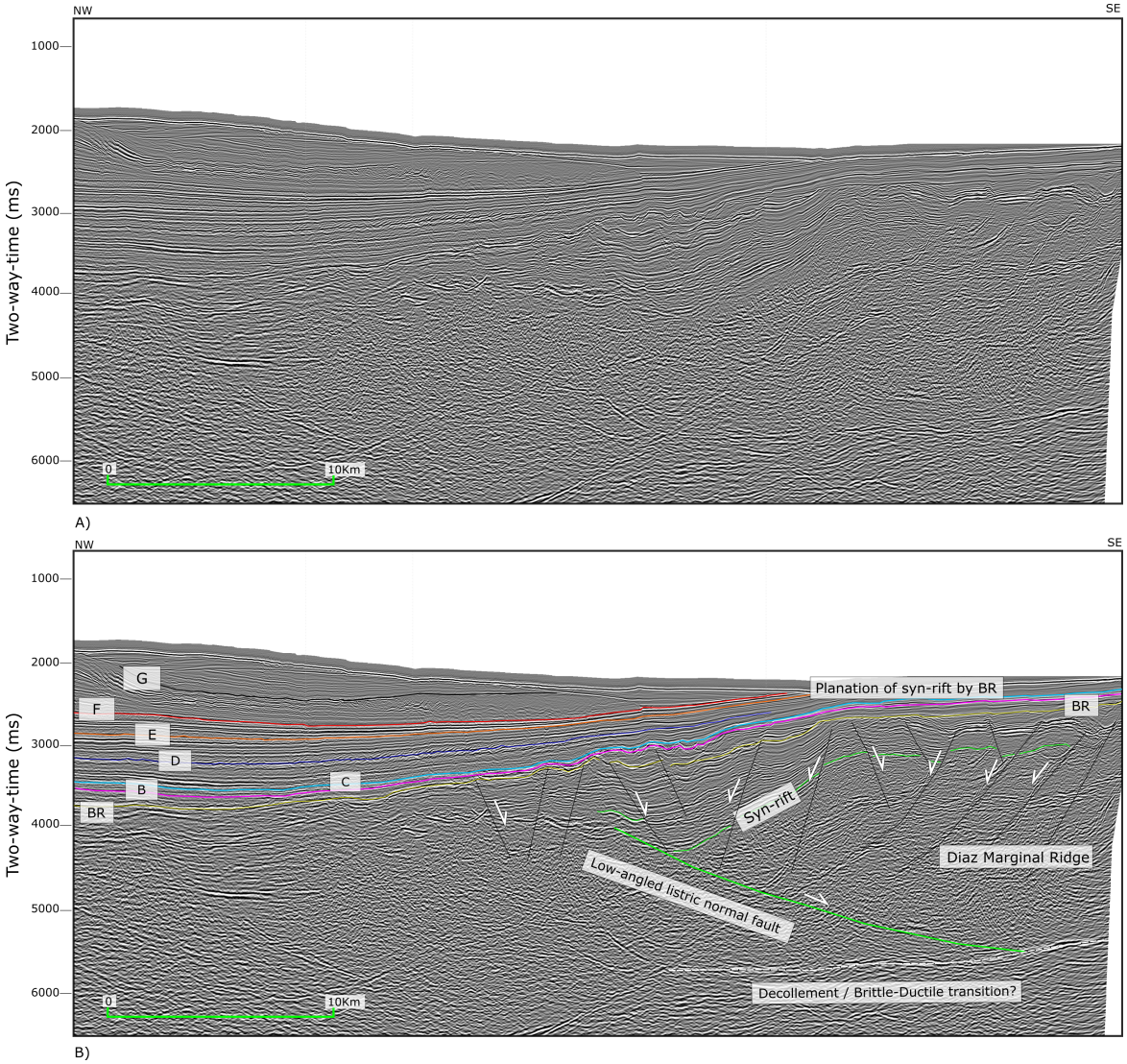


Fig. 4.30 Seismic line 2001-9, in the far-western sector, location shown in Fig. 4.1. Interpreted seismic section demonstrates the change from low-frequency, low-amplitude reflectors of P4 in the north to high-amplitude, high frequency internal reflector patterns in the south before the package pinches out against the DMR.

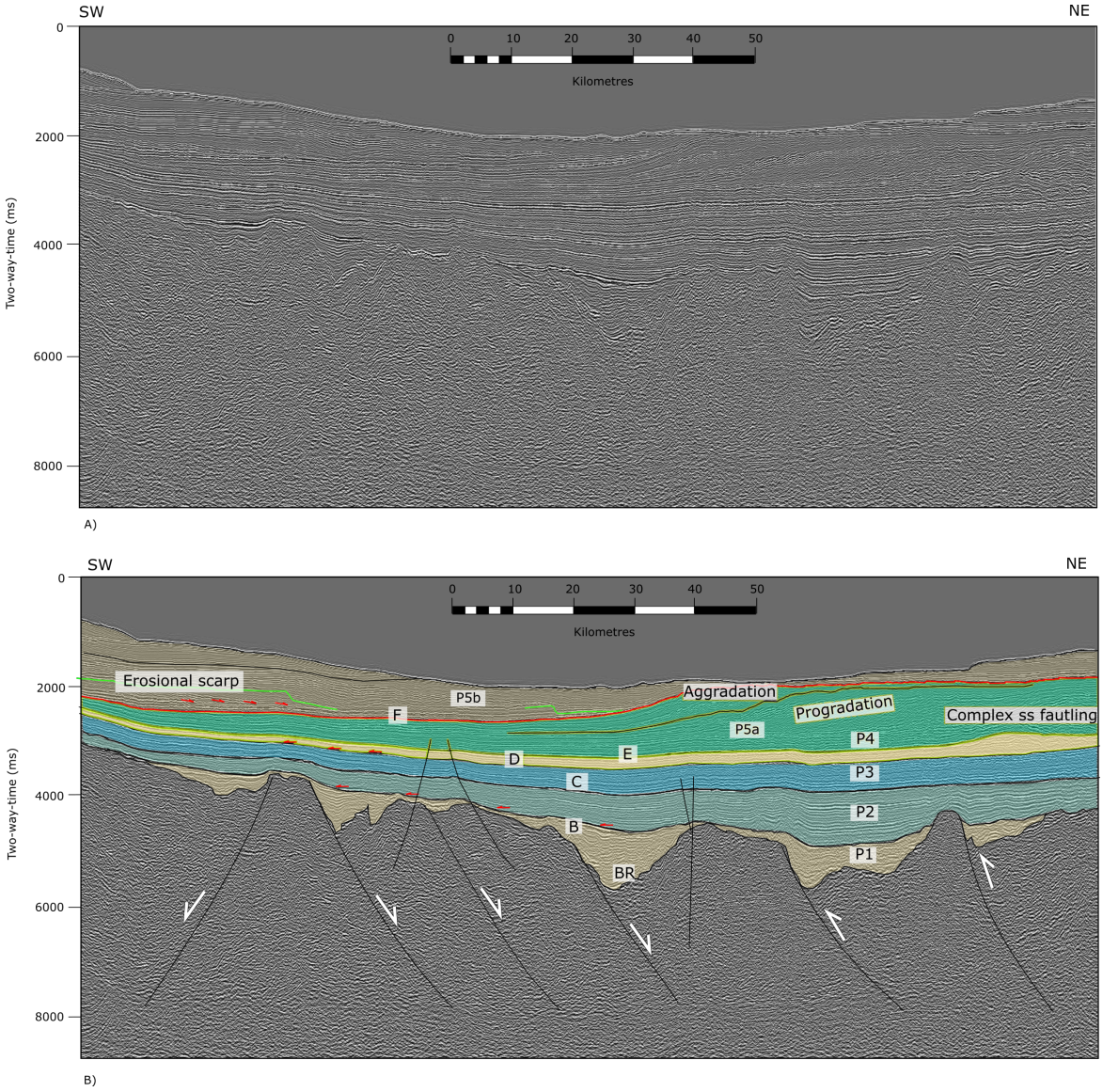


Fig. 4.31 Seismic line 2001-10, crosses the far-western, western and central sectors of the basin, location shown in Fig. 4.1. Interpreted seismic section with megasequence boundaries delineated.The section shows deposition between reflectors E and F, thinning out towards the far-western and western sectors of the basin. Also shown is the change in reflector geometries between Package 5a and 5b, indicating a change in sedimentary provenance.

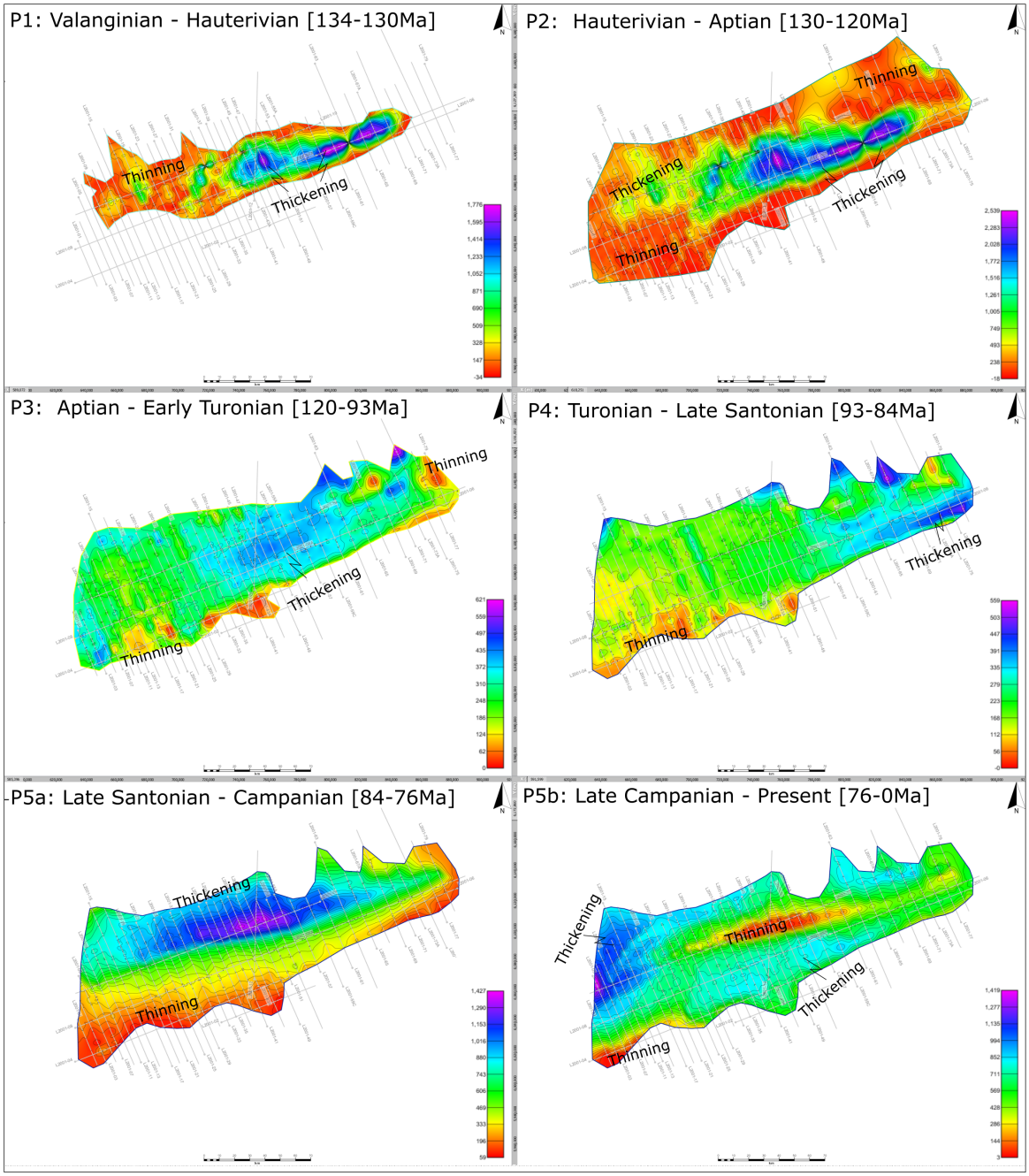


Fig. 4.32 Isochron maps showing the variation in thickness between the seismic packages across the Southern Outeniqua Basin. P1 is the package defining sediments between BR and B. P2 is the package defining sediments between B and C. P3 is the package defining sediments between C and D. P4 is the package defining sediments between D and E. P5a is the package defining sediments between E and F. P5b is the package defining sediments between F and the seabed.

Chapter 5

Structural Interpretation

5.1 Introduction

In this chapter I examine the structure of the Southern Outeniqua Basin and attempt to distinguish between the two end-member hypotheses of extensional-margin basin formation; by either transtensional or orthogonal rifting processes. I will examine satellite gravity and regional magnetics in order to understand the broad scale regional tectonics that would have led to the formation and evolution of the southern African margin and follow up with a more detailed analysis and interpretation of the seismic data acquired over the Southern Outeniqua Basin.

Large-scale tectonics

In this section an analysis of publicly available potential field data was made in order to try an understand the tectonic setting in terms of regional structural orientation and margin evolution.

Gravity Data

Satellite gravity, downloaded from NOAA (National Oceanographic and Atmospheric Administration), is measured using a radar altimeter that detects variations in sea surface height and translates that into a gravitational anomaly. These anomalies can then be analysed in order to identify regions of mass deficit, subsequently interpreted to define basins (Smith and Sandwell, 1997). I have used gravity anomalies to aid reconstruction of the margin prior to the separation of the Falklands and Argentina from South Africa (Fig. 5.1). The Agulhas-Falklands Fracture Zone, labelled AFFZ, along which South America separated from Africa (Ben-Avraham et al., 1997, 1993; Martin and Hartnady, 1986) is very clear in this gravity data where I have rotated South America back along this fault until the continental margins are in contact with each other (Fig. 5.1). Although there may have been some deformation along the continental margin after separation, such a reconstruction allows for a preliminary examination of the margin prior to large-scale transform motion. The Southern Outeniqua Basin aligns closely with a larger basin, known as the Falklands Plateau Basin (FPB), on the Argentinian side of the margin (Fig 1(a)), suggesting that these basin, together, formed a single larger proto-basin prior to the initiation of large-scale strike-slip motion (Lorenzo and Mutter, 1988; Scrutton, 1976; Thomson, 1998). This proto-basin signature is larger, approximately 1.6 million square kilometres, on the South American side, with a similar orientation and morphology to the Southern Outeniqua Basin: both are deep NE-SW trending basins bounded by shallower bathymetry on the continental side of the fracture zone and a marginal ridge high (Scrutton, 1979). In summary, this suggests that there was a pre-existing basin that may have formed by orthogonal rifting prior to being bisected by the AFFZ.

A Bouguer correction was applied to the satellite gravity in order to highlight the different crustal components seen along the margin (Fig.5.2). The correction highlighted the roughly ESE-WNW trend of the Cape Fold Belt in the region onshore of the Southern Outeniqua

Basin. This trend is obliquely orientated relative to the trend of the AFFZ. A mass deficit underlies the Southern Outeniqua Basin (Fig.5.2a). The gravity map also shows the tentative trace of another fault, trending sub-parallel to the AFFZ, with a loss of signature along the northern boundary of the basin.

Magnetic Data

Magnetic data can be used in order to distinguish between oceanic crust, which has a high magnetic response and attenuated continental margin, which has a lower magnetic response. I have used data from the publicly available Earth Magnetic Anomaly Grid (NOAA, 2015) to separate probable oceanic and continental crust and to map major structural trends along the southern African margin (Figure 5.2b). The trace of the AFFZ can readily be followed as a dark magnetic low which separates the South African continental crust, of lower magnetic response, to the north of the fracture zone from the oceanic crust to the south. The striped pattern of the magnetic fabric further away from the continental strata is characteristic oceanic crust that formed at a mid-ocean ridge during alternating periods of normal and reverse polarity magnetism caused by magnetic reversals in the Earth's magnetic field (e.g. Vine and Matthews (1963)). My interpreted continent-ocean boundary, marked by the change in magnetic pattern, is illustrated along the western margin of South Africa where it extends down to and is truncated by the AFFZ. The Agulhas Plateau large igneous province (LIP) is also visible to the south of the AFFZ as a highly magnetic anomaly. A broad, relative magnetic high is observed in the central and western parts of the Southern Outeniqua Basin; perhaps suggesting a highly thinned nature of the crust in that region, or less-likely, basalt under-plating of the crust. A change in magnetic signature to the SW of the LIP may have been caused by an extinct mid-ocean ridge segment.

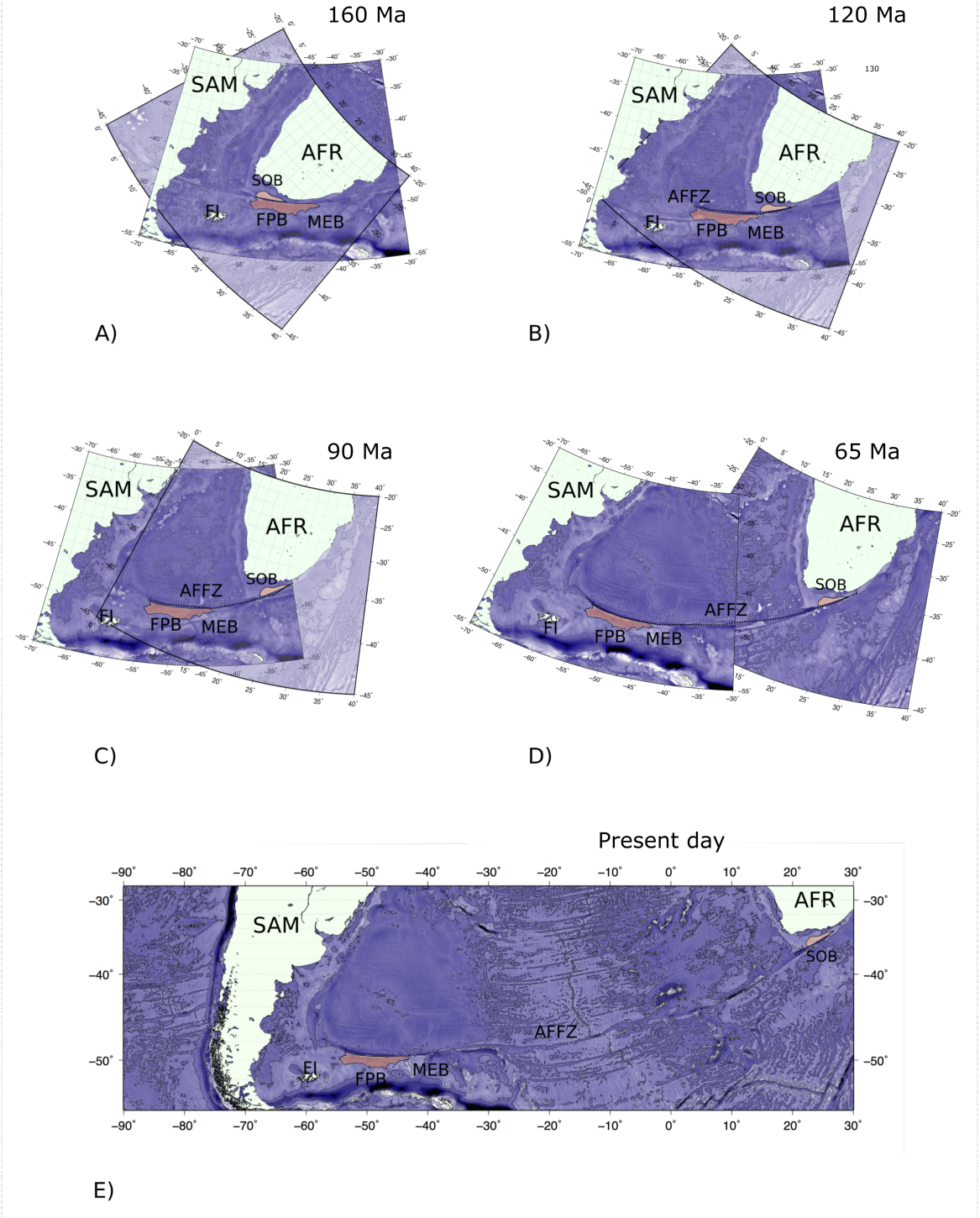
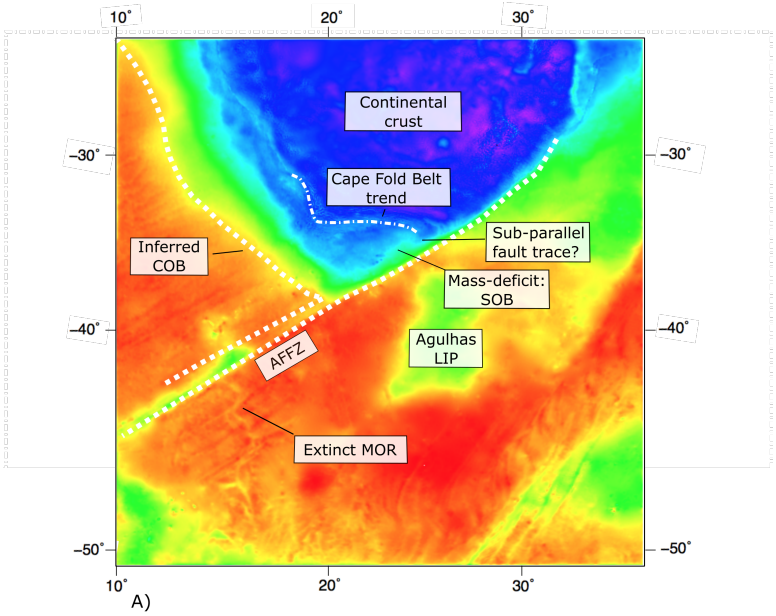


Fig. 5.1 A) Reconstruction based on free-air satellite gravity data of western Gondwana around 160Ma; prior to any translation along the AFFZ. B) Dextral strike-slip movement along the AFFZ approximately 130Ma. C) Further translation along the fracture zone around 110Ma sees the Maurice Ewing Bank clearing the southern tip of the African plate. D) Gravity reconstruction around 90Ma with pronounced rotation of the African plate as the separation from the South American plates continues. E) Present day plate configuration with the AFFZ clearly visible as a distinct quasi-linear gravity low. SAM - South America, AFR - Africa, FI - Falklands Islands, FPB - Falklands Plateau Basin, MEB - Maurice Ewing Bank, SOB - Southern Outeniqua Basin.



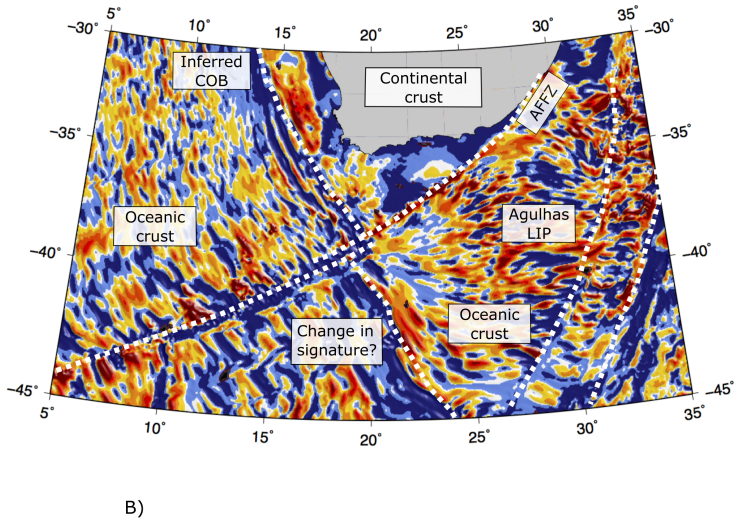


Fig. 5.2 A) Bouguer correction applied to gravity image highlights the trace of the AFFZ and the gravity signatures around the South African margin. The mass deficiency in the crust is highlighted as the bounds of the Southern Outeniqua Basin (SOB) with the faint trace of a fault bounding the northern part of the basin. A sinuous trace inboard of the coastal margin shows the trend of the Cape Fold Belt. B) An EMAG 2 image is annotated to show the different crustal provinces along the offshore South African margin. A change in the magnetic fabric is visible across the trace of the AFFZ outboard of the Southern Outeniqua basin, separating continental from oceanic lithosphere. COB- Continent-Ocean Boundary; LIP - Large Igneous Province; SOB - Southern Outeniqua Basin.

5.2 Interpretation of seismic data

Structural interpretation of the Southern Outeniqua Basin was based on the gridded horizons described in the Chapter 4 and individual seismic lines. Reflectors (see section 4.2) picked on the seismic lines were calibrated with legacy on-shelf well data to determine the relative ages of the stratigraphic sequences and possible structural hierarchies amongst the fault populations. Mapping of the breakup unconformity surface (BR) revealed a number of prominent sub-basins which are bounded by structures in three distinct orientations, NE-SW, NNW-SSE, NW-SE, across the extent of the Southern Outeniqua Basin. The basin is naturally separated into 4 regions, Far-West, West, Centre and East (Fig. 5.3A). The figure shows the approximate location of the AFFZ, on the eastern side of the basin and furthest from the western part, and summarises these trends which are labelled from structural orientation 1-3 (S.O.1-3).

S.O.1 is recognisable in the horizon morphology and trends NE-SW, roughly parallel to coastline and to the strike of the AFFZ. This orientation is dominant in the eastern part of the area, where an approximately 5800ms TWT deep, NE-SW trending basin is flanked by relative highs.

A second distinct orientation defining parts of the interpreted horizon, trends NNE-SSW (S.O. 2); structures in this orientation are most common in the centre of the area and appear to underly the deep basin described above. A final, more tentative trend (S.O. 3), runs NNW-SSE and is observable only in the western part of the area.

Individual seismic lines were interpreted to determine whether these orientations, visible in the surface, correspond with mappable faults and, if so, to determine their sense of slip. Spacing between survey lines varied between 6-10km. In typical continental normal faulting, fault segment lengths range from ca. 10-15km (e.g. Greece; Goldsworthy and Jackson (2001)) to ca. 30-40km (e.g. E-Africa, Muirhead and Kattenhorn (2018)). This means that in

some cases, only one seismic line may cross any particular fault segment. However, some of the basin bounding faults do appear to be traceable across multiple lines.

5.2.1 Structural Orientation 1: NE-SW (045-065)

Normal faults

The mapped BR, Valanginian (134Ma), surface was used in order to better delineate the pre-existing depression geometries prior to major transform motion. Figure 5.4 shows normal faults in S.O.1 along with corresponding seismic lines. Figure 5.5 shows the mapped graben morphologies that are seen along the strike of the basin within the predominant S.O. 1 trend.

Within the eastern part of the basin, major basin bounding faults were observed across multiple lines on both the northern and southern sides of the basin along the shoulders of both relative highs, e.g. the St. Francis Arch and Diaz Marginal Ridge (Fig. 5.7). Along the northern flank of the Diaz Marginal Ridge, these faults dip to the NW and step seawards in an en-echelon configuration towards the southeast. The normal faults in the mid-eastern part of the basin have formed large displacement corresponding to up to 800ms TWT, basin bounding faults that define a the deep NE-SW trending basin. Faults located on the basin-facing shoulder of the DMR appear to be confined to a narrow zone of deformation, approximately 5km wide, and were active until the base Tertiary by the displacement of reflector F (Fig. 5.6). Graben and half-graben structures in this orientation are shallower in the eastern sector of the basin and deepen towards the SW. The graben structures in this eastern sector of the basin are seen to overlap with a northern and southern graben developing between an intra-basinal high, constituting syn-rift strata (Fig. 5.5). The southern-most graben is seen to be defined by larger displacement normal faults than its northern graben counterpart.

Within the major structures, a series of minor displacement, normal faults cut the syn-kinematic strata, with the top of the strata delineated by the horizon BR, in which the faults

are confined. Deformation in this area is however not confined to strata between the syn-rift and BR reflectors, inferred to be Valanginian- Barremian in age, but seems to have been active to the deposition of reflector F, inferred to be Campanian in age. Figure 6 depicts evidence for this reactivation of the DMR-bounding faults into the overlying sediments, displacing those of reflector F.

Large displacement (100's ms TWT) normal faults are observed in the eastern sector of the basin. These normal faults which define the DMR in the southern part of the sector are seen to have been reactivated with a reverse sense of displacement after the deposition of the BR-reflector. The reflectors within this package show distinct folding, which trends in an en-echelon configuration when mapped, along the planes of these re-activated normal faults (Fig. 5.7).

In the western sector of the basin, normal faults tend to dip to the SE closest to the shelf and NW closest to the DMR. These planar faults show minor displacements, up to 200ms TWT, and form half-grabens within the centre of the basin. The mapped trend of these half-grabens is defined by these faults with possible evidence for fault linkage across lines (Fig. 5.5). Normal faults in S.O. 1 can also be seen in the western sector of the basin again defining the basin-ward shoulder of the DMR. These planar faults and are not visible below 7500ms TWT but truncate earlier syn-rift faults and are interpreted to control the morphology and geometry of the DMR in the western sector (Fig. 5.10).

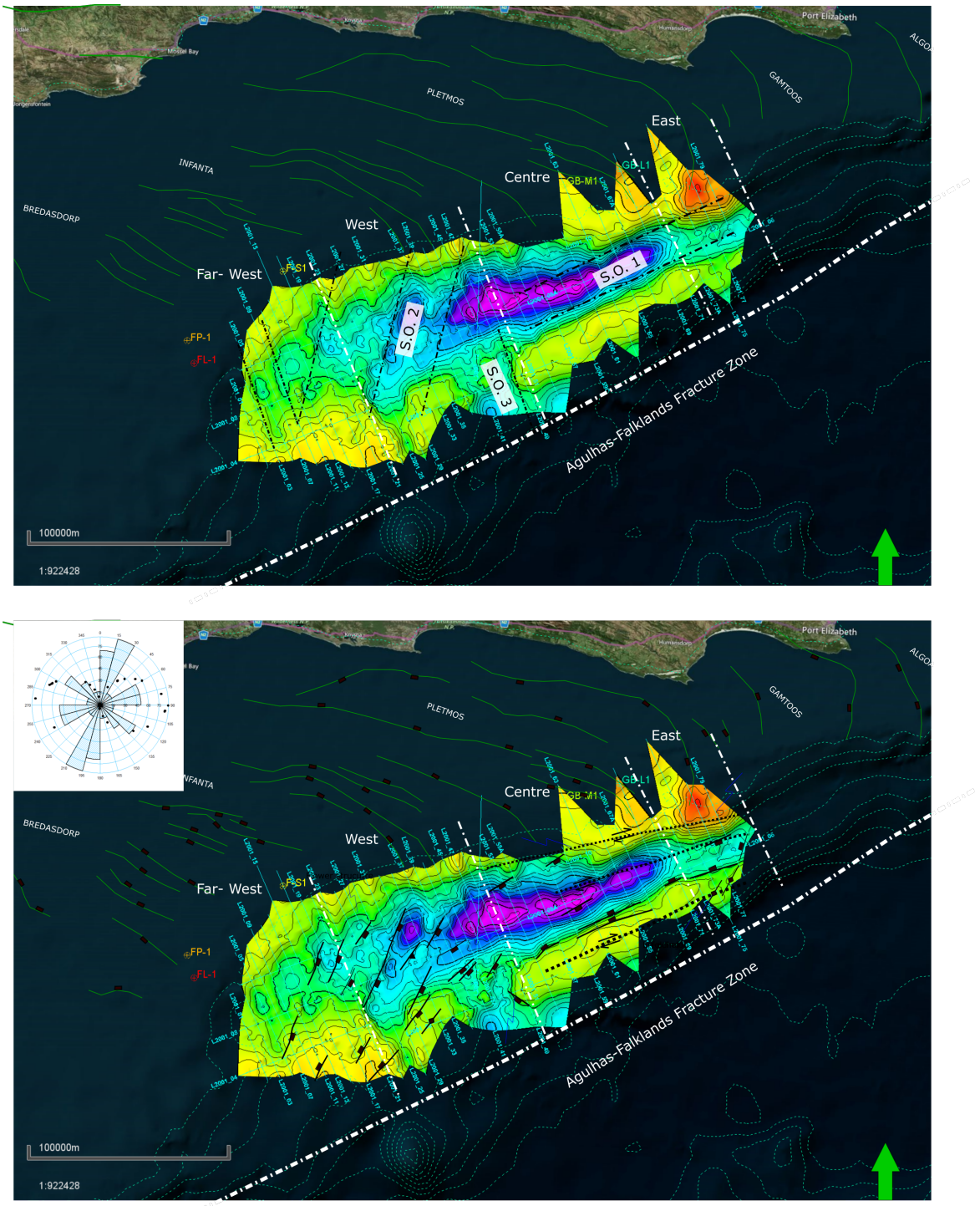


Fig. 5.3 A) The mapped base unconformity (BR - refer to Chapter 4.1) surface is shown, overlain by the observed structural trends and basinal regions in plan view. The structural trends were mapped using the morphological variations in the horizon governed by the inferred existence of faults. B) The mapped faults of this study, in black, are digitised onto the BR surface as well as their corresponding orientations quantified using inset rose-diagram. Shelf area faults were digitised from literature and are shown in green (Broad et al., 2006; Brown et al., 1995; Roux, 1997).

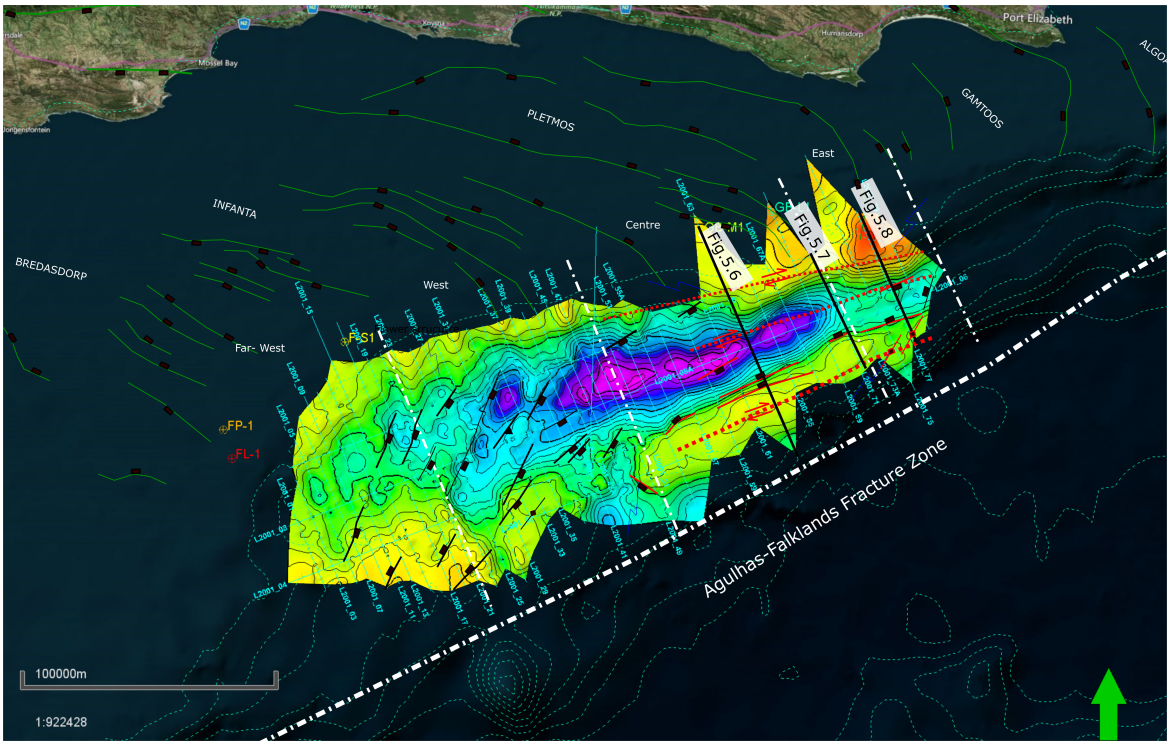


Fig. 5.4 Shows the: A) Mapped BR surface and faults in the Southern Outeniqua Basin. Faults which are in the S.O. 1 orientation are highlighted in red with corresponding seismic lines interpreted in Figs. 5.6-8.

Strike slip faults

Near-vertical faults in S.O.1 display both a normal and reverse sense of displacement and have been mapped across portions of the entire basin (compare Fig. 5.6 to Fig. 5.7). The paleo-highs on the shelf side of the basin, such as the St. Francis basement arch (Fig. 5.6) are affected by the transpressional nature of the movement along these faults seen in the uplifted reflector geometries. An additional, sub-parallel, ca. 20km long strike slip fault trace is mapped in the eastern part of the area with the fault found to be propagating through the middle of the basin. The uplift of the basement arch and parts of the DMR shows the transpression and folding of strata due to the dextral strike slip fault, inferred from the regional context (Fig. 5.8). These faults do not originate from reactivated basement normal faults and appear to constitute a separate family of deformational structures. Along

with the transpressive folding associated with these faults, pop up structures have also been mapped on corresponding seismic lines (Fig. 5.7). Flower structures are prevalent, especially in the eastern part of the basin, where the strata are uplifted and show a reverse sense of displacement. Strike slip faults in S.O.1 are also seen in the central part of the basin, displaying an extensional mode of deformation leading to negative flower structures which interact with the growth faults found on the shelf-break (Fig. 5.6).

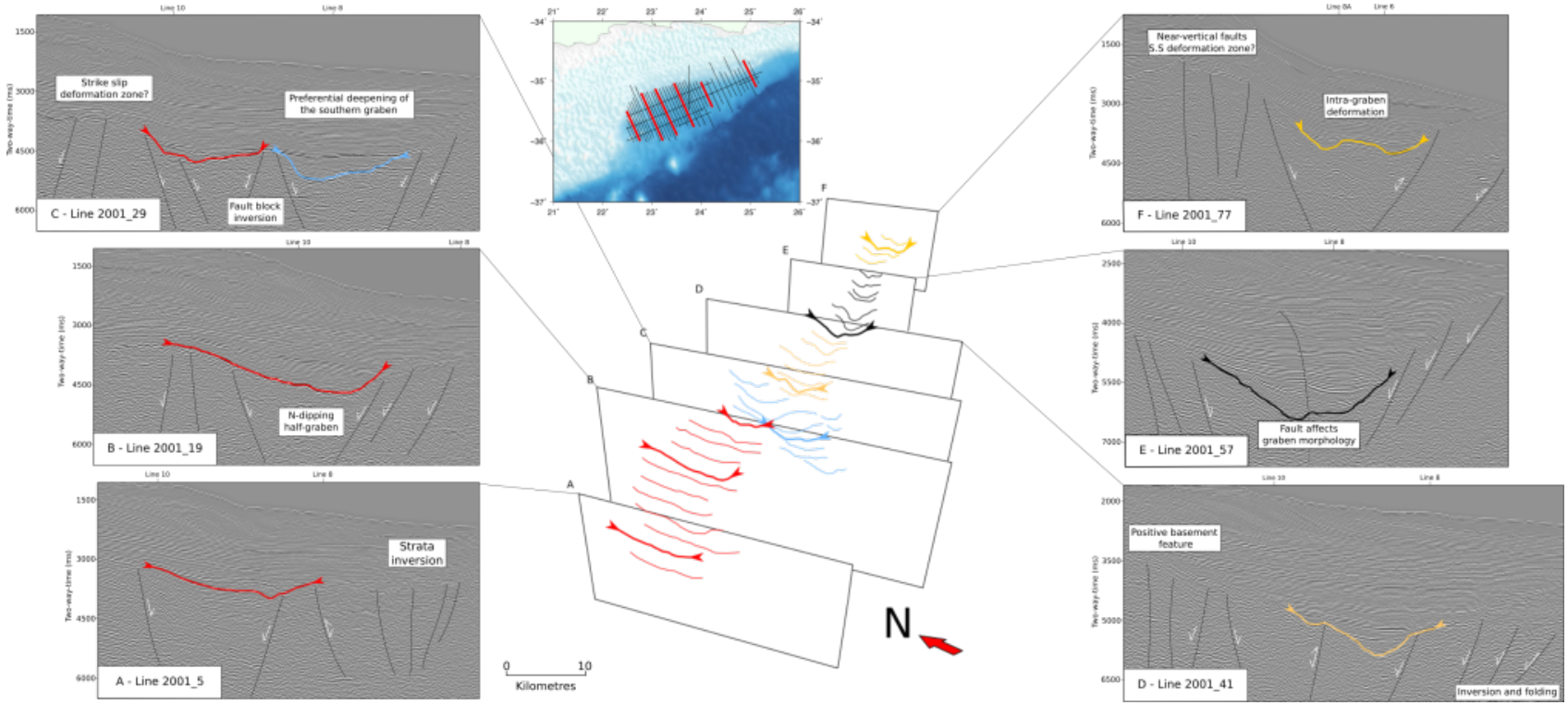


Fig. 5.5 Shows the: The mapped Graben geometries along the strike of the Southern Outeniqua basin. The general trend of the graben is in a NE-SW orientation with a complicating geometry in a NNE-SSW orientation caused by normal faults i that developed during the opening of the Weddell Sea at ca. 147Ma.

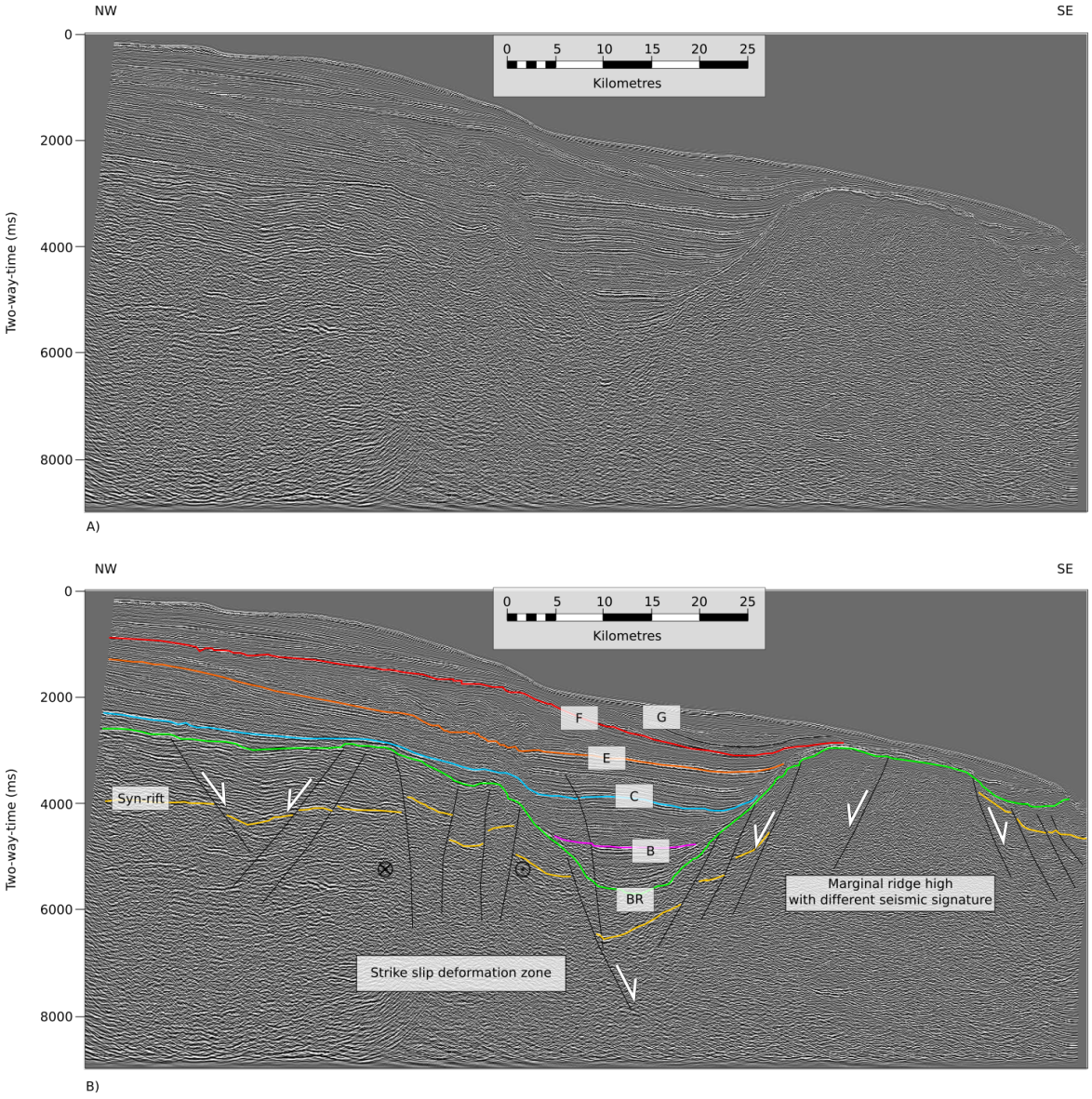


Fig. 5.6 A) Seismic line 2001-63, in the central sector. B) Interpreted line with major stratigraphic horizons and faults annotated; shows the NE-SW trending DMR bounding faults as well as a strike slip fault zone and secondary intra-basinal strike slip fault. See Fig. 5.4 for location.

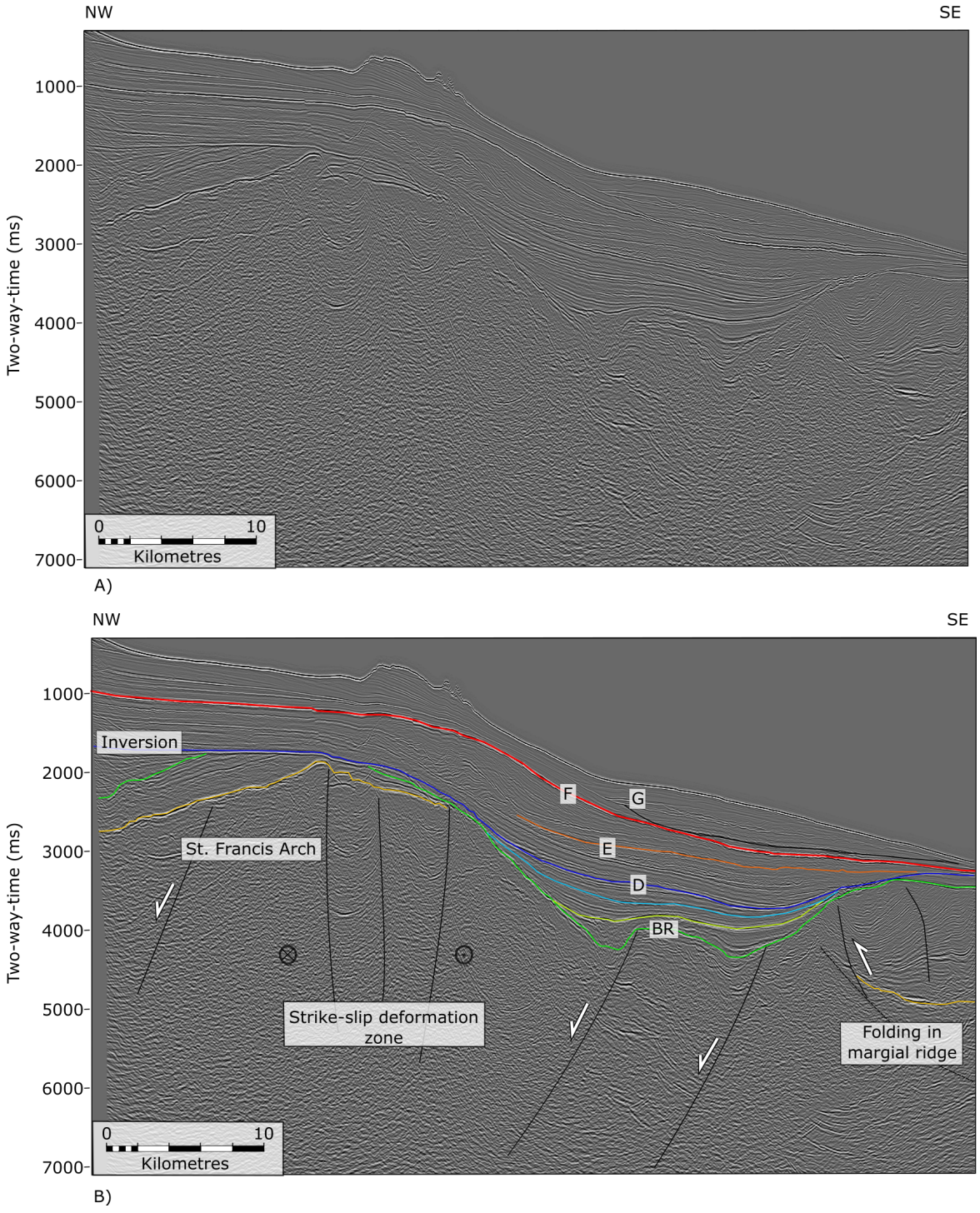


Fig. 5.7 Seismic line 2001-77, in the eastern sector. The interpreted seismic line indicates the second-order stratigraphic unconformities as well as major faults. The large displacement syn-rift fault defines the overall geometry of the basin in this area with smaller, planar-normal faults creating the northern and southern graben seen in the BR reflector interpretation.

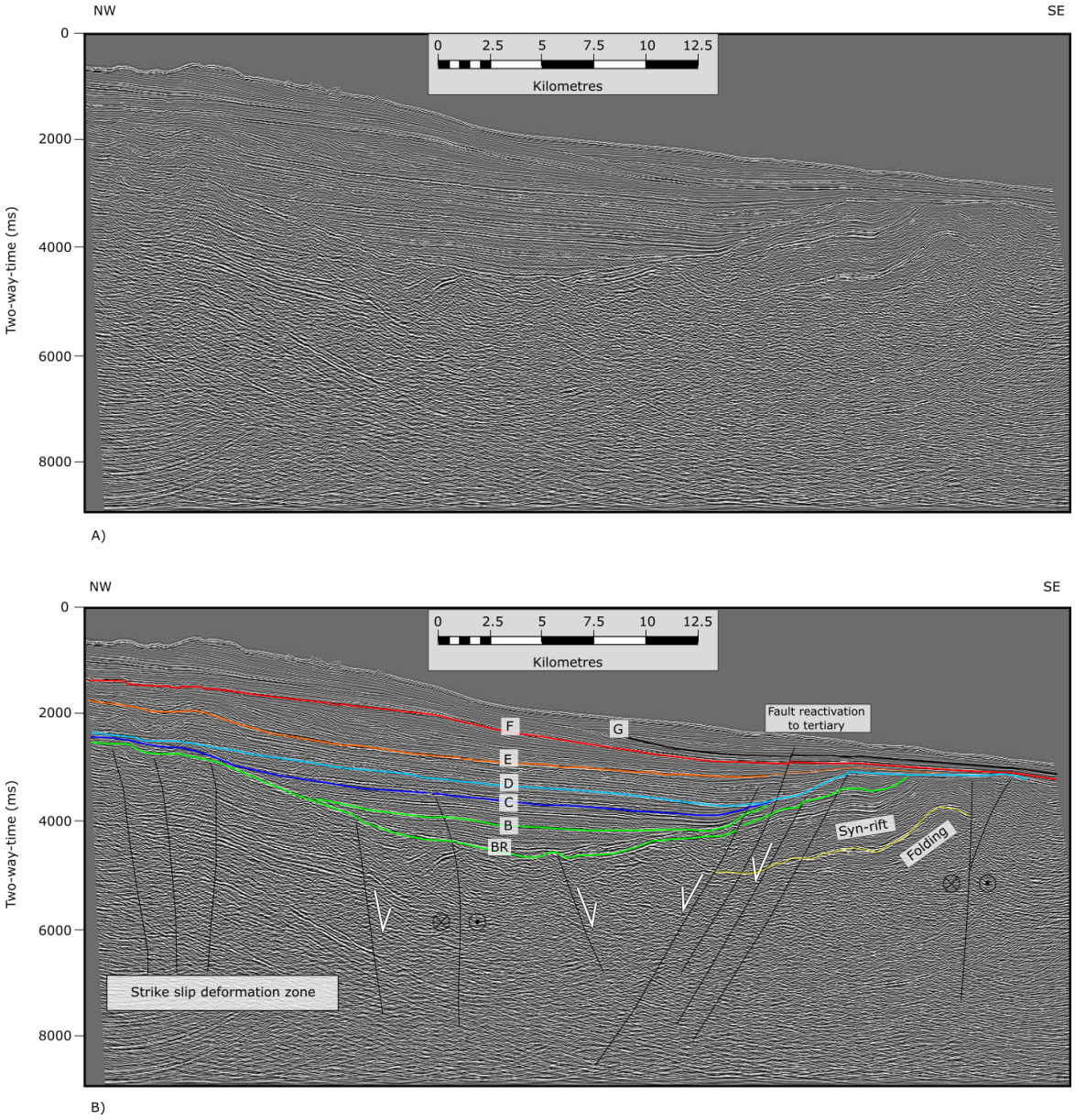


Fig. 5.8 Seismic line 2001-71, in the eastern sector. Faults displaying normal and strike slips sense of displacement, with associated folding, found within the basement and syn-kinematic strata. Reactivation of faults to the Tertiary is seen above the shoulder of the Diaz Marginal Ridge segment to the south of the basin.

5.2.2 Structural Orientation 2: NNE-SSW (020-040)

Normal faults

Faults with a NNW-SSE orientation were mapped from the break-up unconformity reflector surface (Chapter 4. Fig. 4.1). These planar normal faults dip to ESE and define the graben structure within the basin. The geometries of the syn-rift reflectors that are defined by the faults, show rotation of the fault blocks as the basin developed (Fig. 5.10). The graben, mapped by the BR reflector, are filled with sediments, from between the syn-rift and B reflectors, that form distinct wedge geometries (Fig. 5.11). This implies that these sediments were deposited during active extension and rifting till after the deposition of reflector B, inferred to be Hauterivian in age (see Chapter 4). These form a series of en-echelon and eventually linking segments that bound the major NNE-SSW graben morphology (Fig. 5.12). The slip along the faults increases from approximately 500ms to 1s TWT from the SW towards the NE, with the deepest graben occurring in the centre of the basin. Rotation is evident with the formation of an intra-graben high in the southern side of the western sector of the basin. There is some evidence for inversion of some of these fault planes in the form of folding of the syn-rift, BR and B reflectors (Fig. 5.11).

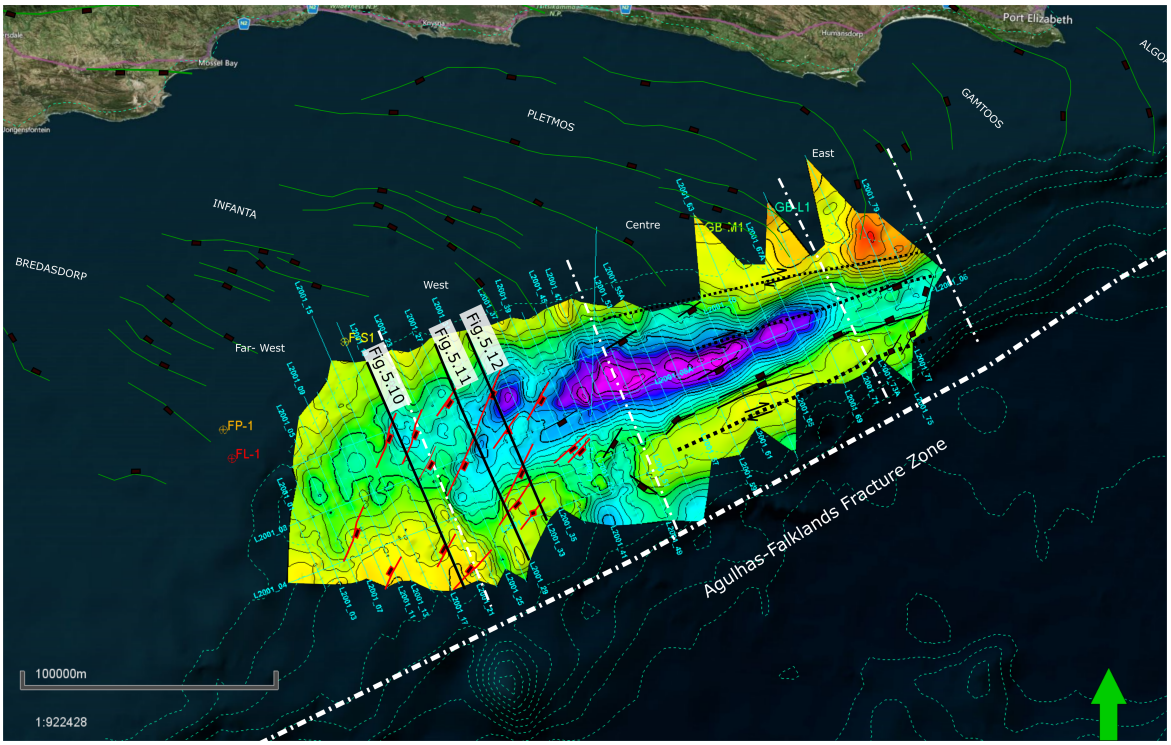


Fig. 5.9 Faults that are mapped within structural orientation 2 are highlighted in red. Individual seismic lines which show the mapped faults are presented as Figs. 5.10-12.

Strike slip faults

Strike slip faults were not observed in S.O.2 . This could be due to the fact that the seismic lines would be highly oblique to the strike direction of the potential faults and consequently near vertical strike slip faults would be difficult to image.

5.2.3 Structural Orientation 3: NW-SE (135-155)

Normal faults

This structural trend is only tentatively identified from a single mappable fault found in the southern part of the western sector of the basin (Fig. 5.14). This fault seems to be important because it truncates the DMR, creating a NW-SE orientated depression, and thus is inferred to be a major deformation geometry regarding the evolution of the basin. The

major basin defining fault and tentative antithetic partner that produced the graben display variations in throw, >500ms and 300ms, dipping to the SW and NE respectively. Hanging-wall strata that bound the fault suggest evidence for later deformation, fault block rotation and inversion during the transition phase between the rift and post-rift reflectors, syn-rift and BR respectively (Fig. 5.14). The continuation of these intra-graben faults is not seen on the adjacent line given that faults in S.O.1 truncate the basinal margin of the depression (Fig. 5.16).

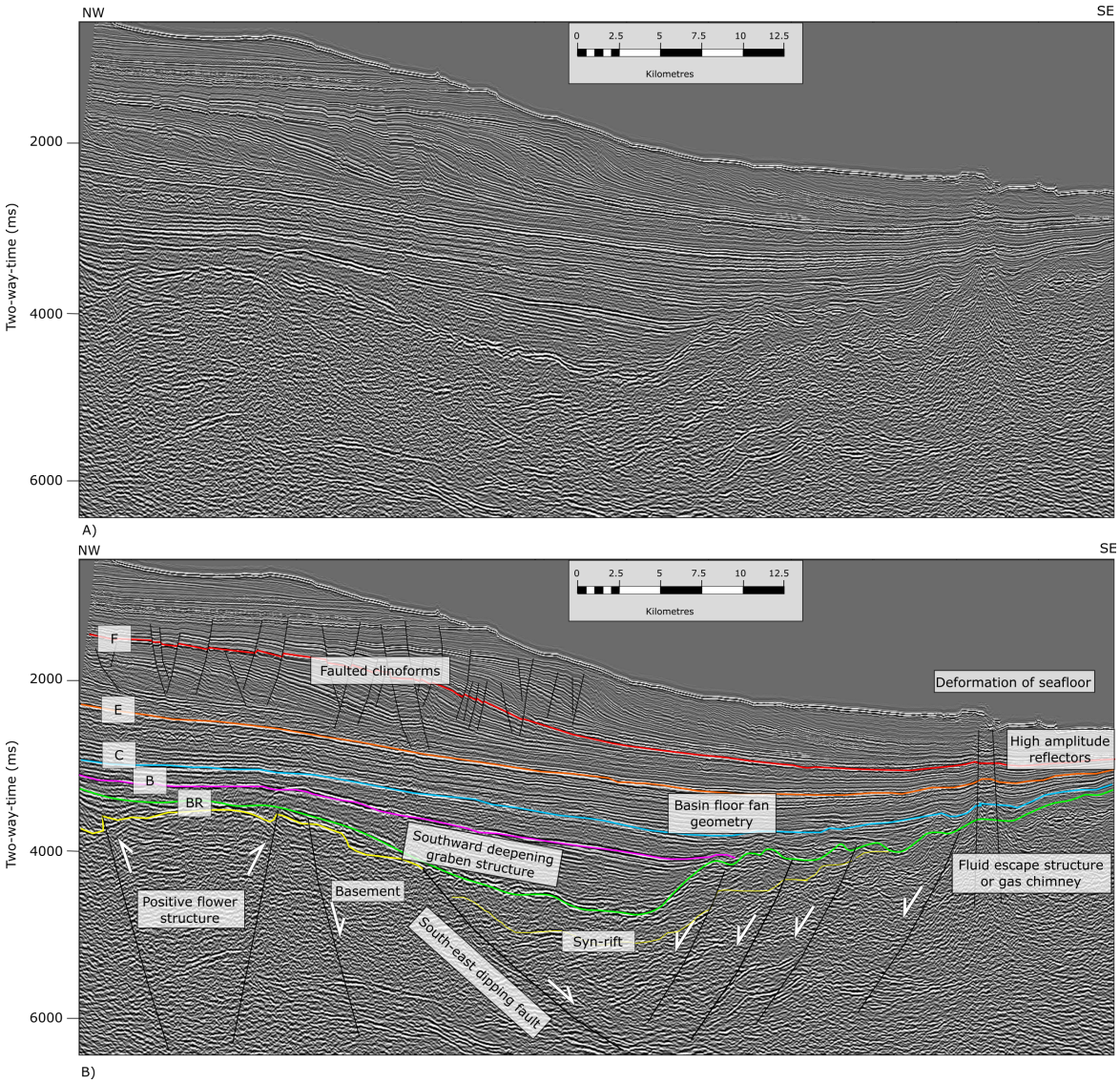


Fig. 5.10 Seismic line 2001-19, in the western sector. The interpreted section shows the block rotation and half-graben deepening to the south of the basin.

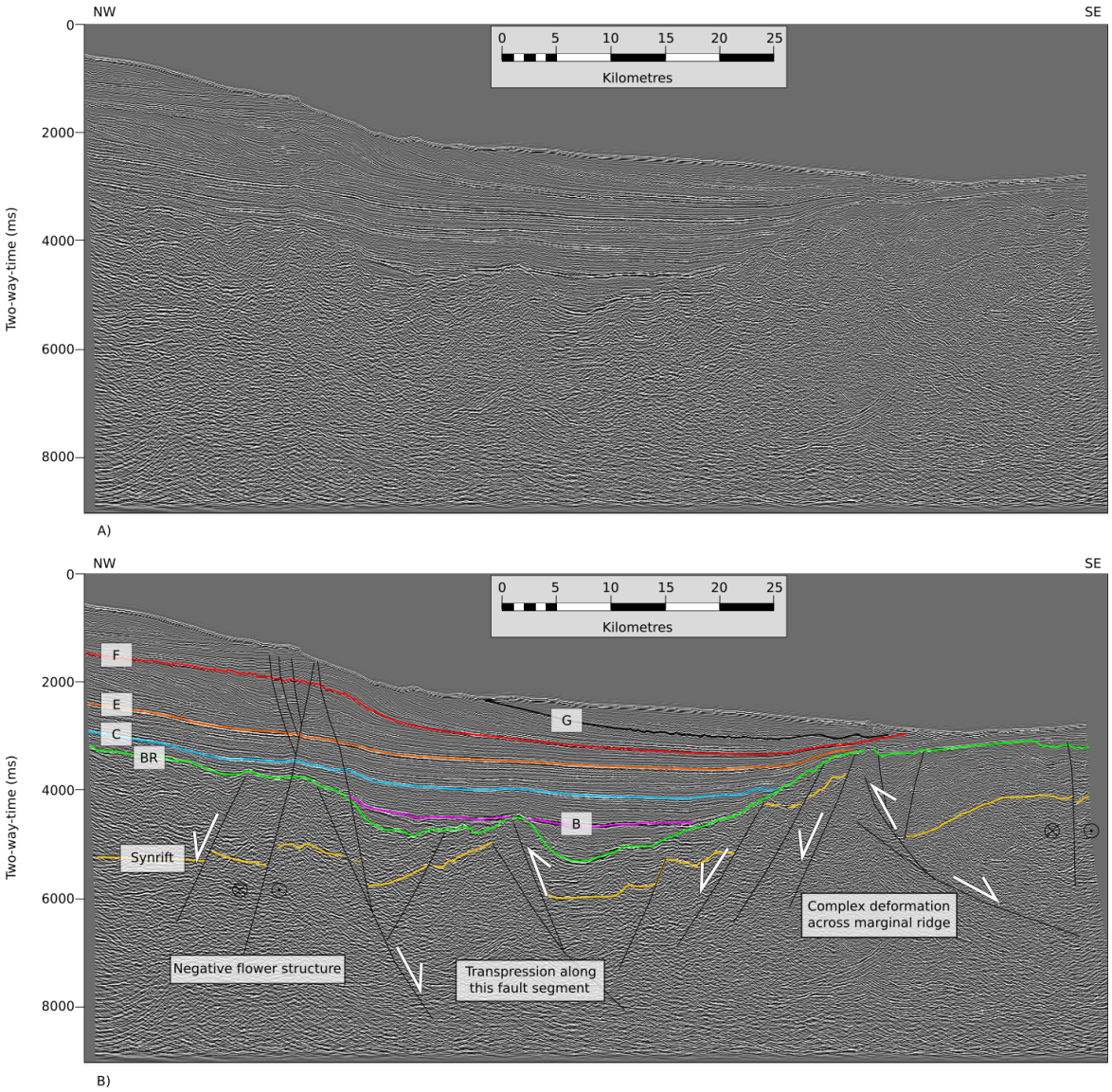


Fig. 5.11 Seismic line 2001-29, in the western sector. Showing block rotation and two half-grabens deepening towards the DMR to the south. A ca. 15km long S.O.1 strike slip fault can be seen propagating on the northern side of the basin where it deforms and interacts with the growth faults in this region.

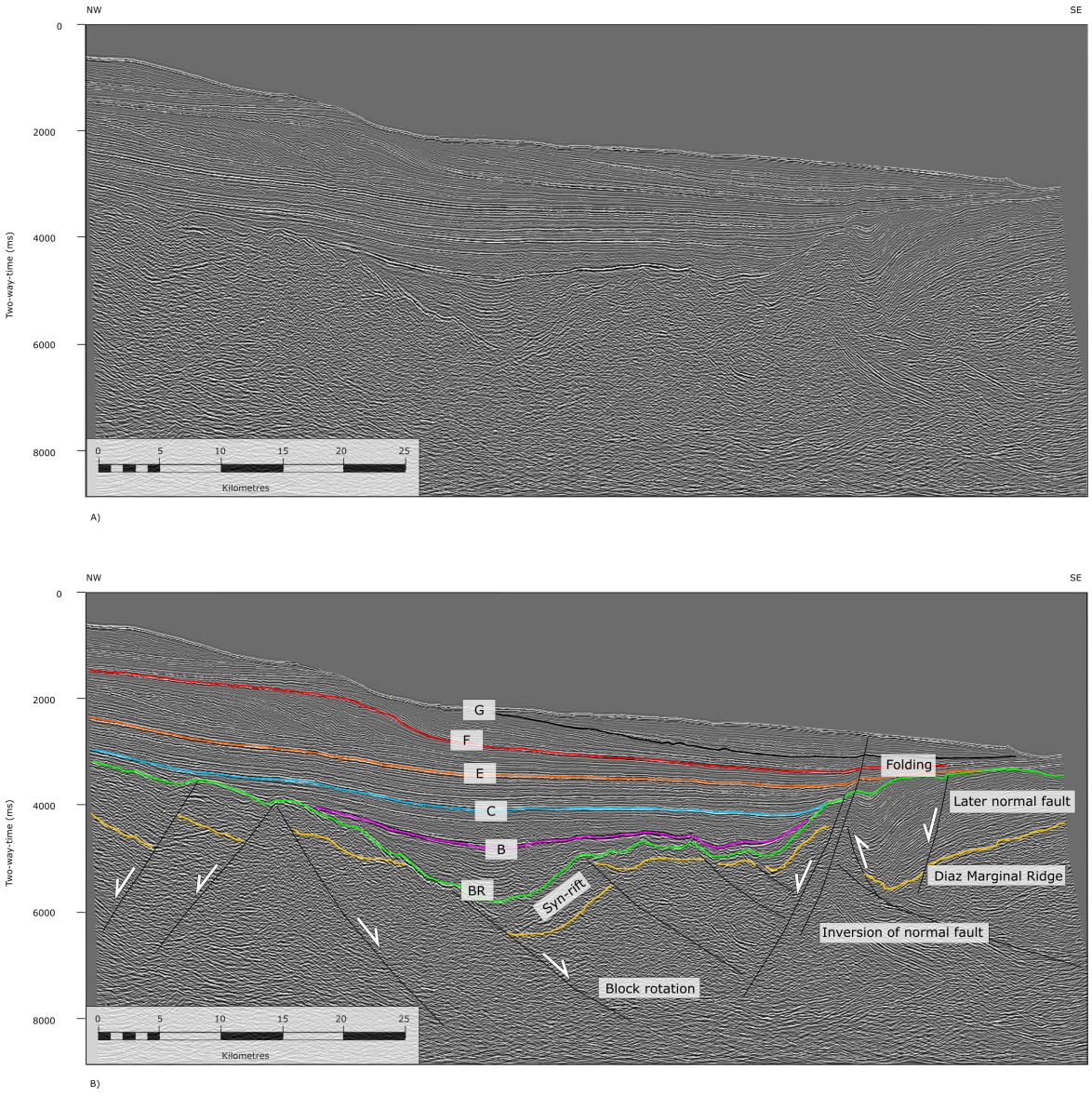


Fig. 5.12 Seismic line 2001-33, in the western sector. Shows block rotation and a half-graben deepening towards the southern part of the basin.

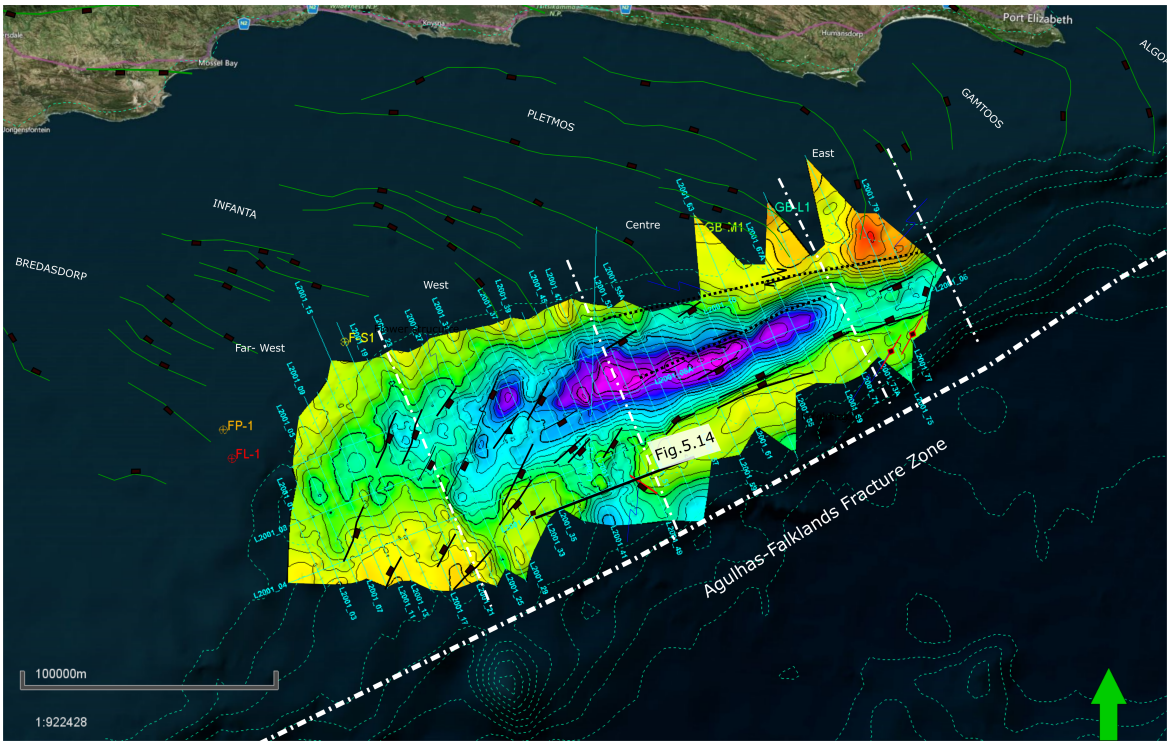


Fig. 5.13 Faults that are mapped within structural orientation 3 are highlighted in red. An individual seismic line, L2001-2, which shows the mapped fault is presented as Fig. 5.14.

5.3 Variation in basin morphology along strike

The study area appears to be separated into four major structural domains; the far-west, west, central and east structural provinces, each having been affected by varying extents and orientations of deformation. The time structure map of the BR- reflector has been annotated to show the four domains as well as the corresponding seismic section figures which highlight the variations in the basin morphology along strike (Fig. 5.16).

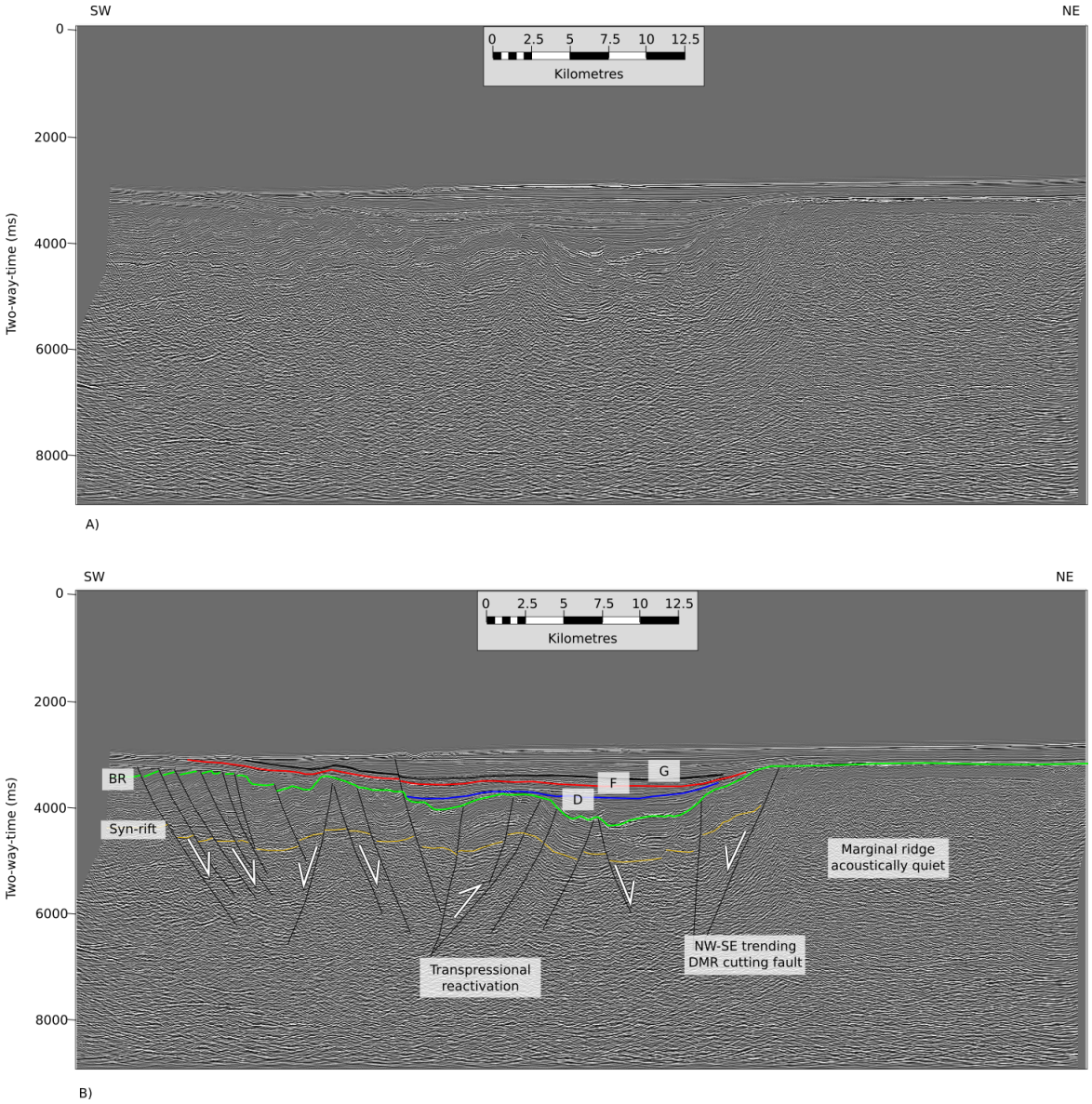


Fig. 5.14 Seismic line 2001-2 in the western sector. The single mapped fault trending in S.O.3 truncates the shoulder of the DMR in the NE of the section, with syn-rift strata being deposited in the subsequently generated accommodation space. Also visible is the deformed and inverted BR surface towards the SW of the section with multiple later generation faults cutting this unit.

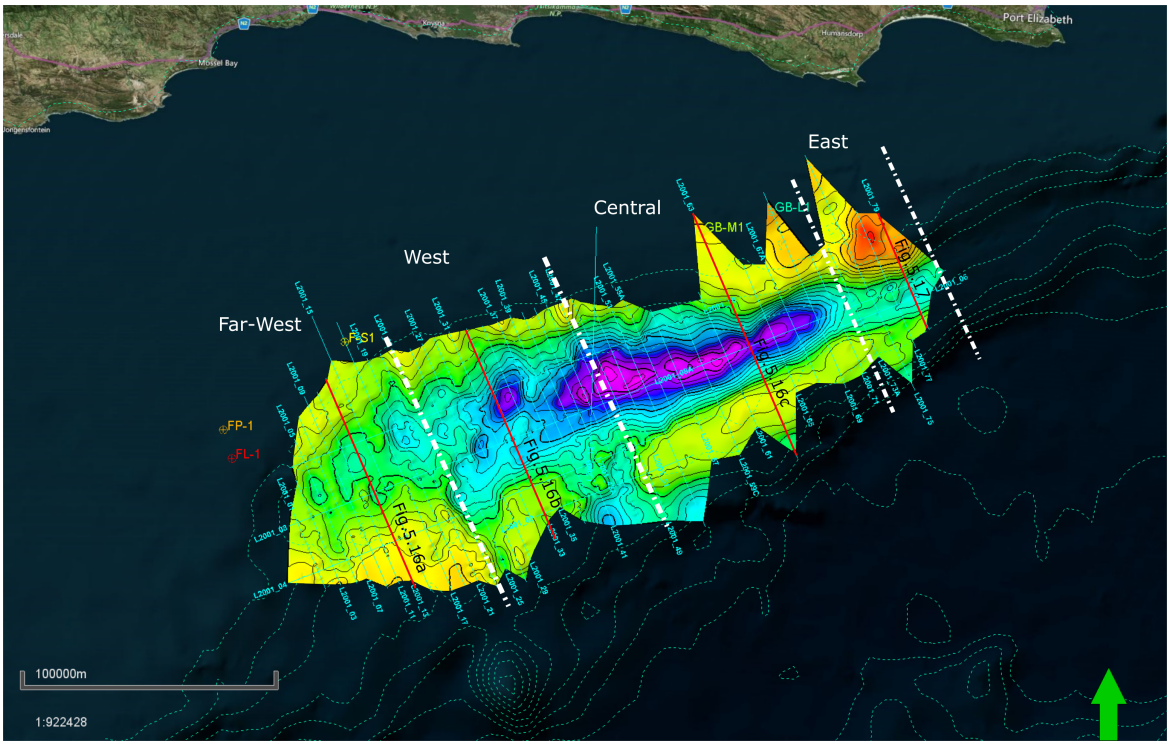


Fig. 5.15 A) The annotated BR-surface time structure map shows the location of figures, labelled Fig. 5.16a-c and Fig. 5.17, chosen in order to display the variation in basin morphology along strike.

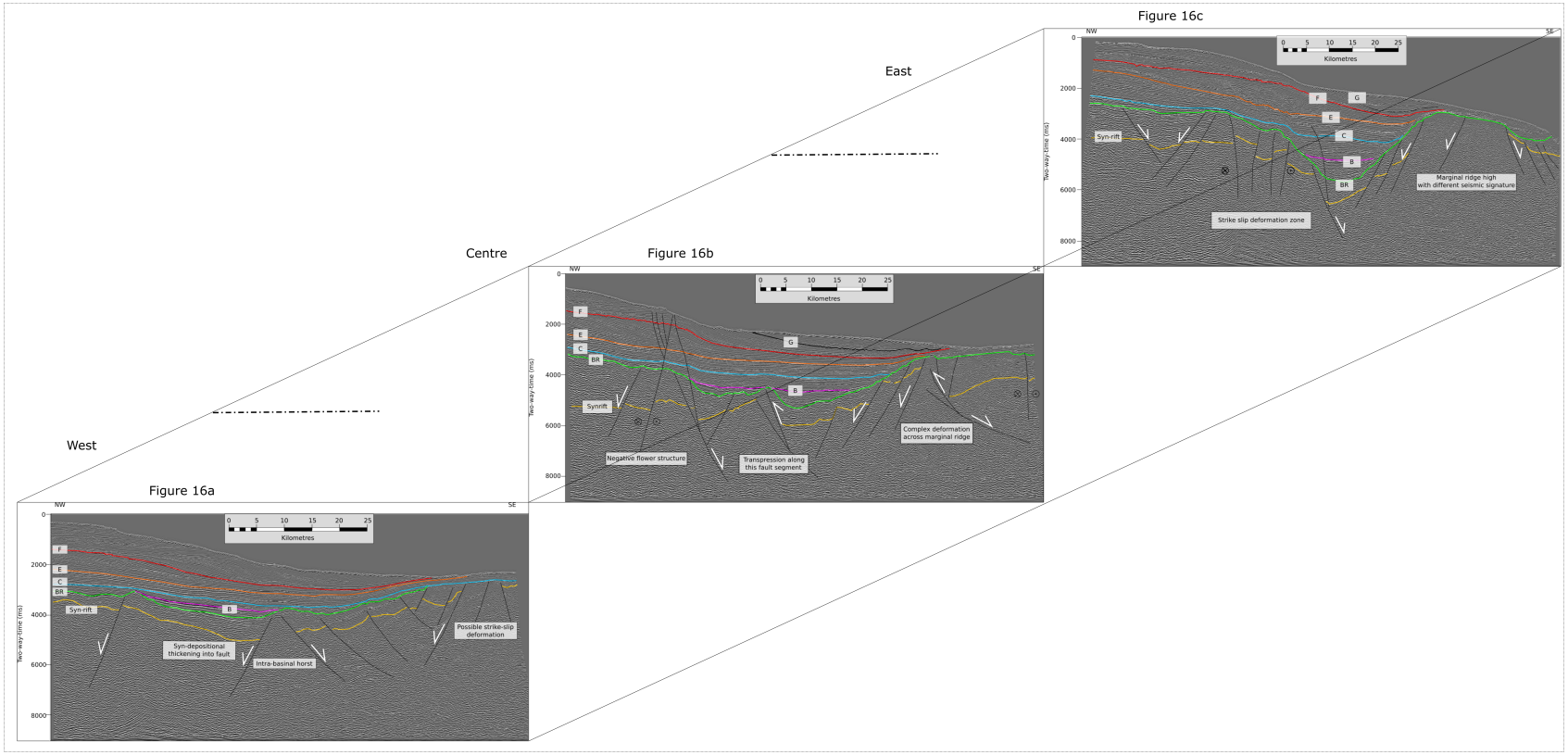


Fig. 5.16 This figure shows: Interpreted seismic sections along the basin strike, with locations for Figs. 5.16a-c. A noticeable increase in deformation complexity can be seen towards the western, central and eastern sectors of the basin.

5.3.1 Far-West

The morphology of the western part of the basin changes from the SW to the NE (Fig. 5.16). The extreme west of the basin is dominated by a shallow graben morphology which deepens and eventually bifurcates into two separate graben, a small, 4 kilometre wide, southern graben and a larger, 10km wide northern graben, separated by an intra-graben basement high (Fig. 5.16a) . This larger northern graben widens and deepens, up to 1.5s TWT, towards the north-east; it is bound by a large displacement, approximately 500ms TWT, normal fault in S.O.2 as well as smaller antithetic normal faults trending in S.O.1 (Fig. 5.17). The syn-rift strata seen in the graben again show a distinct wedge shaped character as well as being deformed by normal faulting. The post-break up unconformity surface, reflector BR, reveals a broad and relatively shallow basin with the half grabens being overlain by sediments up to 1.5 TWT. The major deformation in this region seems to be confined to the sediments below the final break-up unconformity, however evidence for inversion is found over the southern flank of the DMR, between the Lower Campanian and Lower Maastrichtian, where post-rift sediments have experienced folding and reverse faulting (Fig. 5.18). The depth to basement in this area is shallowest with a number of intra-basinal highs defining the geometries of the graben and half-graben structures imaged in the basin.

5.3.2 West

The structural architecture in this region is dominated by S.O.2; constituting large displacement ENE-WSW trending, normal faults in the shelf-bounding basement arch on the northern flank and the DMR, on the southern flank (Fig. 5.10) . Tentative evidence for strike-slip related compression can be seen in the low amplitude folding that appears to be present within the arch. In general, sediments seem to be absent or not easily interpreted in this section of the basin. This is illustrated in Figure 5.14 which shows the seismically transparent and chaotic signature seen within the ridge. Gentle folding of the hanging-wall strata on

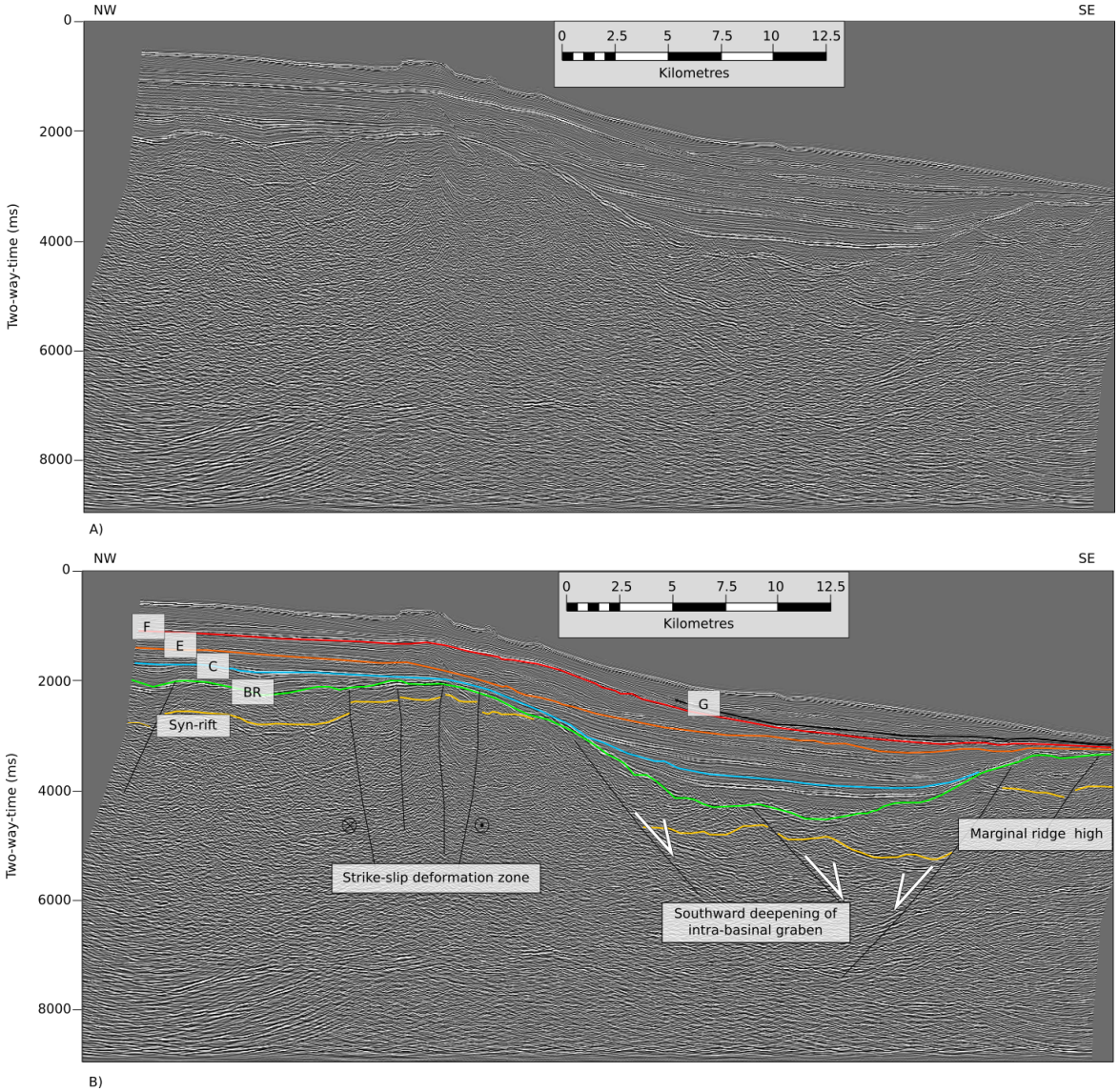


Fig. 5.17 A) Seismic Line 2001-79, in the eastern sector. The interpreted section with major structural and stratigraphic relationships highlighted, showing the folding and faulting of basement arches and the DMR across the basin profile. For reflector ages refer back to stratigraphy section.

the southern flank of the graben, towards the DMR, seems to suggest structural inversion has taken place between horizon BR and horizon C, interpreted to be Valanginain to Aptian in age (Fig. 5.12). Indications of folding and flower structures in the sediments in the shelf side of the the basin are imaged, where the faults seem to be reactivated from the previously deformed basement (Fig. 5.11). Strata within syn-rift are highly folded along

pre-existing fault planes on the flank of the DMR in the southern part of the western sector, supporting the interpretation of inversion. These folds were mapped and form a NE-SW, en-echelon series of anticlines and synclines in the eroded rift and post-rift strata (Fig. 5.12). Folding of the syn-rift strata is observed in the previous figure and suggests the DMR had experienced compression post syn-rift deposition, inferred to be Valanginian in age. A large, near-vertical fault with a normal sense of displacement on the southern side of the trace, is seen to propagate through the basement high on the shelf-side of the basin. Deformation in this region is not confined to the rift and immediate post-rift strata, with the reactivation of basement faults observed on the northern flank of the DMR seen propagating into sediments of Tertiary age (Fig. 5.11). Basement topography in this area is variable - alternating between shallow and wide in the shelf-side of the basin and deep and narrow in the seaward part of the basin bound by the northern shoulder of the DMR.

5.3.3 Centre

The sector designated 'centre' is marked by a single deep, ≈5000ms TWT, and narrow, ≈20km, graben trending in S.O.1 (Fig. 5.19). The major graben bounding faults have been concentrated to the shoulders of the uplifted basement arches and, topographically higher, DMR on the shelf and seaward-sides of the basin respectively. The DMR in this region is structurally more competent with large displacement, greater than 1.5s TWT, normal faults concentrating deformation and creating a deeper basin than anywhere elsewhere along the basin strike. The basement arches, faulted by both normal and strike slip faults, are uplifted by the transpressional strike slip zone which propagates along S.O.1. Inboard of the faulted and uplifted basement arches, sediments deposited prior to reflector C, have been folded and deposited behind the raised basement thereby restricting communication between the shelf basins with the main Southern Outeniqua Basin in this region (Fig. 5.19).

5.3.4 East

In the eastern sector, the basin is floored by a major half-graben bound, to the south by a large-displacement NW dipping normal fault running along the flank of the DMR (Fig. 5.20). Syn-rift sediments form a sedimentary wedge that thickens to the south and reaches a maximum thickness of approximately 800ms TWT. The DMR flanks are defined by normal faults, however evidence for inversion and compression is present in the folded and faulted unit 2 strata, that defines the upper 1.2s TWT of the ridge; refer to figure 6. The graben structure in this area is the narrowest, approximately 10km wide, relative to other regions along the basin strike. The syn-rift strata are shallower than the main basin to the south-west and show a marked increase in folding, uplift and faulting (Fig. 5.12). The basement arches in this region are at a higher elevation than the rest of the basin and are characterised by rotated normal NE-SW trending fault blocks and folded strata. In the rift-border faults of the area, fault-propagation folding may be the cause of the syncline geometry of the hanging-wall strata and the uplift and rotation of footwall block. The strata of unit 2 display a convex downward geometry, with the strata dragging along the fault plane as the propagating fault pushes upwards through the strata (Fig. 5.12). This hanging-wall syncline forms the NE-SW trending, deep, narrow depocentre along the base of the DMR (Fig. 5.12).

The strike slip zone situated along the flanks of the DMR in this region show what appears to be a fault relay system (Fig. 4.16). The timing of fault F1 seen in the figure seems to suggest it was the first to initiate thereby creating accommodation space for the deposition of strata between reflectors C and E. Fault F2 is then inferred to have initiated after F1 as it can be seen to have displaced these sediments down to the NW. The propagation of faults through the basement lithology is imaged by a series of large displacement normal faults whose geometries are confined by the competent rheology of the basement but are seen to diverge and form a wider zone of distributed deformation in the younger sediments, deposited above reflector E, above the marginal ridge high (Fig. 5.16c).

5.4 Diaz Marginal Ridge

The seismic character seen along the trend, sub-parallel to S.O.1, of the DMR varies significantly across the strike of the basin.In the eastern sector of the basin, the marginal ridge high is formed by large displacement, S.O.2 trending, rotated normal faults. The morphology of the shoulders of the DMR is subsequently defined on its northern and southern extremities by a later generation of normal faults that trend in S.O.1. In the central and parts of the western sectors in the basin, the marginal ridge displays a different, acoustically quieter, seismic character and is visibly defined on its extremities by large displacement normal faults (Fig. 5.19). Subsequent minor displacement faulting is seen to deform the middle of the ridge with normal faults trending in S.O.1 with a throw to the NW (Fig. 5.19). In the western part of the basin, the marginal ridge is less topographically pronounced and has a seismic character that appears to be made up of syn-rift strata.

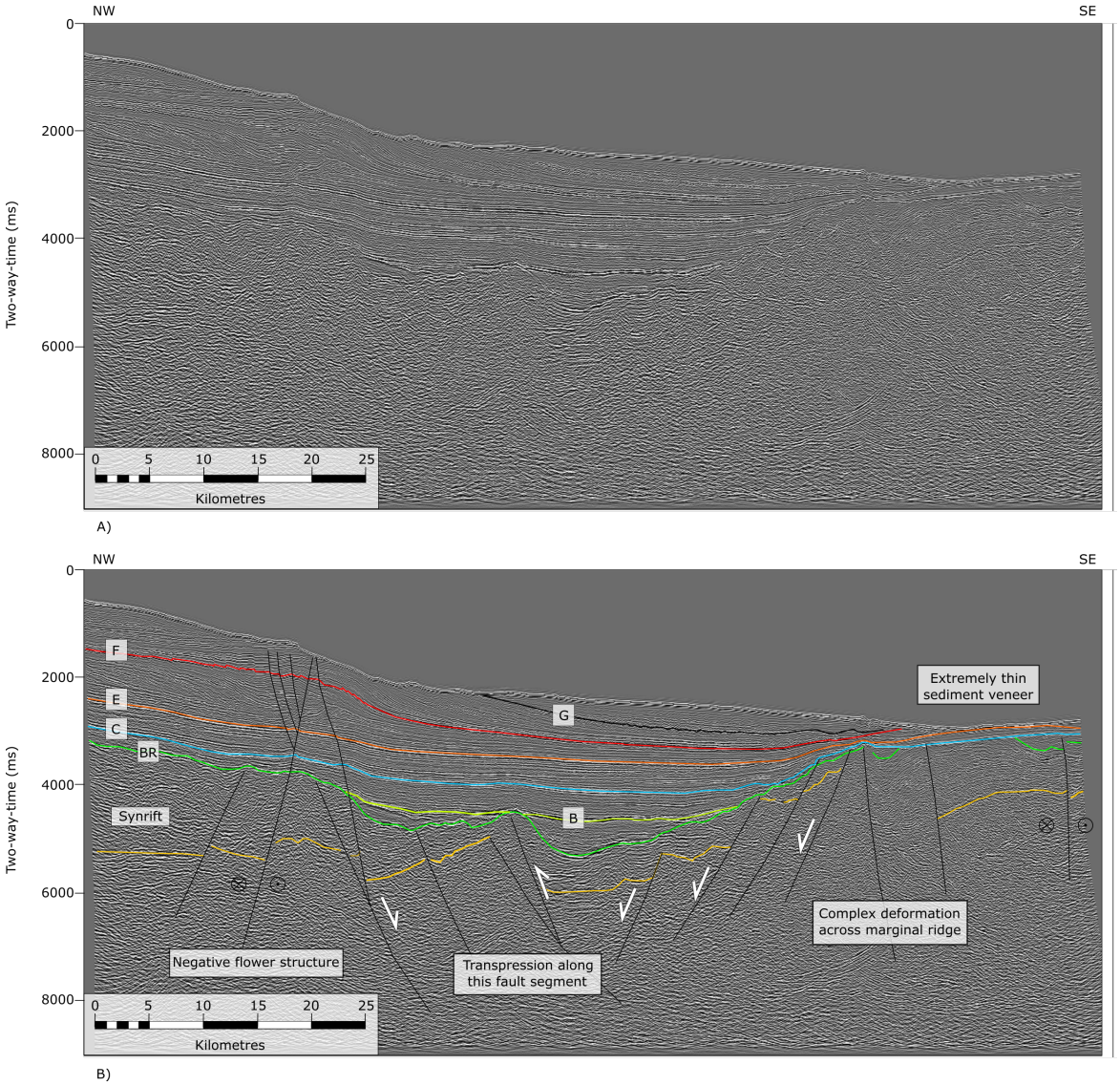


Fig. 5.18 Seismic line 2001-29, in the western sector. Interpreted seismic section shows the tight concave geometry of reflector G as it approaches the DMR high.

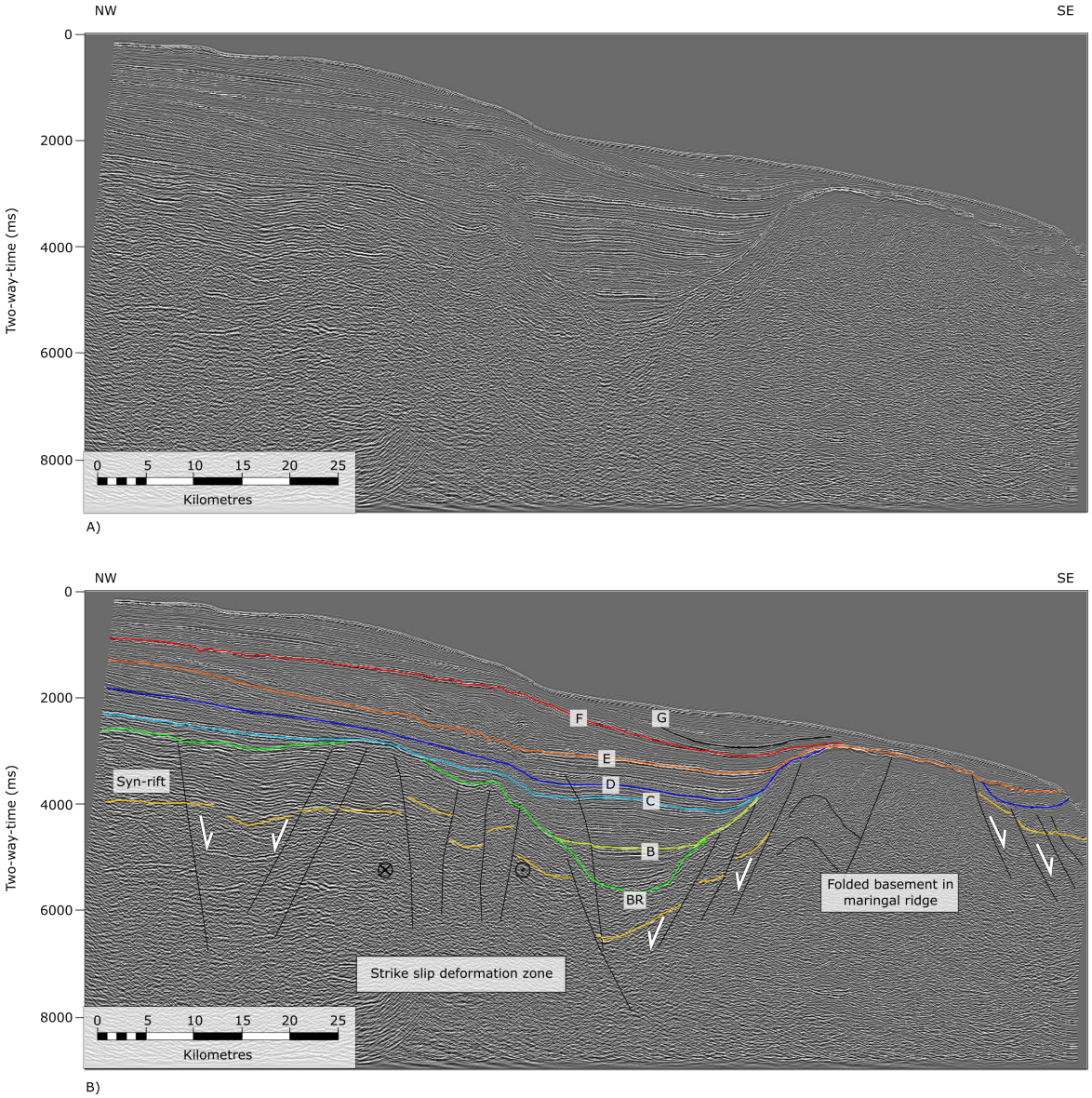


Fig. 5.19 Seismic line 2001-63, in the central sector. Interpreted seismic section shows the major strike-slip zone that is present in the northern part of the central sector.

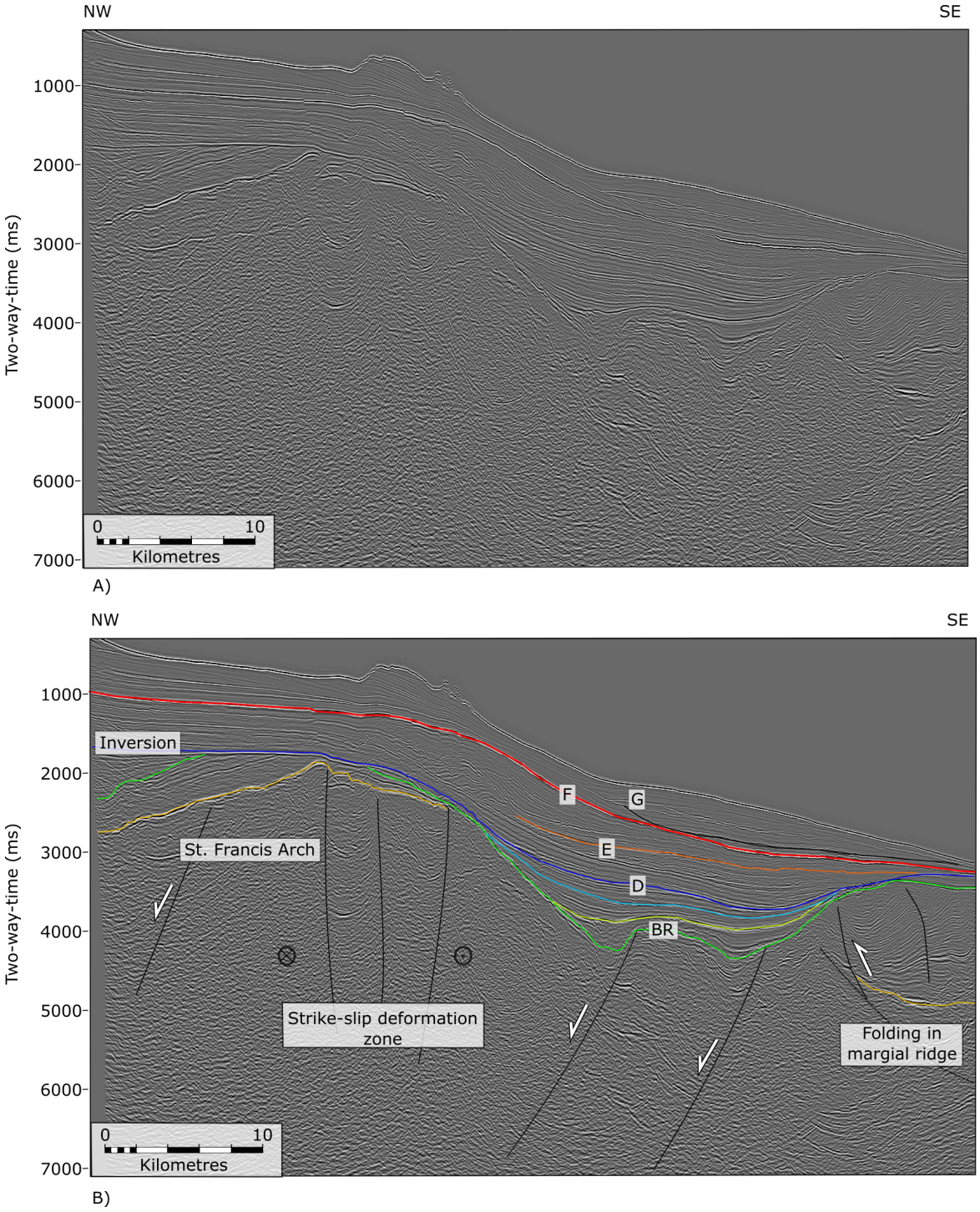


Fig. 5.20 .Seismic line 2001-77, in the eastern sector. Interpreted seismic section shows normal slip along portions of the syn-rift faults and inversion on the upper segments.

5.5 Growth faults

Shoreline progradation in the shallow waters leads to an outward extension of sediments on the slope, which is in turn, affected by the gravity driven collapse of the underlying sediments. Growth faults are visible on the slope in the central sector of the Southern Outeniqua Basin with a combination of regional (basin dipping) and counter-regional (landward dipping), NE-SW trending faults (Fig. 5.21). Some of the faults are large enough as to be traced across the seismic lines and are observed with vertical displacements of between 50 and 200ms TWT (Fig. 5.10). The largest growth faults intersect reflector C, inferred to be Aptian in age, whilst most are confined to interval between reflector E and G, Campanian - Tertiary (93-66Ma). A feature of the growth faults, seen only one seismic line, is interpreted where the faults seem to intersect a detachment surface and become more curved, leading to small scale toe-thrusts, with a wavelength of 400m and an amplitude of 200ms TWT, that develop in response to the vertical slip along the fault (Fig. 5.11).

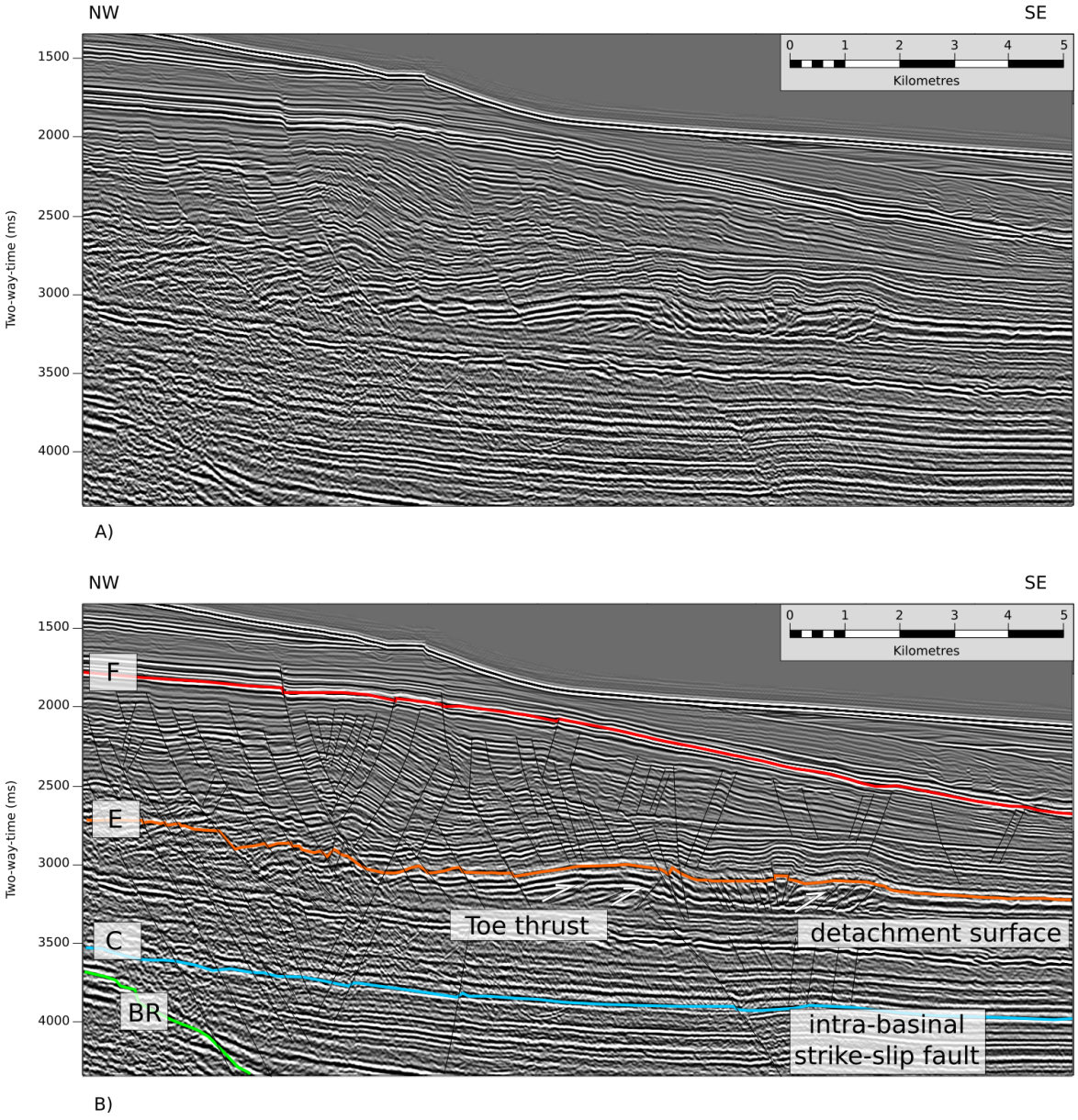


Fig. 5.21 Seismic line L2001-61, in the central sector. The interpreted section highlights the complex growth fault deformation seen along the shelf-side of the basin.

5.6 Summary

The Southern Outeniqua Basin seems to be compartmentalised into two major terrains, consisting of four sub-zoned areas, along its NE-SW trend. A marked change in the deformation which affects the basin occurs in the central zone of the basin with the basement displaying pronounced deepening towards the NE. The structural orientations in this terrain (East and Far-East) generally are orientated 045-065, approximately NE-SW, sub-parallel to the trend of the adjacent Agulhas Falklands Fracture Zone (AFFZ) (Ben Avraham et al., 1997). The oldest faults in this terrain are seen to have concentrated on the shoulder of the Diaz Marginal Ridge with the majority of slip, of the order of 100's of ms TWT, occurring basin-wards with minor deformation evident on the outboard, AFFZ side, of the DMR with a maximum slip of approximately 200ms. (Fig. 5.11). Younger faults which cross-cut or are reactivated from older fault surfaces, such as the strike-slip faults seen in the region, also trend in S.O.1 (045-065); deform existing graben structures as can be seen in the inversion of and infilling beside existing syn-rift strata (Fig.). Old faults in S.O.2 could potentially be present in the basement in this terrain, however poor imaging restricts this interpretation.

The second terrain defined geographically by the far-western and western sectors, shows the oldest, graben-defining, faults oriented in S.O.2 (020-040) and S.O.3. Subsequent faults in S.O.1, truncate these faults and define the sub-parallel nature of the DMR (Fig. 5.12)

Chapter 6

Discussion

6.1 Structural evolution of the Southern Outeniqua Basin

In order to unravel the tectonic and stratigraphic evolution of the Southern Outeniqua Basin, the timing and kinematics of deformation need to be understood in the broader plate tectonic context. This study separates the evolution of the margin into four distinct period of tectonism: 1) Continental rifting between West and West and EastEast Gondwana 2) Continental rifting of West Gondwana, 3) Transcurrent movement along the Agulhas Falklands Fracture Zone, and 4) Passive transform margin development. A series of conceptual cartoons were generated in order to visualise the plate dynamics and associated structures that would be formed during each successive tectonic phase. These structures would then dictate areas of uplift and the generation of accommodation space across the margin through time, which are evaluated against the stratigraphic architecture seen within the basin.

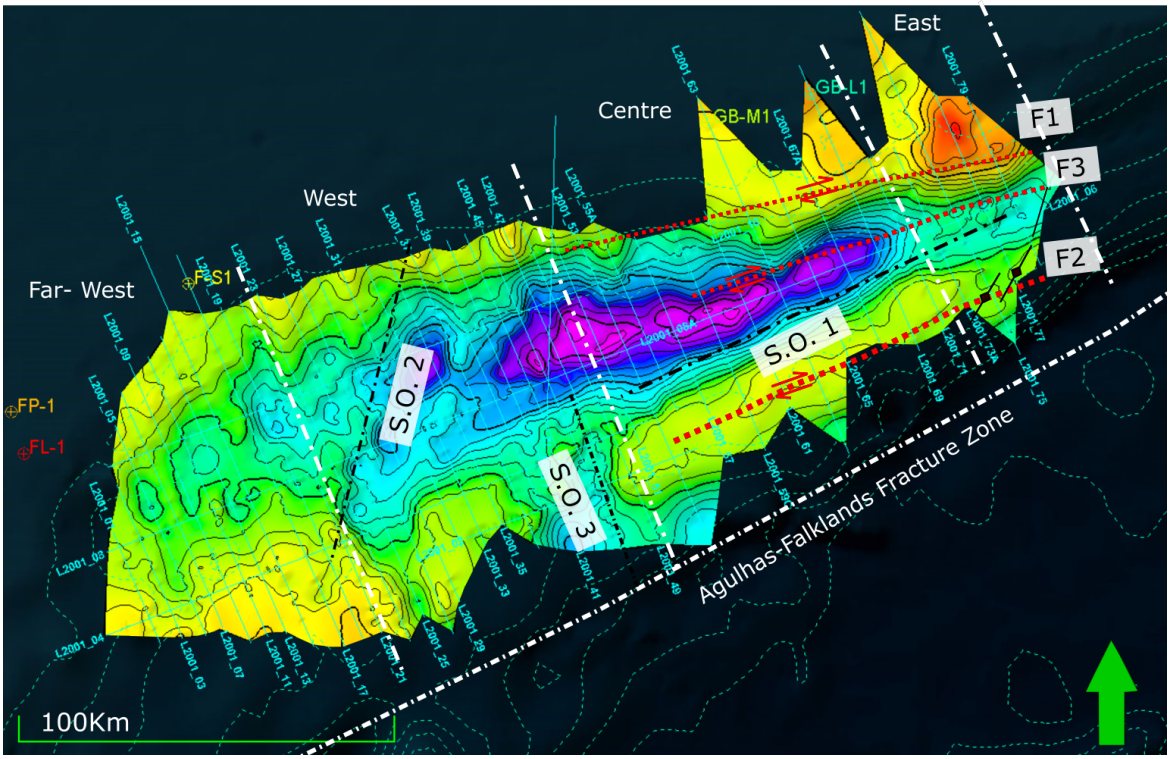


Fig. 6.1 A time structure map of the Valanginian (134Ma) aged unconformity surface, BR, used to illustrate the three depression geometries observed within the basin. The basin has been defined into four sectors given the variation of morphology along strike and are labelled far-west, west, central and east from the SW to NE.

6.1.1 Continental rifting between West-East Gondwana (170 - 150Ma)

The mapping of the BR surface has shown there to be three distinct depression geometries co-existing within the Southern Outeniqua Basin (Fig. 6.1). Based on the relationships of between the faults outlined in Chapter 5, the faults orientated NNE-SSW (S.O. 2) are interpreted to be the oldest (being truncated by a later phase of faults trending NE-SW or S.O. 1) and formed during the initial extension of the basin. The genesis of faults within this orientation is proposed via three models: 1) The faults developed during NW-SE extension that preceded the break-up of West and East Gondwana and incipient formation of the Weddell Sea from the Oxfordian-Valanginian (168-159Ma) (Cooper et al., 2007; Eagles,

2007; Jokat, 2003; König and Jokat, 2006). Evidence for this Early-Jurassic uplift is presented by Thomson et al. (2002) who observed a distinct episode of cooling taking place during the early Jurassic preceding the separation of West and East Gondwana and the formation of the Falklands Plateau Basin. A review of structural orientations in the eastern portion of the conjugate Falklands Plateau Basin has shown a tentative similarity in structures (some faults on the eastern edge of the FPB trend NE-SW (Lorenzo and Mutter, 1988). The orientation of the NNE-SSW trending faults in the western and far-western sectors of the basin however stands in contrast to its proposed conjugate in the western part of the FPB, where faults trend NW-SE (Becker et al., 2012). This discrepancy in fault orientations is explained by the translation of continental slivers along the F1-F3 strike-slip system (Fig. 6.1) before the break-up of the South Atlantic and transcurrent motion of the AFFZ. Data presented by Mitchell et al. (1986) and Taylor and Shaw (1989) whose paleo-magnetic results from a 190Ma dolerite dyke swarm on the Falklands Islands, indicate that the continental block had been translated ≈500km to the south-west and had also been rotated 100 degrees before the opening of the South Atlantic, putting its original position opposite present-day East London (MacDonald et al., 2003; Richardson and Underhill, 2001). Storey et al. (1999) also presented evidence for translation and rotation of the Falklands Islands during the early separation of the Weddell Sea. Assuming that continental slivers (which now make up the western and far-western sectors of the basin) had been translated, along with FPB and Maurice Ewing Bank, before the motion along the AFFZ, a system of en-echelon intra-continental strike slip faults is proposed as the mode of translation. The segmentation of the Agulhas-Falklands Fracture Zone along strike into four distinct zones; 1) Durban segment, 2) East London segment, 3) Diaz Ridge segment and 4) Mallory Trough segment, provide possible validation for this theory given that the AFFZ is the result of a coalescence of individual and sometimes over-stepping strike-slip faults (Ben-Avraham et al., 1997). According to Ben-Avraham et al. (1993) the East London segment of the AFFZ developed first, during the southwards

rifting of the Lafonia (south-eastern Falkland Islands) plate from the African continent at 175-135Ma. It was this initial rifting, brought on by the extension in the incipient Weddell Sea, that created the zones of weakness along which the later fault trace of the AFFZ would propagate (Fig. 6.2). Arguments against this model are brought out by Ramos et al. (2017) who don't believe there is sufficient evidence for the proposed large scale block rotation and accompanying shortening in the crust, given the wealth of new seismic data available in the Falklands region. They propose that no rotation is necessary and that translation of the continental blocks can be accommodated without rotation. The arguments made by Ramos et al., 2017 are preferred over those made by Ben-Avraham et al. (1993) and this study proposes that a model of continental block translation from outside of the original rift zone, brought along intra-continental strike slip faults and then abandoned when the strain is redistributed along more optimally aligned fault traces and the formation of the AFFZ proper, is plausible and worth consideration. A conceptual cartoon (Fig. 6.2) of this phase of extension and intra-continental translation is presented, showing how initial rifting of the Weddell Sea allowed for the isolation of continental slivers, which during the extension between South America and Southern Africa, were translated further to the south-west relative to their original positions. A subsequent re-organisation of stress along more optimally orientated en-echelon strike slip faults (i.e. south of fault plane F3) allowed for the coalescing of individual strike slip fault segments into the larger AFFZ. A conceptual model was generated in order to visualise this Early-Jurassic extension and translation of the continental block hosting the NNE-SSW trending faults (Fig. 6.2).

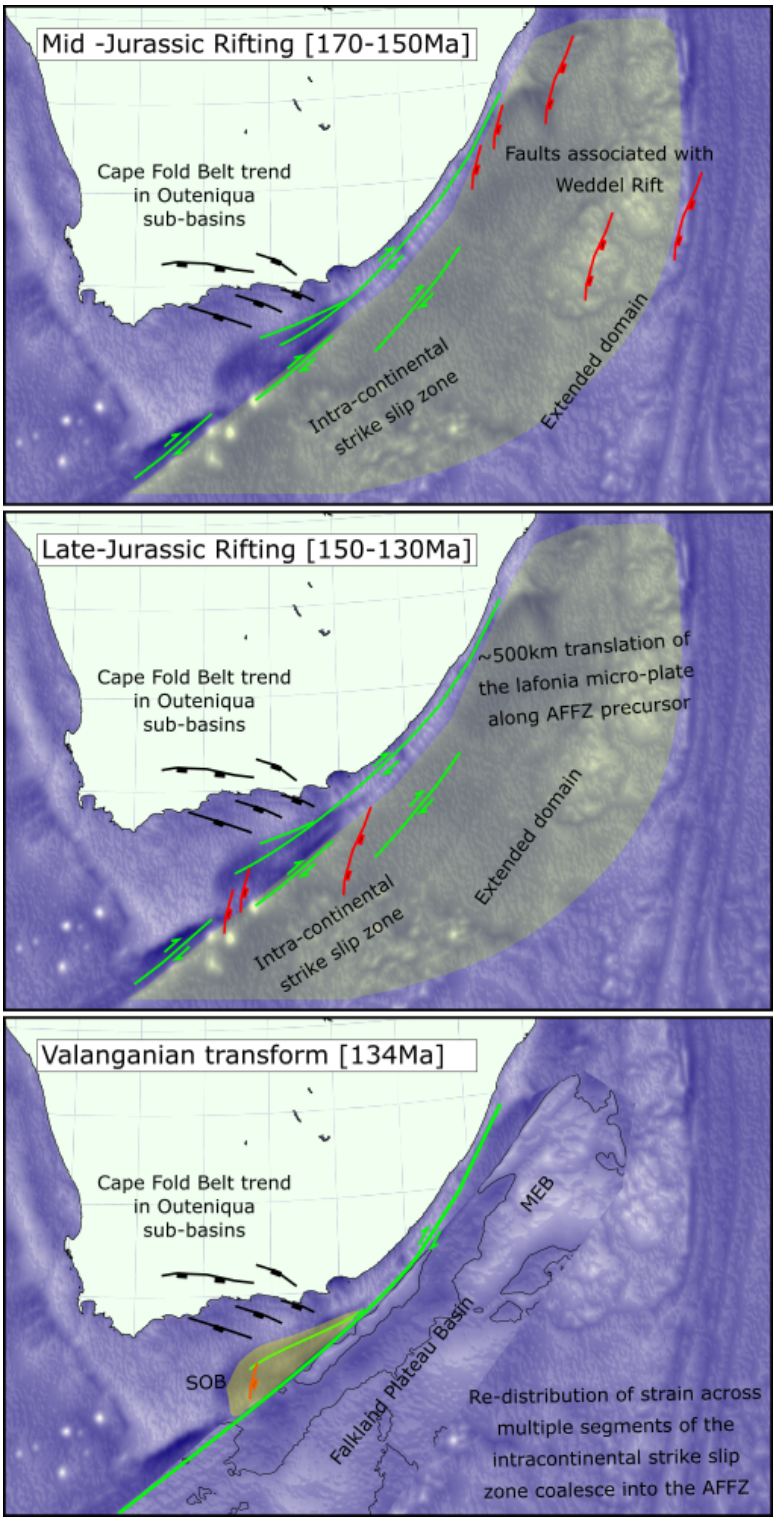


Fig. 6.2 Conceptual cartoon of the first proposed model of the tectonics and structure of the southern margin of South Africa. The cartoon is drawn from regional gravity and magnetic data and the the position of the Maurice Ewing Bank (MEB) during the time of Weddell Sea Rifting. The model shows initial rifting in the Mid-Jurassic and formation of NNE-SSW trending faults. Further extension during the Late Jurassic is proposed to initiate transcurrent motion along intra-continental strike slip faults which then translate the fault blocks from the north-east towards the south-west. A later proposed re-organisation of strain lead to the formation of the incipient AFFZ.

2) The second model proposes that the NNE-SSW (S.O. 2) trending faults were developed during transcurrent motion along en-echelon F1-F3 and proto-AFFZ strike slip faults. In this scenario, rifting in the Weddell Sea induces extension in the proto-Outeniqua (Falkland Plateau Basin and the Southern Outeniqua Basin) with the strain being taken up along the intra-continental strike slip faulting along the trace of the F1-F3 fault and proto-AFFZ faults. The over-stepped configuration between segments of the AFFZ and the F1-F3 faults, produces a transfer zone of strain accumulation between the en-echelon strike slip faults and generates extension and faulting in a NE-SW orientation with additional block rotation creating the final NNE-SSW geometry (Fig. 6.3). Given that the orientation of the NNE-SSW trending faults in the western and far-western sectors of the Southern Outeniqua Basin is highly oblique to the general NW-SE trend of the shelfal Outeniqua sub-basins, a distinction between two separate structural terrains can be made. The results of Parsiegla et al. (2009) of normal ($\approx$25km) thick crust in the western sector of the basin compliments both models presented as to the genesis of the NNE-SSSW trending faults. In both cases thickened crust would be generated, either from the translation of continental material during the movement of Falklands Plateau or during the accumulation of strain leading to shortening of the crust across the transfer zone between the two strike-slip fault traces.

3) The final model for the generation of NNE-SSW trending fault blocks relates the development of the Southern Outeniqua Basin to an extinct spreading ridge located between the Maurice Ewing Bank and the Falkland Islands (Kimbell and Richards, 2008). This model elaborates on the results of Schimschal and Jokat (2019) who undertook wide angle seismic refraction studies along an E-W transect across the Falkland Plateau Basin. Their results indicate the presence of over-thickened oceanic crust beneath the Falklands Plateau Basin proposed to have resulted from extra melt generated between the Weddell Sea Rift and the Falklands Plateau Basin during its formation. The extinct spreading ridge is proposed to have formed due to a difference in extension rates between the formerly connected Maurice

Ewing Bank and Falklands Islands continental blocks (Chemale et al., 2018; Schimschal and Jokat, 2019). Keeping the African plate stationary, the NE-SW trending extinct spreading ridge becomes NNE-SSW trending when aligned back up against South Africa. It is this extension which is proposed to have formed the NNE-SSW trending faults in the western and far-western sectors of the Southern Outeniqua Basin (Fig. 6.4). In addition, this study proposes that the crustal character (both ≈20km thick) of the western and far-western Southern Outeniqua Basin is similar, if not the same, as that of the Falklands Plateau Basin and thus might share a common mode of formation.

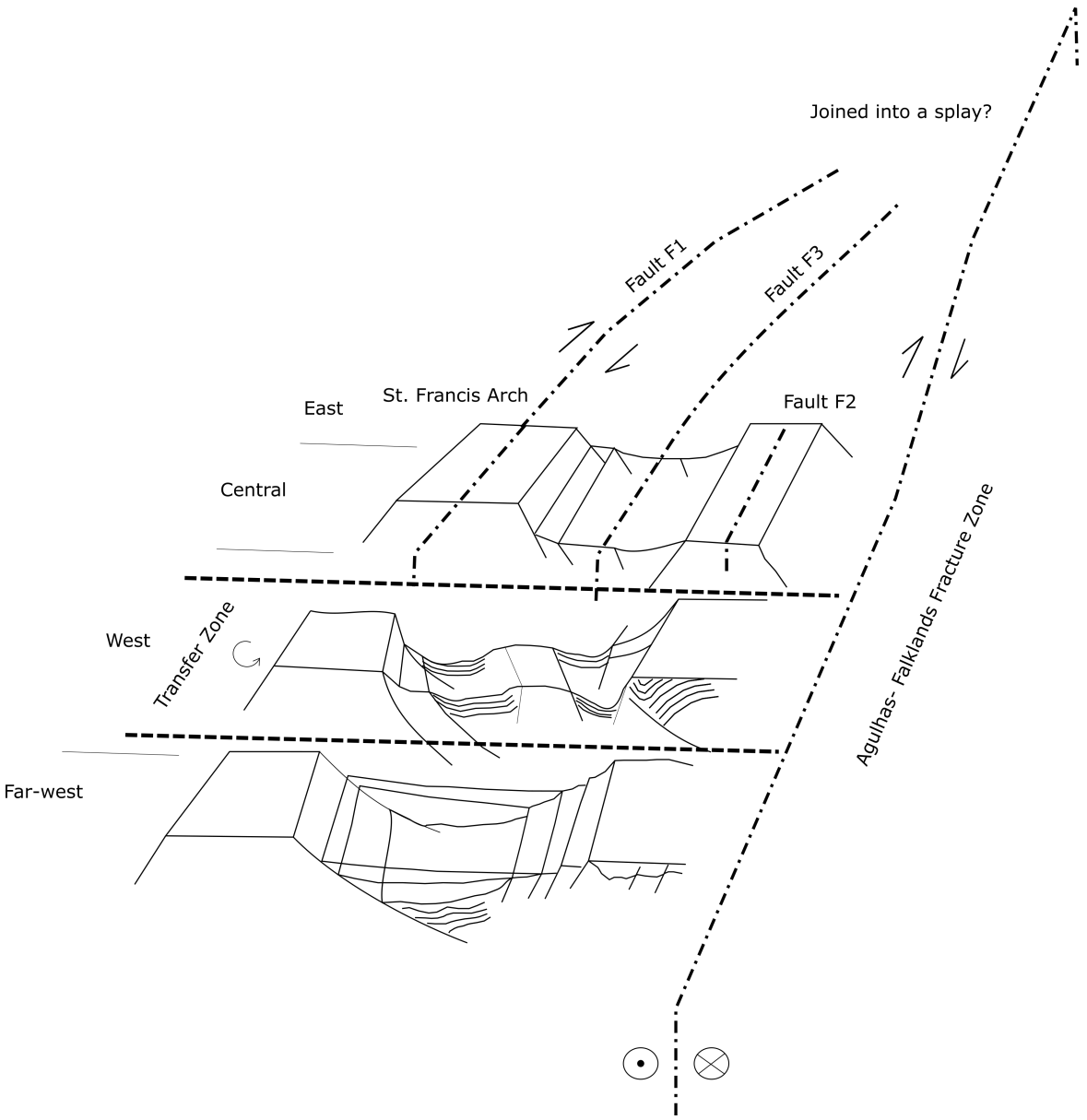


Fig. 6.3 Conceptual cartoon of the second proposed model of the tectonics and structure of the Southern margin of South Africa. The cartoon is drawn from seismic lines in the Central, Western and far-Western sectors of the basin. The lineations labelled F1 and F3 are strike-slip faults visible in seismic in the east and central sectors but lose their character in the western and far-western sectors of the basin (refer to Chapter 4.)

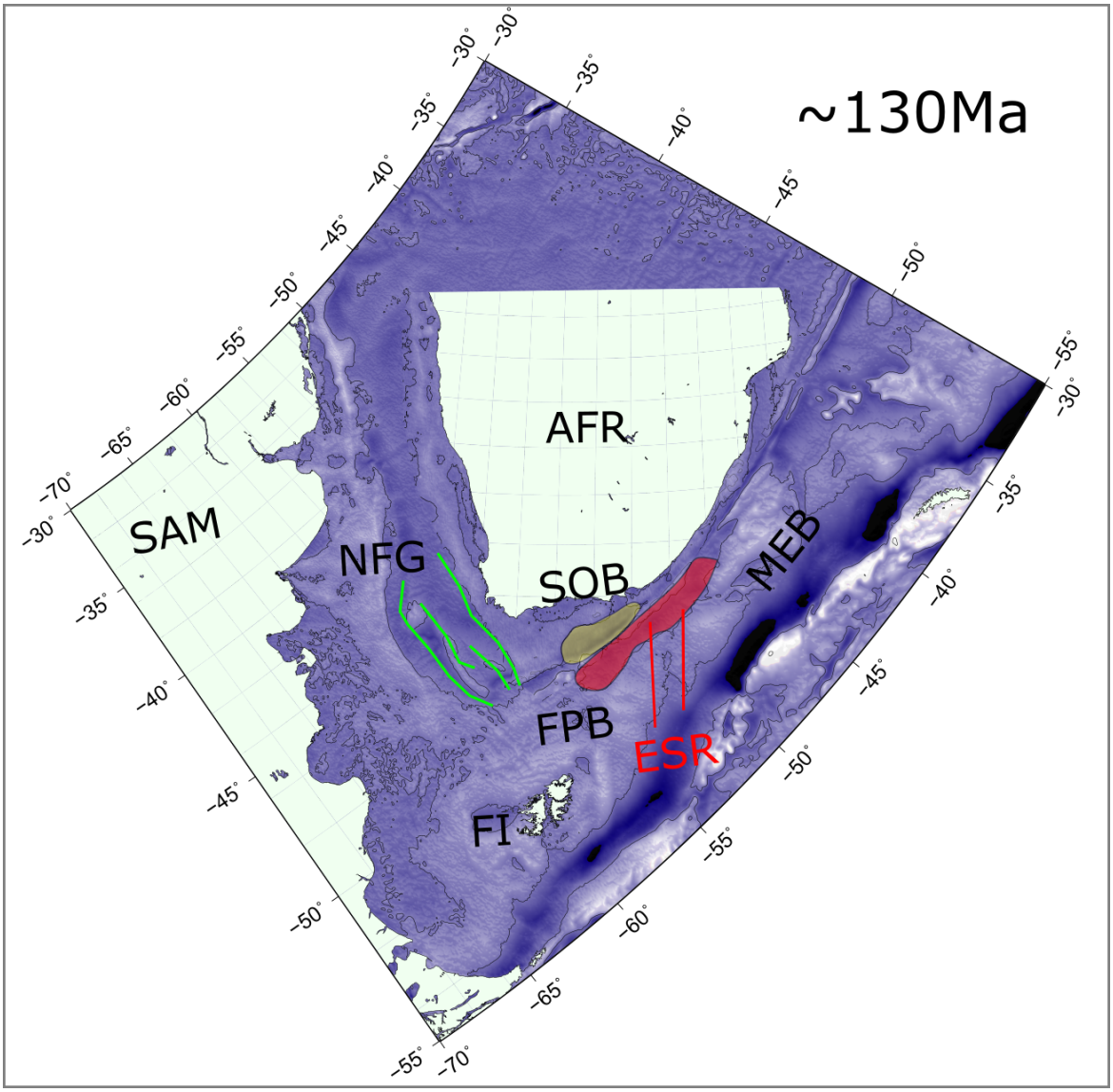


Fig. 6.4 Conceptual cartoon of the third proposed model of the tectonics that created the NNE-SSW trending fault geometries in the far-western sector of the basin. The cartoon is drawn from regional gravity and magnetic data and shows the orientation and position of the extinct spreading ridge between the Maurice Ewing Bank (MEB) and the Falklands Islands (FI).

6.1.2 Continental rifting between South America and Africa (150 -134Ma)

Rifting in the proto-South Atlantic began with a series of isolated rift grabens, of which the North Falklands Graben is best studied (Becker et al., 2012). The northern subsidiary extension of the North falkland Graben is suggested as the focal point of the break-up of West Gondwana and the incipient formation of the South Atlantic. East-West extension from ≈150Ma initiated a series of rifts along the South American and Southern African continental masses, including the San Jorge, San Julian, North Falklands, Bredasdorp, Pletmos, Algoa and Gamtoos Basins. The orientations of the various rift grabens varies and are thus inferred to have developed along pre-existing zones of weakness, such as the thrust planes of the Cape Fold Belt in the South African context (Paton et al., 2006). The East-West extension is proposed in this study to have linked the strike-slip segments of the intra-continental strike-slip zone along the southern portion of the African Plate. These linkages eventually coalesced (≈16myr) into the AFFZ and focused transcurrent motion along this new lineament (Ben-Avraham et al., 1997). A plate reconstruction performed in this study (Fig 6.5) suggests that in order for the southern African and South American plates to move effectively past each other along the AFFZ, an amount of NW-SE extension (orthogonal to the trace of the AFFZ) is necessary. In this case, the genesis of NE-SW (S.O.1) orientated faults is associated with extension prior to and during transcurrent movement along the AFFZ.

6.1.3 Development of structures associated with transform motion (134 - 80Ma)

Movement along the AFFZ is widely agreed to have begun during the late Valanginian to Hauterivian (134-130Ma) (Ben-Avraham et al., 1997; Lorenzo and Mutter, 1988). The mapped BR surface, interpreted as the unconformity marking the onset of motion along the AFFZ, shows deposition within the basin in the form of divergent reflector geometries, typical of syn-tectonic sedimentation. The packages in the western and far-western sector of the

basin are sub-parallel to parallel in configuration and become progressively more deformed towards the north-east into the central and eastern sectors of the basin. Deformation of the sediments between BR-B, Valangian to Hauterivian (134-130Ma), by folding and normal faulting of structures in S.O.1, indicates that strain was taken up both in transtensional and transpressional modes along the pre-existing structures. A significant increase in sediment package thickness between BR-B in the central portion of the basin, relative to the other sectors, and onlap of sediments younger than B, Hauterivian (130Ma), onto the DMR suggest that the basement structure in this sector was a promontory during the deposition of these sediments. The rheological contrast between the basement and sedimentary characters of the DMR, would allow the focusing of strain in the central sector, forming a deep NE-SW trending basin parallel to the marginal ridge, resulting in a greater sediment package thickness between BR and B in this area. Inversion of syn-rift and Package 1 (BR-B) strata on the inboard side of the St. Francis Arch and the formation of an angular unconformity defined by horizon C, Aptian (120Ma), indicates that the main period of transpression in the eastern sector of the basin occurred during Valanginian - Aptian times. This observation is in agreement with Baby et al. (2018) who described planation of relief in the shelfal Algoa and Gamtoos Basins due to uplift and erosion during the same time period (Paton and Underhill, 2004; Thomson et al., 1999). Basin floor fans found within Package 3, Aptian - Cenomanian (120-93Ma), in the western and far-western sectors of the basin indicate that uplift and erosion of the south-western extremity of the Southern Outeniqua Basin. The deposition of these deepwater fans is largely controlled by the morphology of the horizon C surface which shows a marked NE-SW depression along which the gravity transport of these sediments took place. Progradation from the north-east towards the south-west, of sediments in Package 4, Cenomanian - Campanian (93-80Ma), indicate that re-newed uplift and erosion occurred in the eastern sector of the basin and migrated towards the south-west. The cause of this

transient uplift is inferred to be due to the passing of the Natal Valley spreading centre along the trace of the AFFZ during this time (Ben-Avraham et al., 1997; Reznikov et al., 2005).

6.1.4 Development of a passive transform margin (80Ma - Present Day)

A major shift in sedimentary provenance occurs between Package 4 and 5, Campanian-Late (80-76Ma). Deposition of sediments from the north-east towards the south-west abruptly changes and prograding strata start to develop from the south-west towards the north-east. The change in provenance from the eastern sector to the western sector is defined by unconformity F, Campanian (80Ma), which is inferred to be the result of the cessation of transcurrent motion along the AFFZ as the Natal Valley Spreading Centre reaches the South Atlantic. Sediments in sub-unit 5a have been eroded and inverted in the western and central sectors of the basin respectively. This anomalous uplift during the late Campanian-early Maastrichtian (80-72Ma), does not seem to be recorded in any of the shelfal basins and as such seems to be localised to the southern margin of the Southern Outeniqua Basin. The cause of the uplift is suggested to be due to the movement of the southern African continent over the African Superswell (Nyblade and Robinson, 1994). Results from apatite fission track analysis (AFTA) done by Wildman et al. (2015) indicate a cooling event from 80-75Ma which fits well with the observations in this study by the development of unconformity horizons E and F, Campanian - Late Campanian (80-76Ma).

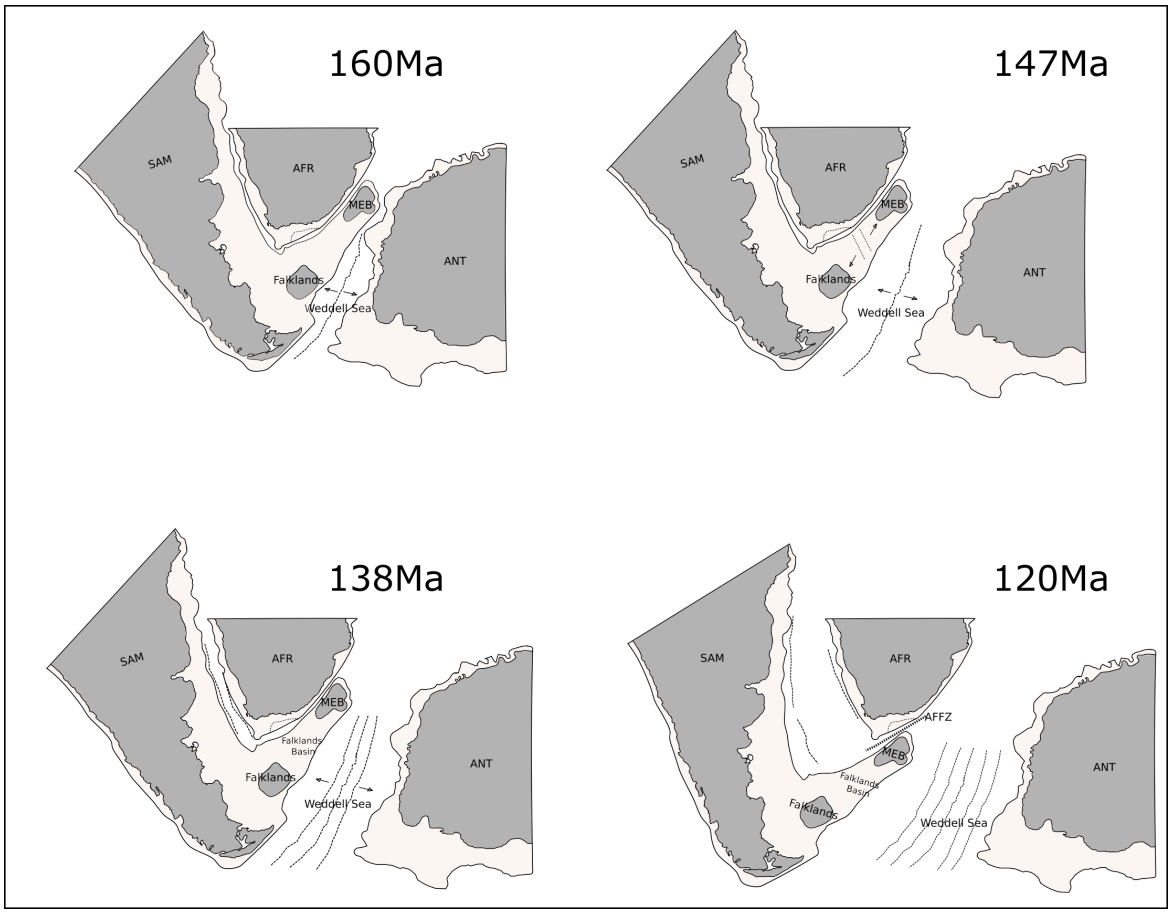


Fig. 6.5 A proposed break up model of Gondwana during the evolution of the Southern Outeniqua Basin. The ages depicted for each phase of the break-up sequence were calibrated by the oceanic magnetic striping interpretation done by Jokat and Herter (2016); Jordan et al. (2017); König and Jokat (2006). 160Ma) Initial NW-SE extension between East and West Gondwana and the development incipient Weddell Sea produces rift shoulder faults that strike NE-SW. 147Ma) The initiation of intracontinental strike slip motion of the proto-Agulhas Falklands Fracture Zone along a new plane of weakness derived during orthogonal rifting of East and West Gondwana. 138Ma) Transform motion along the Agulhas Falklands Fracture Zone juxtaposes the Falkland Plateau Basin and Maurice Ewing Bank against the southern margin of the proto-Southern Outeniqua Basin producing transpression and uplift of a continental sliver, the Diaz Marginal Ridge. 120Ma) True passive margin conditions begin as free connection occurs between the South Atlantic and South Indian Oceans with later (80Ma) transient uplift occurring along the southern African margin with the passage of the Natal Valley Spreading centre.

6.2 Diaz Marginal Ridge

The structure and morphology of the Diaz Marginal Ridge can be seen to vary substantially across the basin, as seen in the eastern versus far-western sectors of the basin. The separation between these sectors is proposed to be controlled by a transverse fault zone (Fig.6.3). The Diaz Marginal Ridge is thought to have been used to accommodate strain throughout the southern portion of the basin and can be seen to be bounding a deep basin in the eastern sector of the basin where the morphology of the DMR is most basement-like in appearance (Fig. 6.6). The timing to which the stress induced by the transverse motion of the Agulhas Falklands Fracture Zone (AFFZ) can also be seen to have been much longer than the effects seen in the Falklands margin. Lorenzo and Mutter (1988) noted that Barremian sediments, roughly correlated with horizon B, show no evidence of deformation and thus infer that the transverse motion of the Agulhas-Falklands Fracture Zone played only a minor part in the deformation of the marginal ridge in the Falklands Plateau Basin. This study however has noted that not only has the AFFZ played a substantial role in the development of the ridge but continued to do so from Valanginian through to Maastrichtian times with normal faults, which also accommodate inversion in some areas, displacing almost all of the horizons picked in the basin (Fig. 6.7). The bevelled top of the DMR seen throughout the basin, and most clearly in the eastern sector, is indicative of wave-action at sea level (Figure 6.6). The timing of the wave erosion is correlated with unconformity Horizon D, Cenomanian (93Ma) with overlying reflectors displaying down-lapping geometries prograding from the south to north from the DMR shoulder into the basin (Figure 6.7) Variations in sediment thickness above the bevelled surface of the DMR form north-east (thinnest) to south-west (thickest) indicate differential uplift of the marginal ridge along the margin between the Aptian-Maastrichtian (121-66Ma). The first phase of uplift is interpreted to be a result of transpression during the early phases of basin evolution due to transform motion along the Agulhas-Falklands Fracture Zone as South America began to rift away from Africa during the Valanginian

(139Ma). A later episode of uplift during the Cenomanian (93Ma) is interpreted to be as a result of the Natal Valley spreading centre migrating along the trace of the Agulhas-Falklands Fracture Zone, which resulted in transient thermally induced uplift of the marginal ridge (Scrutton, 1979). The transient nature of the uplift along the strike of the Diaz Marginal Ridge is complicated by the potential degree of mechanical coupling between the continental fragment of the ridge and the adjacent oceanic crust (Smit et al., 2008). This is clearly observed in the central sector of the basin where sediments from between horizon B-G (Hauterivian to Maastrichtian, 130-66Ma) on-lap the northern shoulder of the Diaz Marginal Ridge and where the overburden thickness above the Diaz Marginal Ridge surface is thinnest, implying that limited thermal subsidence has occurred during and after the movement of the Agulhas-Falklands Fracture Zone as well as the by-passing spreading ridge (Fig. 6.7). The geometries of the sedimentary sequences between reflectors B and F, on the northern flank of the DMR suggest that the feature was a promontory during these depositional times and as such acted as a source of sediment (Fig. 6.7). Based on this evidence it can be concluded that the DMR in the central sector was a continental basement high during the formation of the Southern Outeniqua Basin and existed prior to the onset of major transverse motion. In the eastern, western and far-western sectors of the basin however, the DMR is the direct result of transform motion along the AFFZ as syn-rift strata deposited at the initial break-up of Gondwana are folded and uplifted to create the topographical high of the marginal ridge as shown in the cartoon illustration (Fig.6.8). The configuration of the DMR as an uplifted marginal ridge bounding the seaward side of a deep sedimentary basin is typical of structures that develop along transform margins (Antobreh et al., 2009; Attoh et al., 2004; Basile and Allemand, 2002; Turner et al., 2003; Wilson et al., 2003)

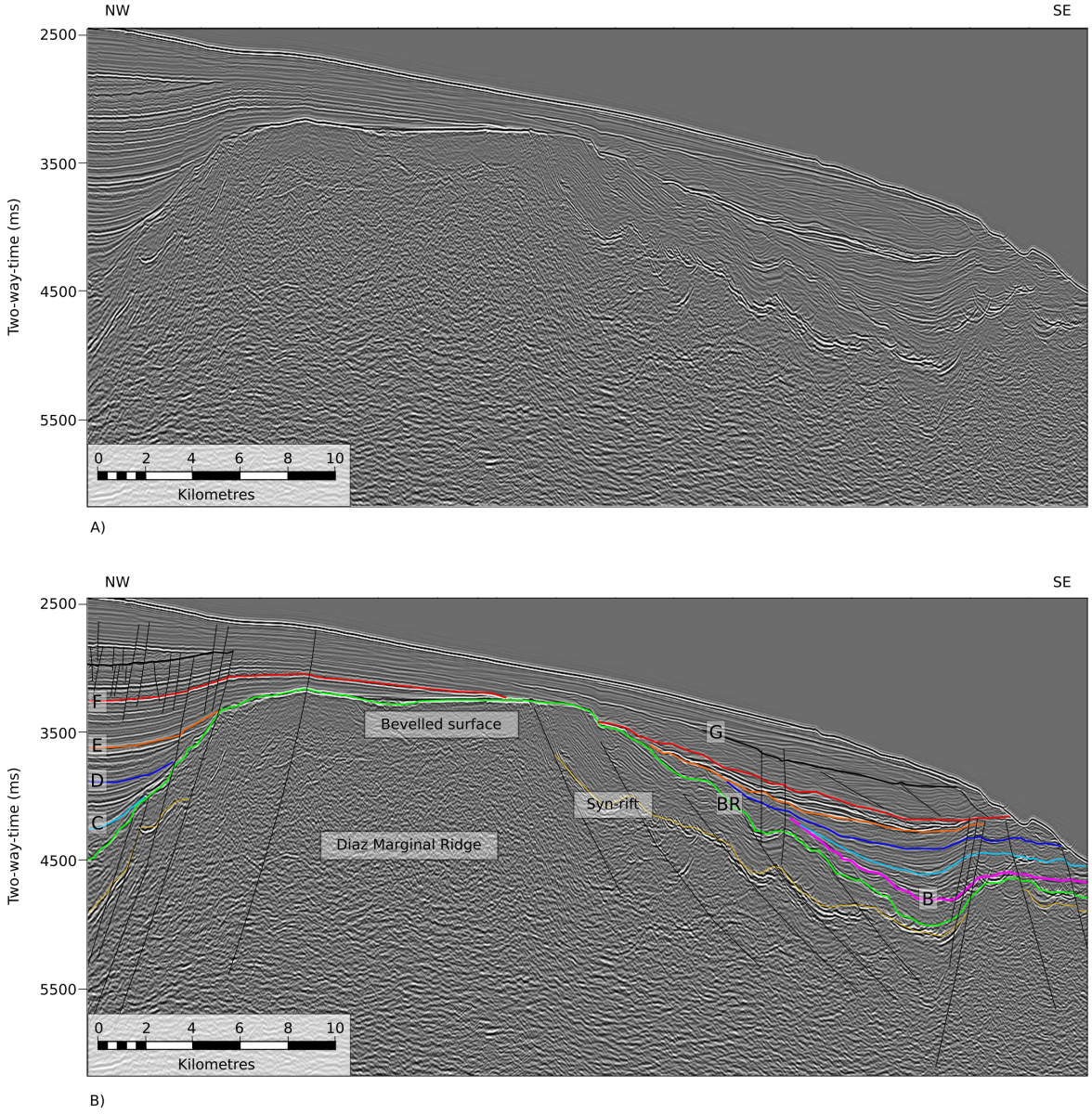


Fig. 6.6 Seismic line 2001-53. Interpretation shows the sediments on the southern (oceanward) side of the DMR are deformed between horizons Br-E, Valanginian - Cenomanian (134-93Ma). Deformation is is assumed to be associated with the transform motion along the AFFZ during this time.

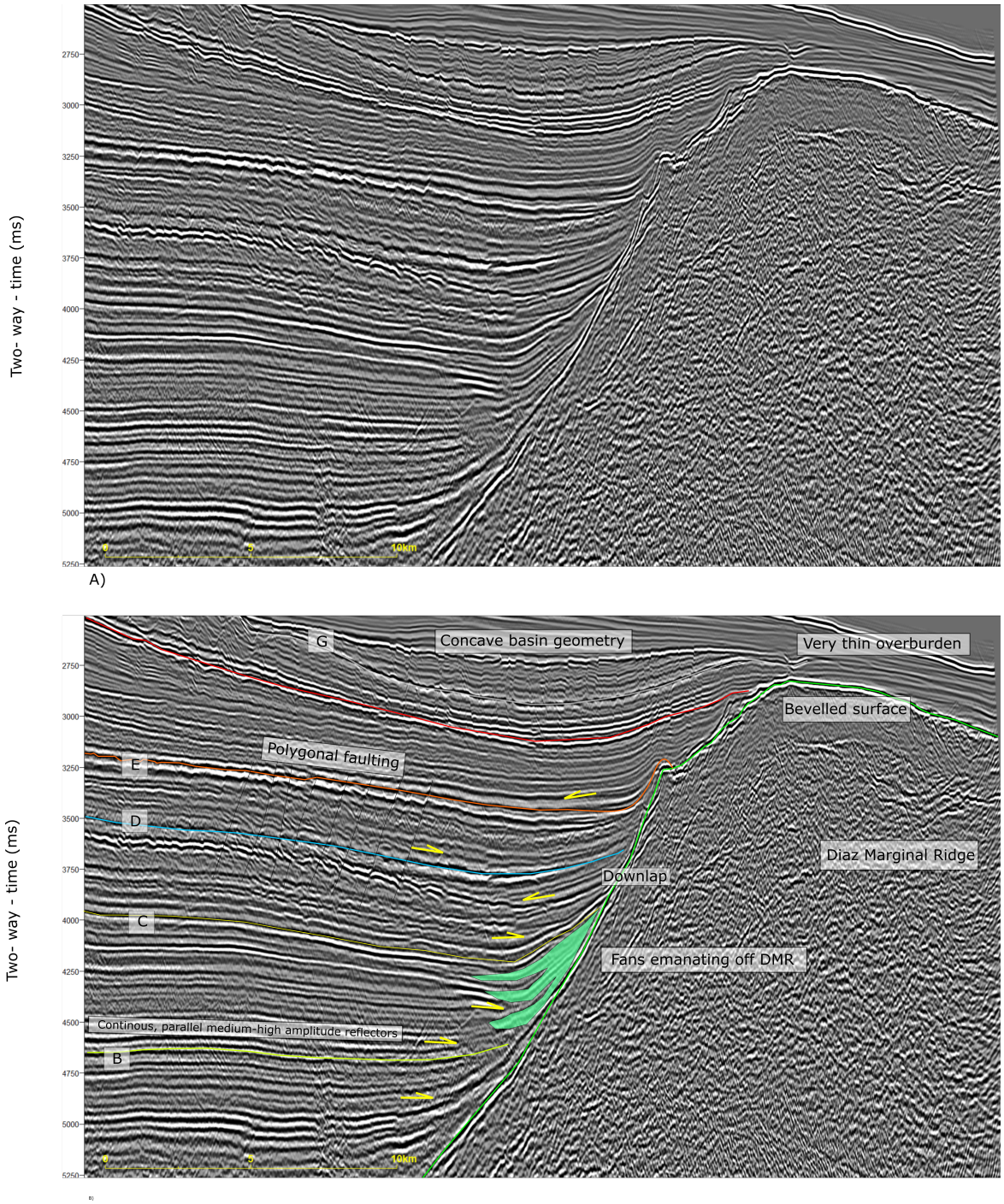


Fig. 6.7 Seismic line 2001-61, in the central sector. Interpreted line with major horizons, faults and the DMR annotated. The sediments between horizon B and F, Hauterivian - Campanian (134-80Ma) on the northern shoulder of the DMR show inclined reflector geometries. This is interpreted to be the result of rotation of the fan sediments due to transpression along the AFFZ and the later transient thermal uplift associated with the migrating Natal Valley spreading centre.

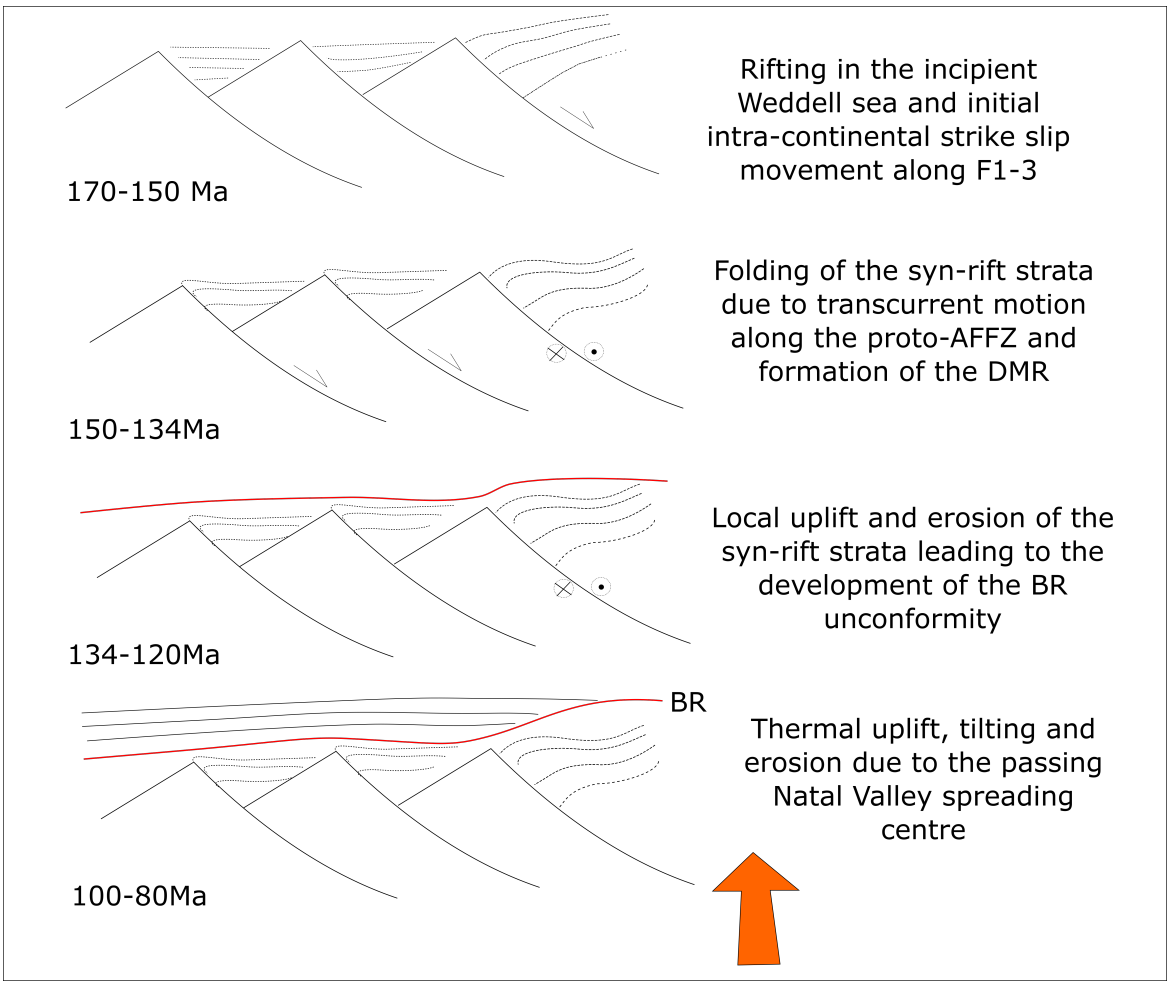


Fig. 6.8 A chronostratigraphic chart with regional, basin and feature specific annotations for the area under study. Relative timings of the various picked reflectors are given alongside the interpreted structural and stratigraphic mega-themes.

6.3 Stratigraphic evolution of the Southern Outeniqua Basin

The variation in sediment deposition along the margin has highlighted the complex and dynamic evolution of the basin fill within the Southern Outeniqua area. Isopach maps illustrate the variation in sediment supply in the Valangian - Aptian (134-120Ma), from what initially appears to be a dual point source to the north-east and south west, to a predominant shift in the provenance direction of the sediment towards the south-western portion of the basin in the late Cretaceous, defined by horizon F, Late Campanian (76Ma). Early infilling of the basin, bounded by reflectors BR and B, likely originated from the rift shoulders in the basin within a shallow marine type of environment. The subsequent filling of sediments seem to have been supplied from the north-east from a basinal high and filling towards the south west as seen in the clinoform geometries of Package 2. The Aptian time subsidence of the central part of the basin then leads sediments to be sourced from the elevated south western portion of the basin. Downlapping of reflectors onto horizon C, Aptian (120Ma), from the west along with the mounded geometries of basin floor fans spreading towards the north-east are evidence for the uplift of the south-western portion of the basin and deposition of sediments into the NE-WS trending depression (Fig. 6.9). During this time, the DMR in the central portion of the basin experienced uplift and as such a number of fans have developed off of the basinal high into the basin (Fig. 6.8). Sediments recovered from the Aptian-Albian boundary ($\approx$113Ma) in DSDP well 330, drilled on the edge of the Falklands Plateau Basin and Maurice Ewing Bank, show the transition from sapropelic claystone to zeolite-rich nanno clay owing to the change from anoxic water-bottom conditions to open ocean circulation along the margin (Barker and Dalziel, 1977). These findings suggest that initially, restricted marine conditions prevailed from the Aptian until at least the Albian due to transpression and uplift along the Diaz Marginal Ridge generated between the African and South-American continental blocks along the Agulhas-Falklands Fracture Zone. During the Cenomanian (93Ma), continued uplift in the far-western, western and central portions

of the basin resulted in sediments being supplied from basinal highs across the basin into a main depocentre located in the western and central sectors, a cartoon has been generated to visualise this (Fig. 6.10). A significant adjustment occurs during Maastrichtian times with the main sediment provenance coming off from the shelf at a time presumably heralding the cessation of transcurrent movement along the AFFZ. It is during this phase that true passive margin conditions are established along the margin, which supports the arguments made by workers in the Falklands Plateau Basin that note the Maastrichtian as the period of relative tectonic quiescence (Lorenzo and Mutter, 1988).

Tinker et al. (2008) have defined three stages of sedimentation during the Valanginian (134Ma), Hauterivian (130Ma) and Cenomanian/Turonian (93Ma) with decreased denudation during the intervening periods along the South African margin. This largely supports the seismic stratigraphic interpretation of this study, however the deposition of sediments between the sequence boundaries of horizons D and E, Cenomanian - Campanian (93-80Ma) indicates that an additional sediment source to the south of the DMR (Fig. 6.6). The cause of this increase in sedimentation over this time period is proposed to be due to the passing of the Falklands Plateau by the Southern Outeniqua Basin along the AFFZ (Thomson et al., 2002). During this movement, transpression on the Falklands side of the transform is suggested to have caused uplift of the continental blocks, leading to sediment being fed into the Southern Outeniqua Basin from the south (Richards et al., 2006). Later Maastrichtian-Tertiary sediment supply was limited as transgressive systems drowned the rivers and led to a relative starvation of the basin (Tinker et al., 2008). Sediments between horizon G, Maastrichtian (66ma) and the seabed show prograding geometries and are interpreted to be contourite deposits generated by the Agulhas western boundary current with the same geometries being described by Uenzelmann-Neben et al. (2007) further up the coast in the Natal Valley Basin. The evolution of the Southern Outeniqua Basin is summarised in a chronostratigraphic chart showing the

major tectonic and stratigraphic events that occurred in the basin and the surrounding area (Fig. 6.11).

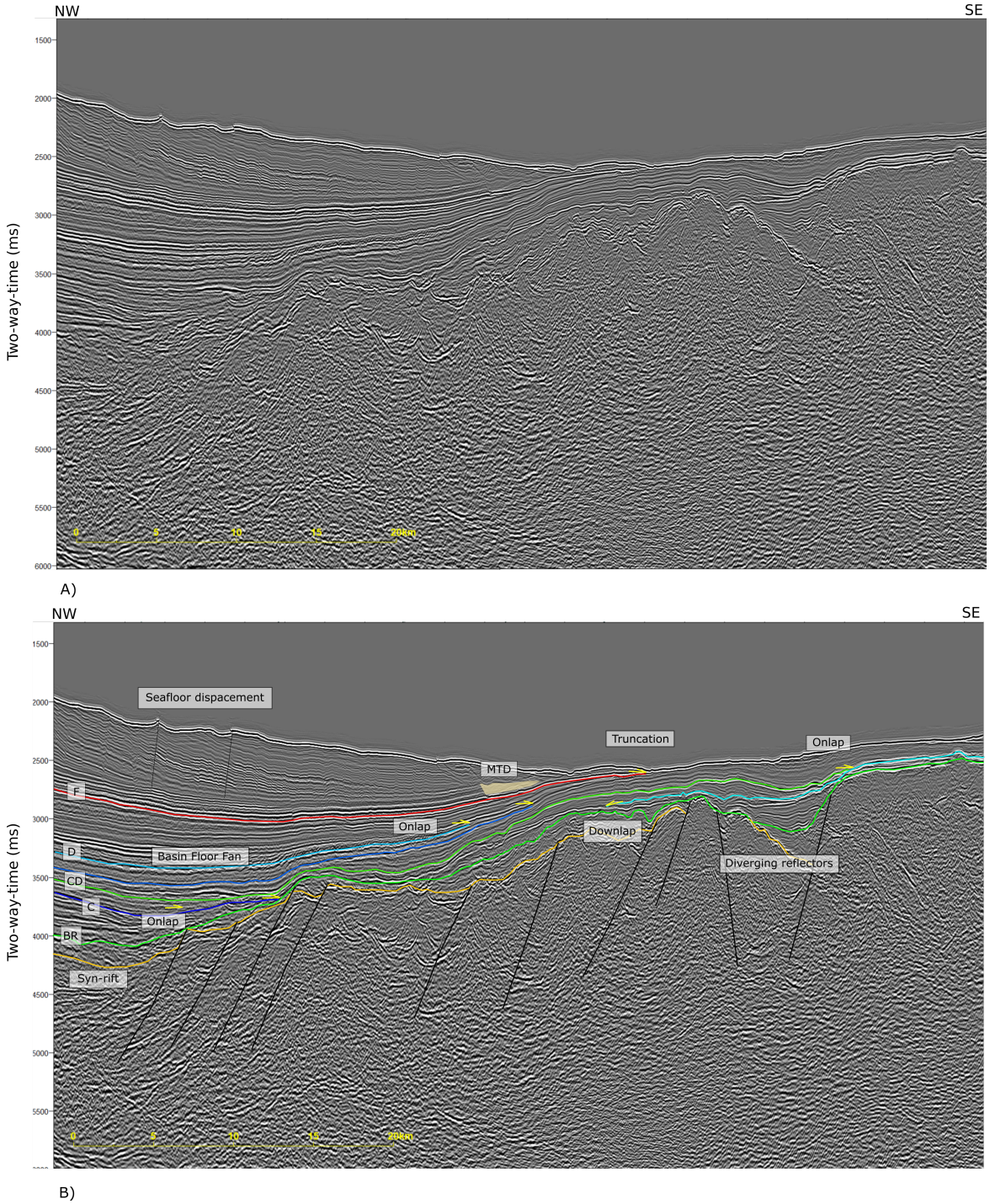


Fig. 6.9 Seismic line 17, in the far-western sector. Interpreted line with major horizons and faults annotated. The south-eastern portion of the line shows a basement promontory that is dissected by faults that show sediments with divergent reflector geometries, typical of syn-rift deposits. Downlapping reflector geometries near the northern shoulder of the DMR, in the far-western sector, create a mounded feature which is typical of basin floor fan deposits. A number of truncational, onlapping and downlapping reflector geometries indicates the multiple phases of subsidence and uplift that have occurred along the trace of the DMR.

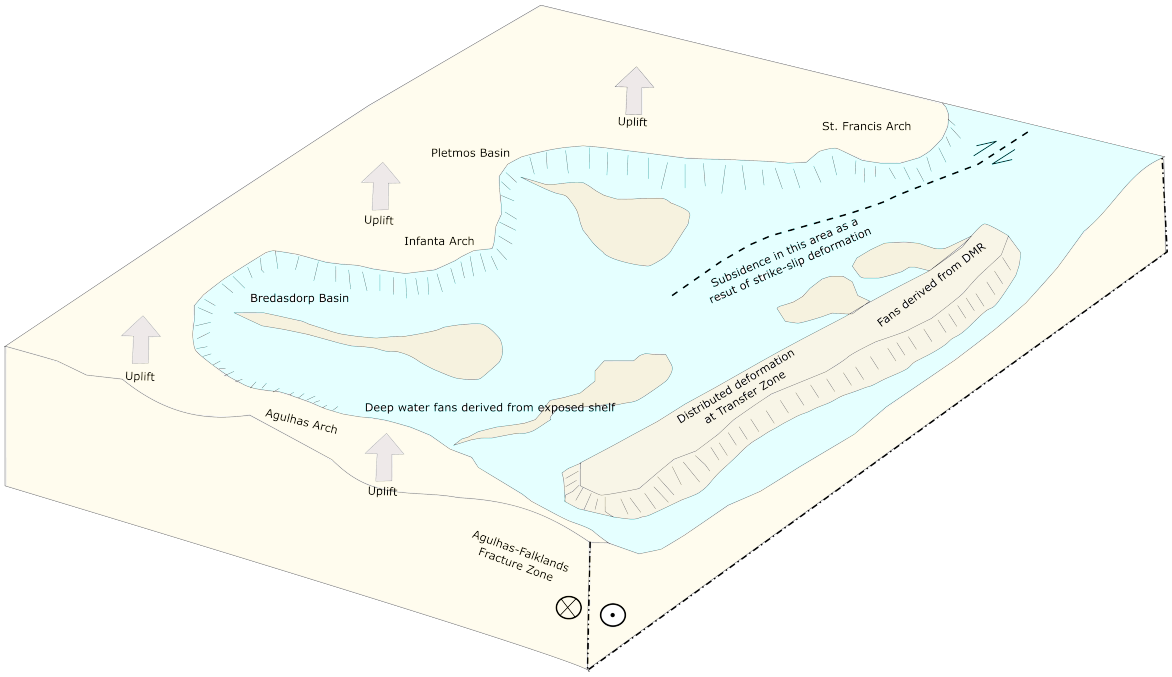


Fig. 6.10 A) A cartoon drawn to reflect the proposed mass transport processes that governed the deposition of Packages 3 and 4, Aptian - Campanian (120-80Ma), along the strike of the basin.

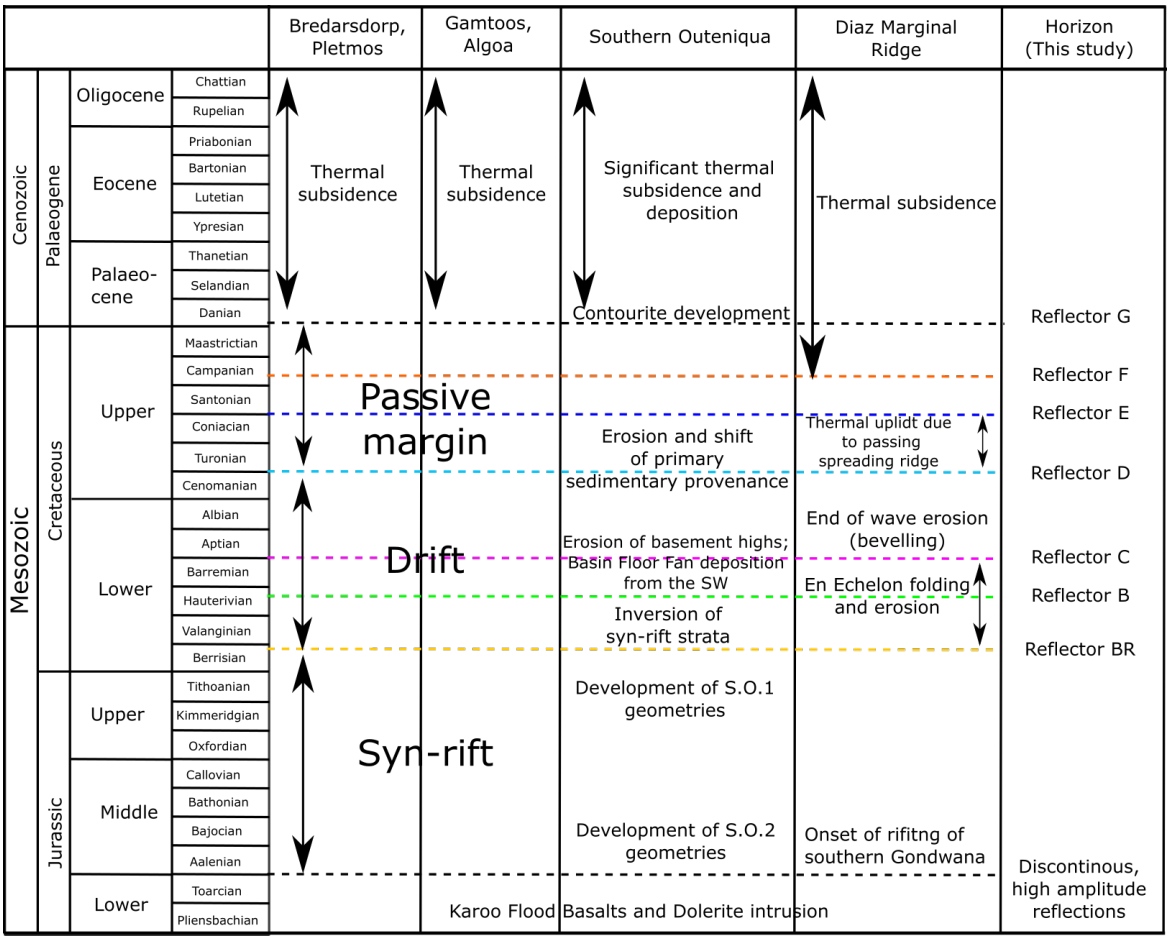


Fig. 6.11 A chronostratigraphic chart with regional, basin and feature specific annotations for the area under study. Relative timings of the various picked reflectors are given alongside the interpreted structural and stratigraphic mega-themes.

Chapter 7

Conclusion

The primary objective of this study was to determine the kinematic evolution of the Southern Outeniqua Basin from the structural and stratigraphic observations made from various geophysical datasets such as 2D seismic, well and regional satellite gravity and magnetic data. The seismic data was calibrated to the wells and specific well top horizons extrapolated from the shelfal area into the deeper basin in order to get a relative timing of deposition for various stratigraphic packages and their related architectures. The mapping of the key unconformities throughout the basin provided a framework for understanding the tectonic controls on the distribution and subsequent accumulation of sediments throughout the basin. Three different fault orientations have been mapped within the basin, grouped geographically in such a way that allowed for the basin to be sub-divided into four sectors; far-west, west, central, east. Faults in the far-western sector predominantly strike NNE-SSW (S.O. 2) and are proposed to have formed in the Mid-Jurassic (170-150Ma), during the breakup of West-East Gondwana. Three models have been proposed in this study to account for the anomalous fault orientations, given that they are highly oblique to both the NE-SW trending basement faults on the shelf to the north and the NE-SW trending Agulhas-Falklands Fracture Zone to the south. This study prefers model 2, which suggests that the formation of a transfer zone between the two en-echelon strike slip fault systems F1-F3 and the AFFZ has created a series

of rotated fault blocks that now trend NNE-SSW. The Late - Jurassic (150-130Ma) break up of West Gondwana provides the extension necessary to generate the NE-SW trending faults (S.O.1) mapped in the western, central and eastern sectors of the basin. Transcurrent movement along the newly created Agulhas-Falklands Fracture Zone induces uplift within the basin and forms the Diaz Marginal Ridge (DMR), which bounds the southern part of the basin. Folded syn-rift strata that form the DMR in the western and eastern sectors of the basin are contrasted against the basement like character of the marginal ridge in the central sector of the basin. This rheological contrast is suggested to have localised strain along the central sector of the basin thereby creating a deep, ridge parallel depocentre during the Valangian-Hauterivian (134-130Ma). The Southern Outeniqua Basin is classified as an active transform margin until after deposition of Package 4, Turonian to Late-Santonian (93-84Ma). A marked change in sedimentation occurs between the Late - Santonian and Campanian where sediments of Package 5 switch from a predominantly north-eastern to a south–western provenance signifying the end of active transform motion and the onset of passive margin conditions. Significant uplift occurs between the Late-Campanian and Tertiary and is proposed to be as a result of a deep thermal perturbation known as the African Superswell. Late Tertiary scouring of the shelf -slope is evidence for an increase in the energy of the western boundary current that is present in the area known as the Agulhas current.

The results of this study have provided an additional interpretation in the understanding of the petroleum system within the Southern Outeniqua Basin. The tectonic models generated in the study indicate a possible early, deep-lacustrine depositional environment within the syn-rift strata which will have a bearing on source rock quality, maturation and will influence the timing of charge of the overlying basin floor fan facies, interpreted in the seismic. Recommendations for future work include the delineation and mapping of the basement and syn-rift intervals, along with a more detailed timing of displacement of the fault systems across the basin. Interpretation of the third-order systems tracts is also recommended in

order to more accurately map the sandy facies across the basin and give a better delineation of petroleum system elements such as reservoir quality, seal integrity and the timing of the hydrocarbon charge.

References

Antobreh, A.A., Faleide, J., Tsikalas, F., and Planke, S. (2009). Rift shear architecture and tectonic development of the Ghana margin deduced from multichannel seismic reflection and potential field data. *Marine and Petroleum Geology*, 26(3):345–368.

Attoh, K., Brown, L., Guo, J., and Heanlein, J. (2004). Seismic stratigraphic record of transpression and uplift on the Romanche transform margin, offshore Ghana. *Tectonophysics*, 378(1-2):1–16.

Baby, G., Guillocheau, F., Boulogne, C., Robin, C., and Dall'Asta, M. (2018). Uplift history of a transform continental margin revealed by the stratigraphic record: The case of the Agulhas transform margin along the Southern African Plateau. *Tectonophysics*, 731-732(October 2017):104–130.

Barker, P. F. and Dalziel, I. W. D. (1977). The Mesozoic South Atlantic Ocean and Evolution of Its ... *Initial Reports of the Deep Sea Drilling Project, 36*, page 1080.

Basile, C. and Allemand, P. (2002). Erosion and flexural uplift along transform faults. *Geophysical Journal International*, 151(2):646–653.

Becker, K., Franke, D., Schnabel, M., Schreckenberger, B., Heyde, I., and Krawczyk, C. M. (2012). The crustal structure of the southern Argentine margin. *Geophysical Journal International*, 189(3):1483–1504.

Ben-Avraham, Z., Hartnady, C. J., and Kitchin, K. A. (1997). Structure and tectonics of the Agulhas-Falkland fracture zone. *Tectonophysics*, 282(1-4):83–98.

Ben-Avraham, Z., Hartnady, C. J., and Malan, J. A. (1993). Early tectonic extension between the Agulhas Bank and the Falkland Plateau due to the rotation of the Lafonia microplate. *Earth and Planetary Science Letters*, 117(1-2):43–58.

Ben-Avraham, Z., Hartnady, C. J., and Roex, A. P. (1995). Neotectonic activity on continental fragments Agulhas Plateau and Mozambique Ridge. *Journal of Geophysical Research*, 100(B4):6199–6211.

Booth, P. W. K. and Shone, R. W. (1999). Complex thrusting at Uniondale, eastern sector of the Cape Fold Belt, Republic of South Africa: Structural evidence for the need to revise the lithostratigraphy. *Journal of African Earth Sciences*, 29(1):125–133.

Broad, D., Jungslager, E., McLachlan, I., and Roux, J. (2006). Offshore mesozoic basins. In Johnson, M. R., R, A. C., and Thomas, R. J., editors, *The Geology of South Africa*, pages 553–571. Geological Society of South Africa/ Council for Geoscience, Johannesburg/Pretoria.

References

Brown, L. F. et al. (1995). *Sequence Stratigraphy in Offshore South African Divergent Basins: An Atlas on Exploration for Cretaceous Lowstand Traps by Soekor (Pty) Ltd.* Number 41 in AAPG Stud. Geol. AAPG.

Chemale, F., Ramos, V. A., Naipauer, M., Girelli, T. J., and Vargas, M. (2018). Age of basement rocks from the Maurice Ewing Bank and the Falkland/Malvinas Plateau. *Precambrian Research*, 314(July 2017):28–40.

Cooper, A., Raymond, C., and et al., editors (2007). *Break-up of Gondwana and opening of the South Atlantic : Review of existing plate tectonic models in Antartica*, number 2007–1047 in Online Proceedings of the 10th ISAES.

Davies, C. P. (1997). *Hydrocarbon evolution of the Bredasdorp Basin, offshore South Africa: from source to reservoir*. PhD thesis, Stellenbosch.

de Vera, J., Granado, P., and McClay, K. (2010). Structural evolution of the Orange Basin gravity-driven system, offshore Namibia. *Marine and Petroleum Geology*, 27(1):223–237.

Eagles, G. (2007). New angles on South Atlantic opening. *Geophysical Journal International*, 168(1):353–361.

Goldsworthy, M. and Jackson, J. (2001). Migration of activity within normal fault systems: examples from the quaternary of mainland greece. *Journal of Structural Geology*, 23(2):489 – 506.

Haq, B., Hardenbohl, J., and Vail, P. R. (1987). Chronology of fluctuating sea levels since the Triasic (250 million years ago to present). *Science*, 235(4):1156–1167.

Hirsch, K. K., Scheck-Wenderoth, M., van Wees, J.-D., Kuhlmann, G., and Paton, D. a. (2010). Tectonic subsidence history and thermal evolution of the Orange Basin. *Marine and Petroleum Geology*, 27(3):565–584.

Jokat, W. (2003). Timing and geometry of early Gondwana breakup. *Journal of Geophysical Research*, 108(B9):2428.

Jokat, W. and Herter, U. (2016). Jurassic failed rift system below the Filchner-Ronne-Shelf, Antarctica: New evidence from geophysical data. *Tectonophysics*, 688:65–83.

Jordan, T. A., Ferraccioli, F., and Leat, P. T. (2017). New geophysical compilations link crustal block motion to Jurassic extension and strike-slip faulting in the Weddell Sea Rift System of West Antarctica. *Gondwana Research*, 42:29–48.

Jungslager, E. H. A. (1996). Geological evaluation of the remaining prospectivity for oil and gas of the pre-1At1 "syn-rift" succession in Block 9, Republic of South Africa. Technical report, Soekor (Pty.) Ltd.

Jungslager, E. H. A. (1999). Petroleum habitats of the Atlantic margin of South Africa. *Geological Society, London, Special Publications*, 153(1):153–168.

Kimbell, G. S. and Richards, P. C. (2008). The three-dimensional lithospheric structure of the Falkland Plateau region based on gravity modelling. *Journal of the Geological Society*, 165(4):795–806.

König, M. and Jokat, W. (2006). The Mesozoic breakup of the Weddell Sea. *Journal of Geophysical Research*, 111(B12):B12102.

Kuhlmann, G., Adams, S., Campher, C., van der Spuy, D., di Primio, R., and Horsfield, B. (2010). Passive margin evolution and its controls on natural gas leakage in the southern Orange Basin, blocks 3/4, offshore South Africa. *Marine and Petroleum Geology*, 27(4):973–992.

Le Pichon, X. and Hayes, D. (1971). Marginal offsets, fracture zones, and the early opening of the south atlantic. *Journal of Geophysical Research (1896-1977)*, 76(26):6283–6293.

Lister, G., Etheridge, M., and Symonds, P. (1986). Detachment faulting and the evolution of passive continental margins. *Geology*, 14(3):246–250.

Lorenzo, J. and Wessel, P. (1997). Flexure across a continent-ocean fracture zone: The northern falkland/malvinas plateau, south atlantic. *Geo-Marine Letters*, 17:110–118.

Lorenzo, J. M. and Mutter, J. C. (1988). Seismic stratigraphy and tectonic evolution of the Falkland/Malvinas Plateau. *Rev.Bras.Geoci*, 18:191–200.

MacDonald, D., Gomez-Perez, I., Franzese, J., Spalletti, L., Lawver, L., Gahagan, L., Dalziel, I., Thomas, C., Trewin, N., Hole, M., and Paton, D. (2003). Mesozoic break-up of SW Gondwana: Implications for regional hydrocarbon potential of the southern South Atlantic. *Marine and Petroleum Geology*, 20(3-4):287–308.

Martin, A. and Hartnady, C. (1986). Plate tectonic development of the south wets indian ocean: a revised reconstruction of east antartica and africa. *J. Geophys. Res*, 84(B12):4767–4786.

Maus, S., Barckhausen, U., Berkenbosch, H., Bournas, N., Brozena, J., Childers, V., Dostaler, F., Fairhead, J. D., Finn, C., von Frese, R. R. B., Gaina, C., Golynsky, S., Kucks, R., Lühr, H., Milligan, P., Mogren, S., Müller, R. D., Olesen, O., Pilkington, M., Saltus, R., Schreckenberger, B., Thébault, E., and Caratori Tontini, F. (2009). Emag2: A 2–arc min resolution earth magnetic anomaly grid compiled from satellite, airborne, and marine magnetic measurements. *Geochemistry, Geophysics, Geosystems*, 10(8).

McKenzie, D. (1978). Some remarks on the development of sedimentary basins. *Earth and Planetary Science Letters*, 40(1):25–32.

McMillan, I. K. (2003). Foraminiferally defined biostratigraphic episodes and sedimentation pattern of the Cretaceous drift succession (Early Barremian to Late Maastrichtian) in seven basins on the South African and southern Namibian continental margin. *S. Afr. J. Sci*, 99(December):537–544.

McMillan, I. K., Brink, G. I., Broad, D. S., and Maier, J. J. (1997). Late Mesozoic Sedimentary Basins off the south coast of South Africa. In Selley, R. C., editor, *African Basins*, pages 319–376. Elsevier, Amsterdam.

Mitchell, C., Taylor, G., Cox, K., and Shaw, J. (1986). Are the falkland islands a rotated microplate? *Nature*, 319:131–134.

Mitchum, R.M and Vail, P.R, S. T. I. (1977). Seismic Stratigraphy and Global Changes of Sea Level: Part 2. The Depositional Sequence as a Basic Unit for Stratigraphic Analysis: Section 2. Application of Seismic Reflection Configuration to Stratigraphic Interpretation. *Seismic Stratigraphy - Applications to Hydrocarbon Exploration.*, 165:53–62.

Mueller, C. O. and Jokat, W. (2017). Geophysical evidence for the crustal variation and distribution of magmatism along the central coast of Mozambique. *Tectonophysics*, 712-713:684–703.

Muirhead, J. D. and Kattenhorn, S. A. (2018). Activation of preexisting transverse structures in an evolving magmatic rift in East Africa. *Journal of Structural Geology*, 106(September):1–18.

Nyblade, A. A. and Robinson, S. W. (1994). The african superswell. *Geophysical Research Letters*, 21(9):765–768.

Parsiegla, N. (2008). The Agulhas Plateau: structure and evolution of a Large Igneous Province. *Geophys. J. Int*, 174:336–350.

Parsiegla, N., Stankiewicz, J., Gohl, K., Ryberg, T., and Uenzelmann-Neben, G. (2009). Southern African continental margin: Dynamic processes of a transform margin. *Geochemistry, Geophysics, Geosystems*, 10(3).

Paton, D. A., MacDonald, D. I., and Underhill, J. R. (2006). Applicability of thin or thick skinned structural models in a region of multiple inversion episodes; southern South Africa. *Journal of Structural Geology*, 28(11):1933–1947.

Paton, D. a. and Underhill, J. R. (2004). Role of crustal anisotropy in modifying the structural and sedimentological evolution of extensional basins: the Gamtoos Basin, South Africa. *Basin Research*, 16(3):339–359.

Platt, N. H., Sussex, W., Onz, R. H., and Philip, P. R. (1995). Structure of the southern Falkland Islands continental shelf : initial results from new seismic data. *Marine and Petroleum Geology*, 12(7):759–771.

Rabinowitz, P. D. and Labrecque, J. (1979). The Mesozoic South Atlantic Ocean and Evolution of Its ... *Journal of Geophysical Research*, 84(B11):5973–6002.

Ramos, V. A., Cingolani, C., Chemale, F., Naipauer, M., and Rapalini, A. (2017). Journal of South American Earth Sciences The Malvinas (Falkland) Islands revisited : The tectonic evolution of southern Gondwana based on U-Pb and Lu-Hf detrital zircon isotopes in the Paleozoic cover. *Journal of South American Earth Sciences*, 76:320–345.

Reznikov, M., Ben-Avraham, Z., Hartnady, C., and Niemi, T. M. (2005). Structure of the Transkei Basin and Natal Valley, Southwest Indian Ocean, from seismic reflection and potential field data. *Tectonophysics*, 397(1-2 SPEC. ISS.):127–141.

Richards, P., Duncan, I., Phipps, C., Pickering, G., Grzywacz, J., Hoult, R., and Merritt, J. (2006). Exploring for fan and delta sandstones in the offshore Falklands Basins. *Journal of Petroleum Geology*, 29(3):199–214.

Richardson, N. J. and Underhill, J. R. (2001). ABSTRACT: Controls on the Structural and Stratigraphic Architecture of Syn-Rift Sequences, North Falkland Basin, South Atlantic. *AAPG Bulletin*, 85:1–6.

Roux, J. (1997). Potential outlined in southern outeniqua basin off s. africa. *Oil and Gas Journal*, 95(29).

Schimschal, C. M. and Jokat, W. (2019). The Falkland Plateau in the context of Gondwana breakup. *submitted to Gondwana Research*, 68:108–115.

Scrutton, R. (1979). On sheared passive continental margins. *Tectonophysics*, 59(1-4):293–305.

Scrutton, R. A. (1976). Crustal Structure at the Continental Margin South of South Africa. *Geophysical Journal of the Royal Astronomical Society*, 44(3):601–623.

Smit, J., Brun, J. P., Cloetingh, S., and Ben-Avraham, Z. (2008). Pull-apart basin formation and development in narrow transform zones with application to the Dead Sea basin. *Tectonics*, 27(6):1–17.

Smith, W. H. F. and Sandwell, D. T. (1997). Global sea floor topography from satellite altimetry and ship depth soundings. *Science*, 277(5334):1956–1962.

Sonibare, W. a., Sippel, J., Scheck-Wenderoth, M., and Mikeš, D. (2014). Crust-scale 3D model of the Western Bredasdorp Basin (Southern South Africa): data-based insights from combined isostatic and 3D gravity modelling. *Basin Research*, pages n/a–n/a.

Storey, B. C., Curtis, M. L., Ferris, J. K., Hunter, M. a., and Livermore, R. a. (1999). Reconstruction and break-out model for the Falkland Islands within Gondwana. *Journal of African Earth Sciences*, 29(1):153–163.

Tankard, A., Welsink, H., Aukes, P., Newton, R., and Stettler, E. (2009). Tectonic evolution of the Cape and Karoo basins of South Africa. *Marine and Petroleum Geology*, 26(8):1379–1412.

Taylor, G. and Shaw, J. (1989). The falkland islands: new palaeo-magnetic data and their origin as a displaced terrane from southern africa. In Hillhouse, J., editor, *Deep structure and past kinematics of accreted terranes*, volume 50 of *Geophysical Monograph*, pages 59–72. IUGG.

Thomson, K. (1998). When did the Falklands rotate? *Marine and Petroleum Geology*, 15(8):723–736.

Thomson, K. (1999). Role of continental break-up, mantle plume development and fault reactivation in the evolution of the Gamtoos Basin, South Africa. *Marine and Petroleum Geology*, 16(5):409–429.

Thomson, K., Hegarty, K. A., Marshallsea, S. J., and Green, P. F. (2002). Thermal and tectonic evolution of the Falkland Islands: Implications for hydrocarbon exploration in the adjacent offshore region. *Marine and Petroleum Geology*, 19(2):95–116.

Thomson, K., Underhill, and John R. (1999). Frontier Exploration in the South Atlantic: Structural Prospectivity hi the North Falkland Basin. *AAPG Bulletin*, 83(5):778–797.

Tinker, J., de Wit, M., and Brown, R. (2008). Mesozoic exhumation of the southern Cape, South Africa, quantified using apatite fission track thermochronology. *Tectonophysics*, 455(1-4):77–93.

Turner, J. P., Rosendahl, B. R., and Wilson, P. G. (2003). Structure and evolution of an obliquely sheared continental margin: Rio Muni, West Africa. *Tectonophysics*, 374(1-2):41–55.

Uenzelmann-Neben, G., Schlüter, P., and Weigelt, E. (2007). Cenozoic oceanic circulation within the South African gateway: Indications from seismic stratigraphy. *South African Journal of Geology*, 110(2-3):275–294.

Vail, P. R., Mitchum, R., and Thompson, S. (1977). Seismic stratigraphy and global changes of sea level: Part 3. relative changes of sea level from coastal onlap. In Payton, C., editor, *Seismic stratigraphy - Application to Hydrocarbon Exploration*, pages 63–81. American Association of Petroleum Geologists Special Volumes.

Vine, F. J. and Matthews, D. H. (1963). Magnetic anomalies over oceanic ridges. *Nature*, 199(4897):947–949.

Wernicke, B. (1985). Uniform-sense normal simple shear of the continental lithosphere. *Canadian Journal of Earth Sciences*, 22(1):108–125.

Wildman, M., Brown, R., Watkins, R., Carter, A., Gleadow, A., and Summerfield, M. (2015). Post break-up tectonic inversion across the southwestern cape of South Africa: New insights from apatite and zircon fission track thermochronometry. *Tectonophysics*, 654:30–55.

Wilson, P. G., Turner, J. P., and Westbrook, G. K. (2003). Structural architecture of the ocean-continent boundary at an oblique transform margin through deep-imaging seismic interpretation and gravity modelling: Equatorial Guinea, West Africa. *Tectonophysics*, 374(1-2):19–40.